Use Authorization

In presenting this thesis in partial fulfillment of the requirements for an advanced degree at Idaho State University, I agree that the Library shall make it freely available for inspection. I further state that permission for extensive copying of my thesis for scholarly purposes may be granted by the Dean of Graduate School, Dean of my academic division, or by the University Librarian. It is understood that any copying or publication of this thesis for financial gain shall not be allowed without my written permission.

Signature ___________________________

Date___________________________

Experimental Investigation of Titanium Alloy Bars (TiABs) for Seismic Resilient and Durable Concrete Bridge Piers

by

Mahesh Acharya

A thesis

submitted in partial fulfillment

of the requirements for the degree of

Master of Science in the Department of Civil and Environmental Engineering

Idaho State University

Spring 2021

Committee Approval

To the Graduate Faculty:

The members of the committee appointed to examine the thesis of Mahesh Acharya find it satisfactory and recommend that it be accepted.

Major Advisor

Dr. Mustafa Mashal

Committee Member

Dr. Arya Ebrahimpour

Graduate Faculty Representative

Dr. Andrew Chrysler

Acknowledgments

I would like to acknowledge my family, colleagues, and advisors who helped throughout this project. With genuine pleasure, I would like to express my genuine gratitude to my primary advisor and mentor Dr. Mustafa Mashal whose continuous intellectual guidance and extended support was crucial for completion of this project. His enthusiasm and expertise kept me motivated and provided invaluable suggestion and supervision to accomplish the research. I would also like to thank the committee member Dr. Arya Ebrahimpour and the Graduate Faculty Representative Dr. Andrew Chrysler.

I also owe my sincere thanks to Jared Cantrell, Karma Tenzing Gurung, Mahesh Mahat, Corey Marshall, Katie Hogarth, and Ali Shokrgozar for their friendship, patience, and support during the research. Their continuous help and moral support kept me inspired throughout this project. I would also like to thank the entire structural and earthquake engineering research group at Idaho State University who helped execute and make this project a success. I would also like to acknowledge the Idaho Transportation Department (ITD), Idaho State Board of Education, Idaho State University, Perryman Company, BarSplice Products Inc., and Premier Technology for supporting the research.

I am extremely grateful to my parents Madhav and Mithila Acharya, my brother Manish Acharya, my uncle Naba Raj Gautam and my entire family for their love and support throughout my career. Their belief in me has always kept me going.

TABLE OF CONTENTS

LIST OF FIGURES

LIST OF TABLES

Experimental Investigation of Titanium Alloy Bars (TiABs) for Seismic Resilient and Durable Concrete Bridge Piers

Thesis Abstract – Idaho State University (2021)

The research introduces Titanium Alloy Bars (TiABs) for flexural and transverse reinforcing in new bridge piers located in seismic zones. TiABs offer higher strength, good ductility, excellent durability, and enhanced fatigue-resistance compared to traditional reinforcing bars. The research focuses on the applications of TiABs in construction of new bridges located in seismic and corrosive environment. A bridge pier system was introduced that incorporated both seismic resiliency and durability in a single package. Application of TiABs in bridge piers increases service life, reduces rebar congestion, yields to lower overstrength factor, and limits residual displacement following an earthquake. An approximately 1/3rd scale bridge pier reinforced with TiABs rebars and spirals is tested under quasi-static cyclic loading protocol to investigate seismic performance. Results are compared against a benchmark specimen reinforced with normal steel rebars and spirals. The thesis also introduces the available options for splicing of TiABs using mechanical systems to optimize construction costs.

Key Words: Titanium alloy bars; Ti6Al4V; Bridge piers; Seismic resiliency; 100-year service life; Large-scale testing; Innovative materials; Durable bridges; Splicing of TiABs

CHAPTER 1. INTRODUCTION

1.1 Motivation and Background

Human civilization has utilized numerous materials for construction of civil infrastructure through stone age till now. Titanium, an emerging material in 21st century, is considered 7th most abundant metal and 9th most abundant element in the earth's crust [8]. It can be considered innovative material not only for construction, but also for retrofitting of civil infrastructure. The most widely used grade of titanium is Grade 5 (Ti6Al4V).

According to the American Society of Civil Engineers (ASCE) Infrastructure Report Card-2021, there are more than 617,000 bridges in the United States, of which 47% were at least 50 years or older. 7.5% of the US bridges were structurally deficient, and on average 178 million trips are taken across these structurally deficient bridges every day in the United States [32]. Structurally deficient means classification of a structure indicating one or more elements of the structures require repair or monitoring. Most of the bridges in the United States are designed for a service life of 50 years and 42% of bridges in the US are already past the service life. The rate of deterioration of bridges is increasing the rate of repair, rehabilitation, and replacement, all while the number of bridges sliding into the 'fair' category is growing as shown in Figure 1 [32].

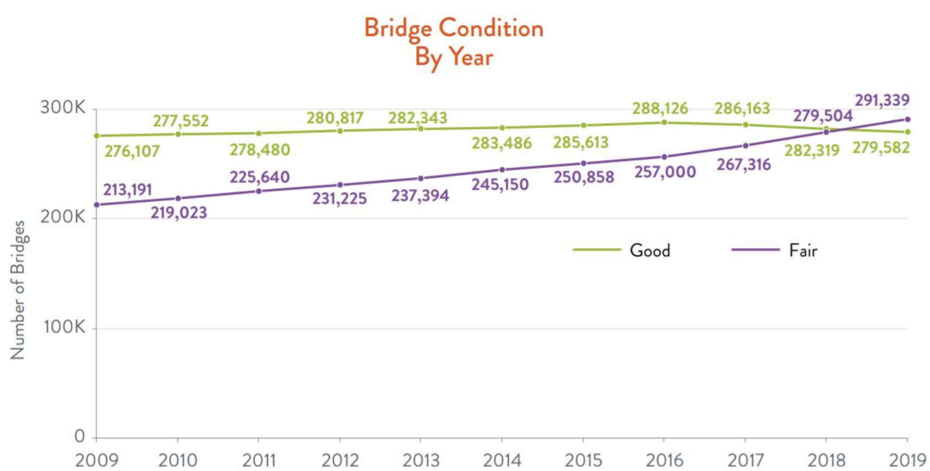

Figure 1. Bridge Condition of the United States as of Year 2019 [32]

Bridges reaching their service life require frequent maintenance and possible replacement. Many of the Departments of Transportations (DOTs) do not have available funds to replace all structurally deficient bridges that have reached their service life at once. The estimate by ASCE Infrastructure Report Card – 2021 estimates the need of $125 billion to overcome the backlog of bridge rehabilitation at the United States [32]. One of the approaches to deal with this issue has been to reduce the traffic on the bridge and impose speed limits. This approach has a significant economic impact.

In the recent years, the Oregon State University (OSU) has conducted several research projects in collaboration with Oregon Department of Transportation (ODOT) to identify the potential use of titanium alloy bars for retrofitting of deficient bridges in the state of Oregon. Research has shown that Titanium Alloy Bars (TiABs) can significantly increase shear and flexural capacity of existing reinforced concrete bridges using Near-Surface Mount (NSM) techniques. The research encouraged ODOT to successfully retrofit several bridges in Oregon using NSM techniques. For example, a bridge on Oregon's main East-West Route I-84 was retrofitted using titanium alloy bars by ODOT with less than 3% of the bridge replacement cost ($4.6 million), and 30% less expensive than rehabilitation using FRP sheets or stainless-steel bars [9] [12]. Recently, the Texas Department of Transportation (TxDOT) utilized TiABs with NSM techniques to repair the substructure for San Jacinto River Bridge on I-10 that was damaged during the 2019 Imelda tropical storm. Past applications have shown that TiABs have contributed to saving costs for labor and materials, less traffic interruption, durable and accelerated retrofitting process with being less expensive than other materials in terms of life-cycle costs over 50 years.

One of the main causes of aging infrastructure in the United States is corrosion of reinforcing bars. Corrosion is a major concern in evaluating the seismic resilience of both existing and new bridges. Titanium has a stable oxide layer making it impervious to chlorides and rapid corrosion. These properties also make titanium alloys ideal for application in the field to strengthen a bridge. Given the advantages of TiABs, the research focuses on its application for seismic resilient and durable bridges with a service life of 100 year or more. As the first step toward more resilient and durable bridges, seismic testing is conducted on a pier reinforced with TiABs and the results are compared against a benchmark pier with normal steel rebars.

1.2 Scope

The scope of the research is to perform large-scale experimental investigation of a concrete bridge pier reinforced with grade 5 titanium alloy (Ti6Al4V) bars and spirals. Then, compare the results with a benchmark specimen reinforced with normal steel rebar and spiral. The research analyzes the results obtained from quasi-static cyclic loading protocol for the specimens and explores application of titanium alloy bars in construction of new concrete bridge piers in seismic zones.

1.3 Objectives

The objectives of the research are:

1. Literature review of new and advanced materials in civil engineering industry with a focus on the concrete bridges.
2. Development of design procedures, detailing considerations and construction technology for cast-in-place bridge piers reinforced with TiABs.
3. Large-scale experimental testing of a cast-in-place concrete bridge pier reinforced with TiABs under quasi-static cyclic loading protocol.

    a. Large-scale experimental testing of a benchmark cast-in-place concrete bridge pier reinforced with normal steel rebar under a similar quasi-static cyclic loading protocol.
    b. Compare the performance of cast-in-place pier reinforced with TiABs against the cast-in-place pier reinforced with normal steel rebars.
    c. Provide recommendations regarding the use of TiABs in concrete bridge piers and appropriate mechanical coupler for its use.
4. Identify an appropriate mechanical coupler to splice smooth and pseudo-threaded TiABs subjected to tension tests performed in accordance with ASTM International Standards.

Objective 1 is accomplished by summarizing literature review from the past studies on TiABs. Objectives 2-3 are accomplished through testing of two large-scale concrete bridge piers. One of the specimens is cast-in-place (CIP) pier reinforced with normal steel rebars and the other is a CIP pier reinforced with TiABs. Objective 4 is accomplished by conducting tension tests to demonstrate the adequacy of some available mechanical couplers for splicing of TiABs. The use of mechanical couplers would avoid lap splicing of TiABs as well as saving materials cost.

1.4 Thesis Structure

Figure 2 presents a structure of the thesis.

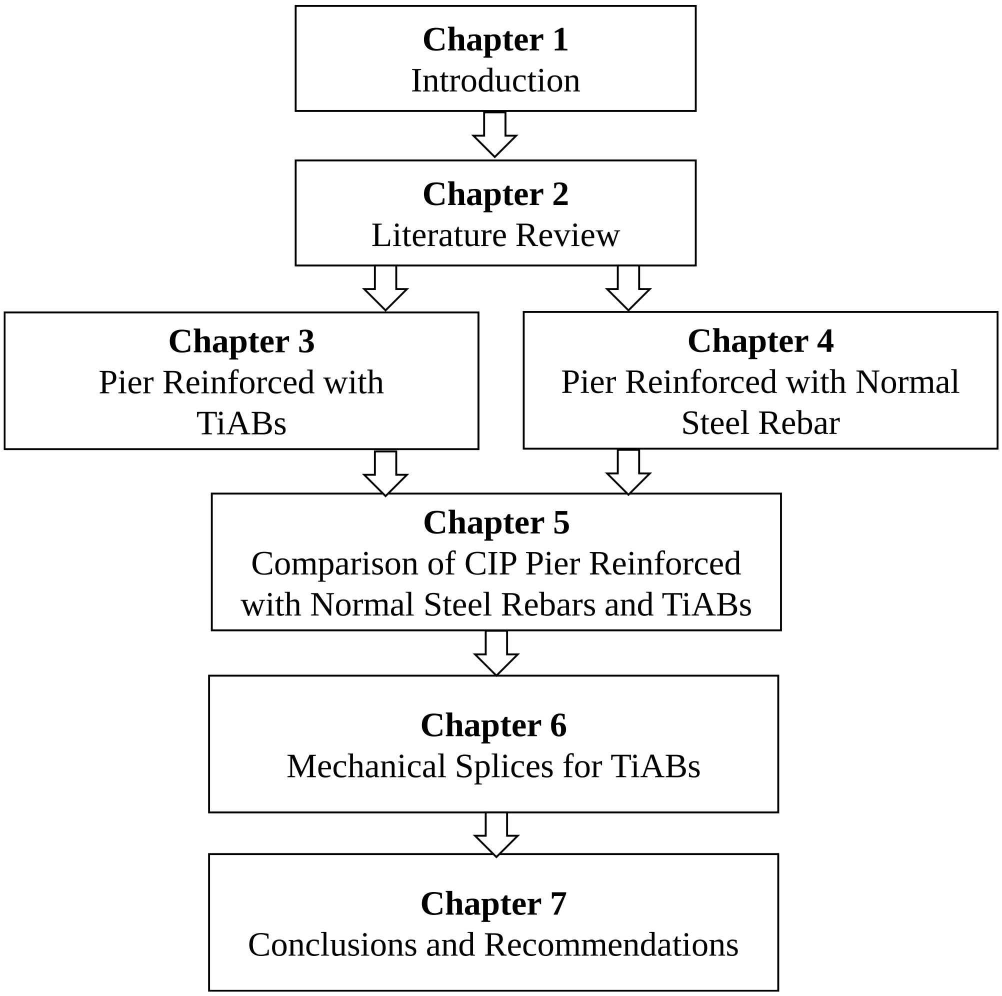

Figure 2. Thesis Structure

Chapter 1 provides an introduction of the research. Background, problem statement, scope and objectives of the thesis are discussed in this chapter.

Chapter 2 presents literature review and recent applications of some novel advanced materials, including TiABs, for construction and retrofitting of bridges.

Chapter 3 presents construction, and experimental testing of a CIP bridge pier reinforced with TiABs. In the first part of the chapter, the design procedure, detailing consideration, construction process and experimental testing of a 1/3rd scale cantilever pier reinforced with TiABs is discussed. In the second part of the chapter, results and observations from testing are presented.

Chapter 4 discusses the construction and experimental testing of a CIP pier reinforced with normal steel rebars. This pier is used as a benchmark specimen. The pier has similar capacity, dimensions, and detailing to the pier with TiABs.

Chapter 5 compares observations and testing results between the pier reinforced with TiABs and the benchmark pier.

Chapter 6 discusses some available options for mechanical splicing of the TiABs. The appropriate mechanical splicing option is then identified to splice pseudo-threaded TiABs.

Chapter 7 summarizes research findings and conclusions. This chapter also provides recommendation for future research on applications of TiABs in bridges.

CHAPTER 2. LITERATURE REVIEW

This section of thesis discusses several novel materials that have recently been incorporated in construction and retrofitting of bridges. The advantages and disadvantages of each material is discussed.

2.1 Advanced Materials for Bridges

Civil Engineering industry is continuously evolving with numerous bridges being constructed all the time. Many concrete bridges in the United States are in poor condition which implies that they require frequent maintenance and upgrades. Advanced materials have been introduced in bridges lately that would improve structural performance and durability. Some of these advanced materials include Shape Memory Alloy (SMA), Engineered Cementitious Composites (ECC), Fiber Reinforced Polymer (FRP) and Titanium Alloy Bars (TiABs)

2.1.1 Shape Memory Alloy (SMA)

Shape Memory Alloy belongs to a class of metallic materials that is capable to recover its original shape on heating or loading-and-unloading. This property of SMA can be summarized as shape memory effect or super-elastic effect. An alloy of Nickel and Titanium (NiTi), SMA has gained more popularity due to its high corrosion resistance, and superelastic strain capacity compared to conventional steel. Researchers have carried out both analytical and experimental investigations in-order-to identify the use of SMA in bridge structures. For SMA, the alloy will deform similar to conventional steel beyond the yield point, however it will return to its undeformed shape after unloading. This means the alloy is super elastic and can be explored in bridge piers (e.g., plastic hinges) located in seismic zones to reduce and possibly eliminate residual displacement after an earthquake. Energy can still be dissipated by stretching the SMA and, once the earthquake motions diminish, the SMA will return to its original shape. The two-dimensional stress-strain behavior of SMA compared with normal steel can be seen in Figure 3. Similarly, the stress-strain diagram of shape-memory alloys and the schematic crystal structures at different temperatures is presented in Figure 4.

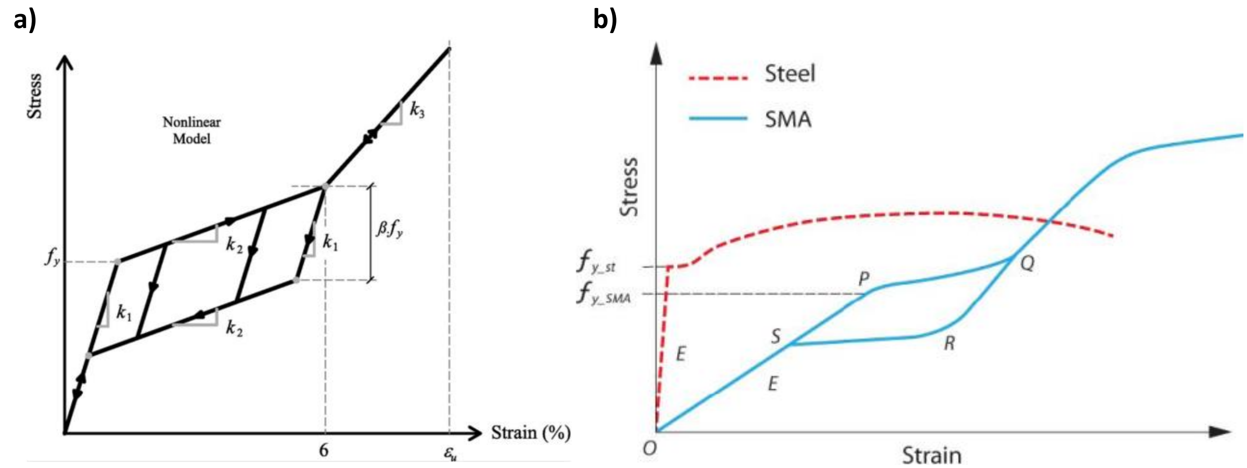

Figure 3. Stress-Strain a) NiTi Superelastic SMA [1], b) Comparison of Steel and SMA [2]

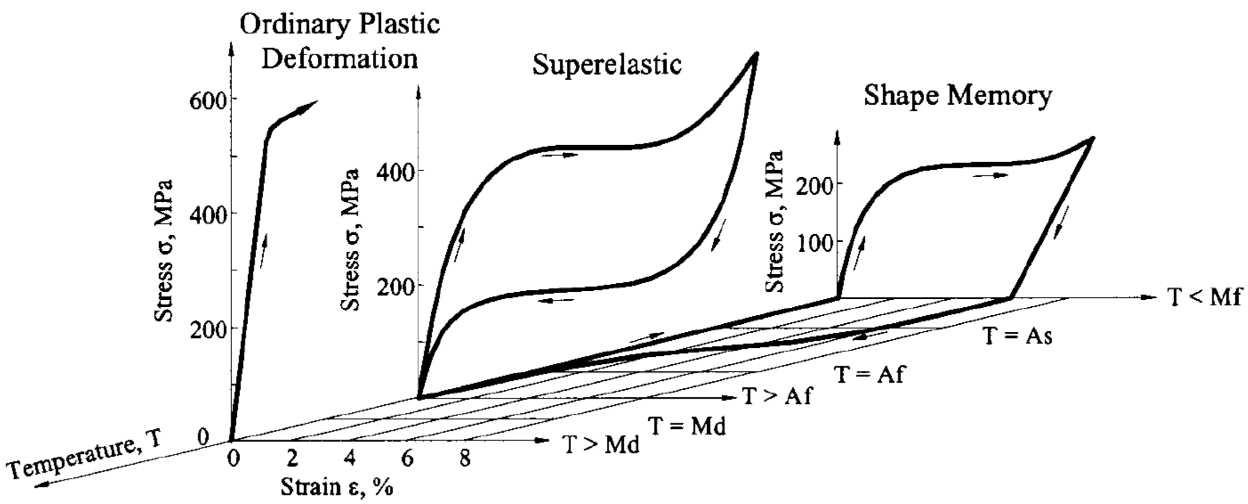

Figure 4. Three-Dimensional Stress-Strain Diagram with Temperature [4]

Past studies showed that reinforcing SMA can substantially reduce residual displacement especially in bridge piers even after undergoing large deformations [28]. The Washington Department of Transportation (WSDOT) recently constructed the first SMA bridge in the world in Seattle. This project was funded by the FHWA Innovative Bridge Research and Deployment (IBRD) program. Figure 5 shows the bridge that was successfully constructed by WSDOT in

Seattle, WA. Also, Figure 6 shows the No. 10 (1.25 inch) SMA bars spliced with normal steel rebars using mechanical couplers for longitudinal reinforcement. SMA is an expensive material. So, it was used only in the plastic hinge region of the pier to reduce construction costs.

Figure 5. SMA reinforced ECC bridge in Seattle, WA

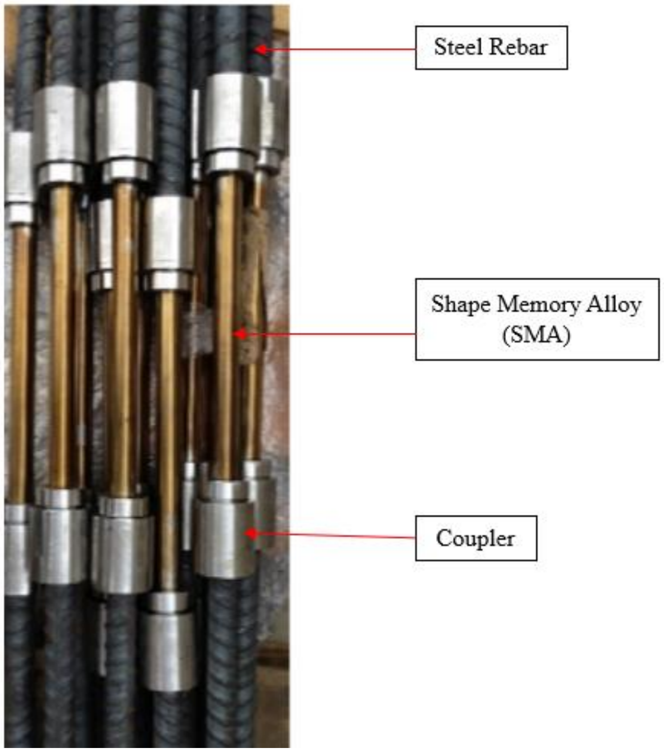

Figure 6. SMA coupled with Steel Rebar

Even though SMA has some good mechanical properties, it has some disadvantages such as material cost and poor fatigue properties.

2.1.2 Engineered Cementitious Composites (ECC)

ECC is a type of fiber-reinforced cementitious materials with high tensile ductility. Compressive strength of ECC concrete is comparatively higher than the normal-weight concrete. A typical ECC mix design is presented in Table 1 [5].

Table 1. Typical ECC Mix Design [5]

Material	Percent by Weight
Cement	37.0
Fly Ash	31.5
Sand	24.7
Silica Powder	5.4
PVA Fiber	1.4
Superplasticizer	---

Note: Water to Cement & Fly Ash ratio= 0.315; Fly Ash to Cement ratio= 0.85

The fibers that are used in ECC Mix are used to maximize the tensile ductility by developing multiple microcracks. This can be reached only if the fibers are coated with material that allows fibers to slip partially when they are overloaded, preventing fiber fracture and leading to formation of many hairline cracks instead of a few wide cracks [6]. Mechanical properties of ECC can vary depending on the mix design and the type of fiber used. Experiments have shown that ECC provides better ductility and significant reduction of shear reinforcement. A plot of stress-strain relationships for ECC is provided in Figure 7.

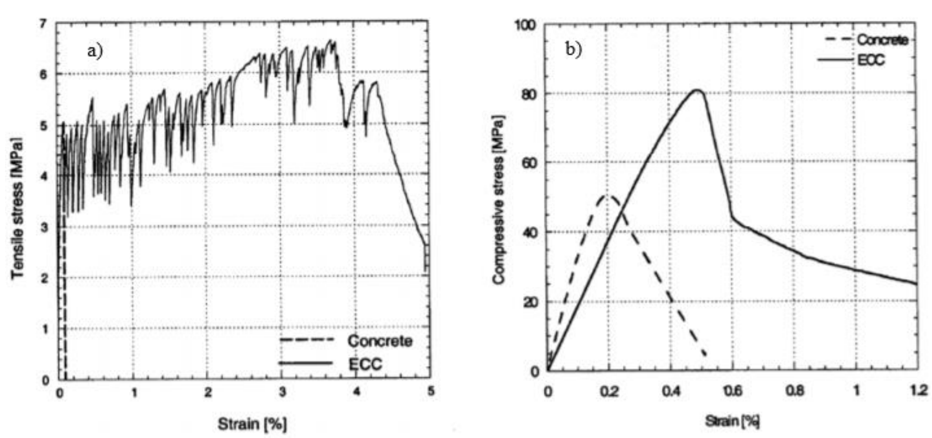

Figure 7. Stress-Strain of ECC vs. Concrete a) Tensile, b) Compression [6]

Researchers at the University of Nevada-Reno performed large-scale experimental testing of bridge columns with ECC in plastic hinges [29]. Research showed that ECC bridge columns experiences less damage during an earthquake and would require limited post-earthquake repair. Even though many research projects were carried out in ECC, the use of ECC in bridge piers has been very limited. Applications of ECC have been limited to repairing bridge decks and retaining walls. In 2019, Washington Department of Transportation (WSDOT) successfully used ECC in combination with SMA in a bridge in Seattle, WA.

2.1.3 Fiber Reinforced Polymer (FRP)

Fiber reinforced polymers are composite materials known for their linear elastic behavior and greater strength. Different types of FRP are currently used in civil engineering industry. Some of these include glass FRP, carbon FRP, aramid FRP, silicon carbide FRP and others. According to ACI 440.1R-06, compressive strength of FRP is neglected because of micro-buckling of fibers or shear failure when stressed under compressive actions. However, stress-strain plot of various FRP's is shown in Figure 8.

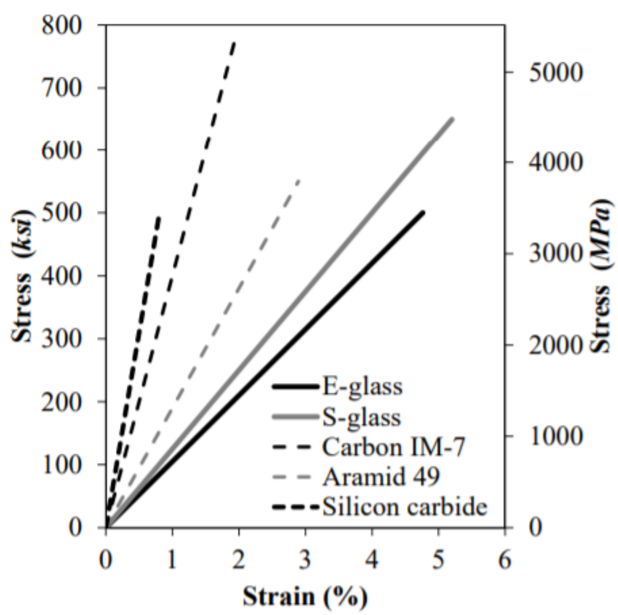

Figure 8. Stress-Strain Plot of FRP [5]

FRP has been widely used in civil engineering industry, mostly for repair and retrofit of bridges and other structures. Various design guidelines, codes and standards are developed for FRP. ACI 440.1R-06 (Guide for the Design and Construction of Structural Concrete Reinforced with FRP Bars) has also proposed a range of mechanical properties for different FRP bars (glass FRP-GFRP, carbon FRP-CFRP, and aramid FRP-AFRP), as presented in Table 2. Although FRP is popular in repair and retrofit of structures, it has some disadvantages. It has lower modulus of elasticity compared to steel. FRP is considered to have poor long-term temperature resistance and the strength decreases when stressed under high temperature for long time. Aging phenomenon is a common defect of FRP. It is easy to cause performance degradation under effect of ultraviolet rays, wind, rain, snow, or other mechanical stress. Also, there is no effective method to recycle FRP.

Table 2. ACI proposed properties of FRP [7]

Properties	GFRP	CFRP	AFRP
Tensile Strength, *ksi* (*MPa*)	70 to 230 (483 to 1600)	87 to 535 (600 to 3690)	250 to 368 (1720 to 2540)
Modulus of Elasticity, *ksi* (*GPa*)	5100 to 7400 (35 to 51)	15900 to 84000 (120 to 580)	6000 to 18200 (41 to 125)
Rupture Tensile Strain (%)	1.2 to 3.1	0.5 to 1.7	1.9 to 4.4

2.1.4 Titanium Alloys

Titanium alloys are mostly used in the aerospace industry. It is gaining popularity lately in civil infrastructures and have emerged as a new advanced material. Great corrosion resistance, high strength to weight ratio, low density, flexibility, ductility, and composite compatibility features of titanium alloys have placed themselves as potential material in construction and retrofitting of bridges. Presently, titanium alloy bars are used to retrofit bridge in civil engineering industry. Titanium alloy bars have lower modulus of elasticity and higher modulus of resilience compared to conventional steel. Titanium alloy bars are strong, durable, and naturally resistant to rust and corrosion but, at the same time it cannot be cast like aluminum, or iron, and tends to cost more than other metals. This makes titanium alloy bars an expensive material compared to steel, stainless steel, aluminum, etc.

In March 2020, the American Association of State Highway and Transportation Officials (AASHTO) released a new publication for the use of Titanium Alloy Bars (TiABs) (Figure 9). The publication is titled 'Guide for Design and Construction of Near-Surface Mounted Titanium Alloy Bars for Strengthening Concrete Structures'. The publication provides recommendations for strengthening of existing reinforced concrete structures with TiABs using the Near-Surface Mounted or NSM techniques.

Currently, the widely used grade of titanium alloy is Grade 5, i.e., Ti6Al4V which is an alloy of Titanium, Aluminum, and Vanadium. Recently, there have been several research studies and applications of TiABs in civil infrastructure in the United States as summarized below.

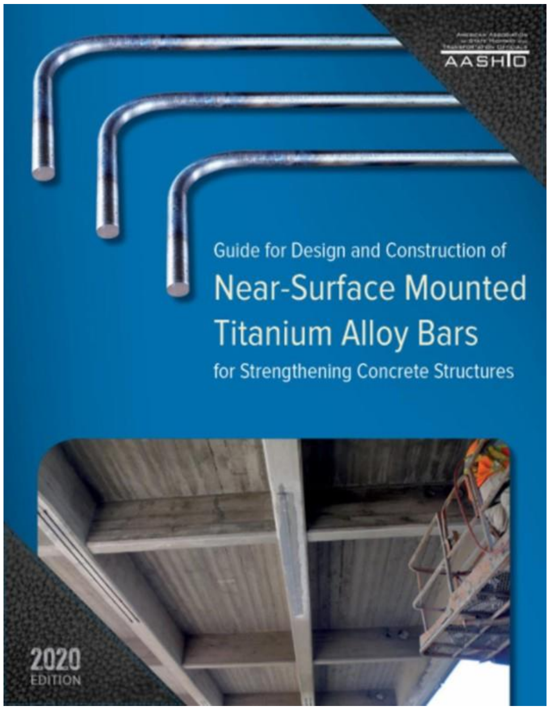

Figure 9. AASHTO Guide for Design and Construction of Near-Surface Mounted Titanium Alloy Bars for Strengthening Concrete Structures, 1st Edition

2.1.4.1 *Idaho State University*

Recently, Idaho State university (ISU) conducted an extensive experimental and analytical research to identify mechanical properties for TiABs and compare them with a high strength alloy (e.g., grade 150 ksi). One of the important tests was the tension test to compare TiABs against the 150 ksi high strength steel alloy. Many specimens were tested, results were used to develop analytical models for stress-strain and other mechanical properties for TiABs [30]. The average analytical stress-strain plot comparing Ti6Al4V, and high strength (150 ksi) steel is presented in Figure 10.

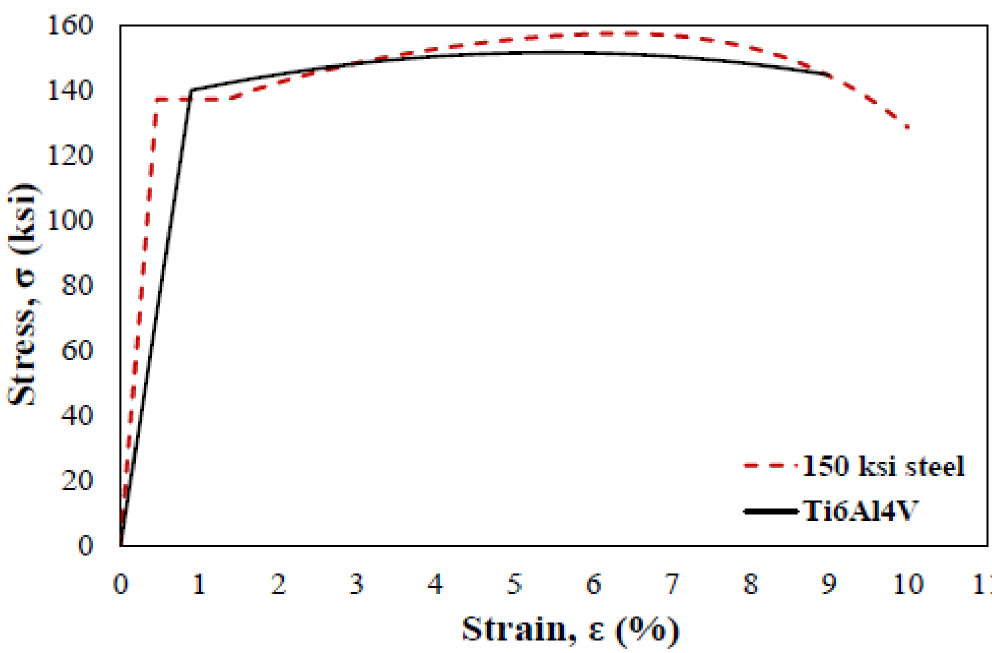

Figure 10. Average Analytical Stress-Strain Plot for TiABs and 150 ksi Steel Specimens [8]

The results from the research at ISU showed that titanium alloys (Ti6Al4V) can perform better than the high strength steel. The titanium alloys had about one and half times more ductility and about one quarter time more modulus of resilience than the 150 ksi high strength steel. These advantageous mechanical properties of the titanium alloy bars can surely be utilized in civil engineering industry, especially bridge piers.

2.1.4.2 Oregon State University

Oregon State University (OSU) has conducted several research projects in collaboration with the Oregon Department of Transportation (ODOT) to identify potential use of TiABs for retrofitting of deficient bridges in Oregon. One of these projects included retrofitting of square column presented as in Figure 11 and Figure 12. The research at OSU was performed to investigate seismic performance of poorly detailed square reinforced concrete columns retrofitted with TiABs. The use of TiABs to retrofit reinforced columns successfully increased drift capacity of deficient columns and altered the failure mode from non-ductile to ductile. The research supported the use of externally anchored TiABs to enhance the performance of rectangular reinforced columns. The use of TiABs for retrofitting offers improved ductility for the pier, enhanced flexural and shear capacity, simple application procedure, long-term environmental durability, and easy inspection of the retrofitted pier [11]. The research concluded that an improved seismic performance of the column could be achieved using TiABs.

Figure 11. Experimental Testing of Retrofitted Square Column [31]

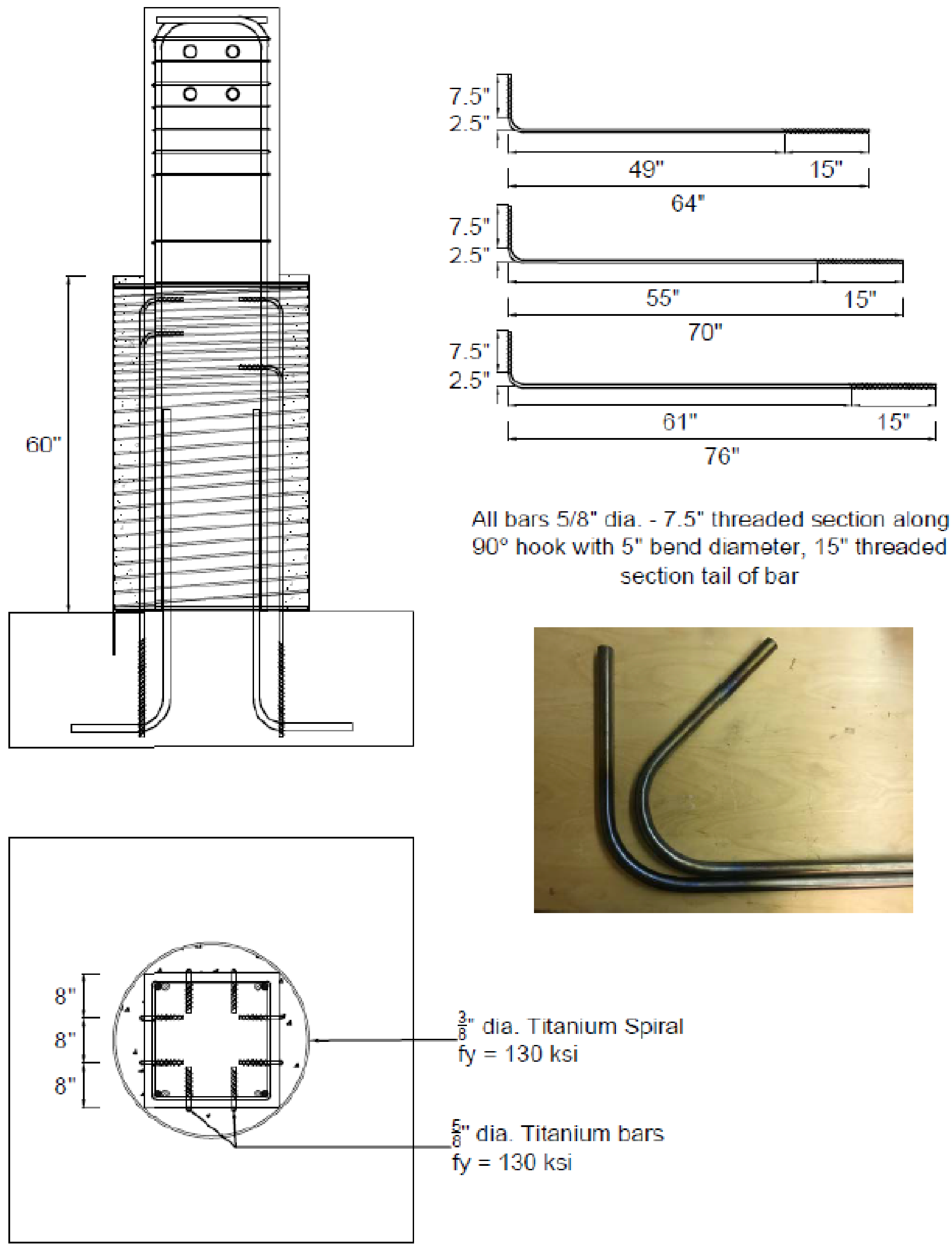

Figure 12. Retrofit Detail Prepared by OSU [31]

Similarly, OSU performed other research studies on retrofitting of deficient reinforced concrete girders. The girders were strengthened for flexure and shear using NSM technology. In this research, NSM technology was combined with TiABs instead of commonly used Fiber

Reinforced Polymer (FRP) sheets or stainless-steel bars. Research showed that use of TiABs for retrofitting is very effective in increasing the shear and flexural capacity of existing reinforced concrete bridges. Testing results showed that the girder strength increased by a factor of two and were well above required factored load effects using only four TiABs. Similarly, the NSM TiABs used for shear strengthening provided increased capacity (40%) and shifted the failure mechanism for the girder from a nonductile shear failure to ductile flexural failure [13]. The detail of design which was created by the research from OSU is presented in Figure 13.

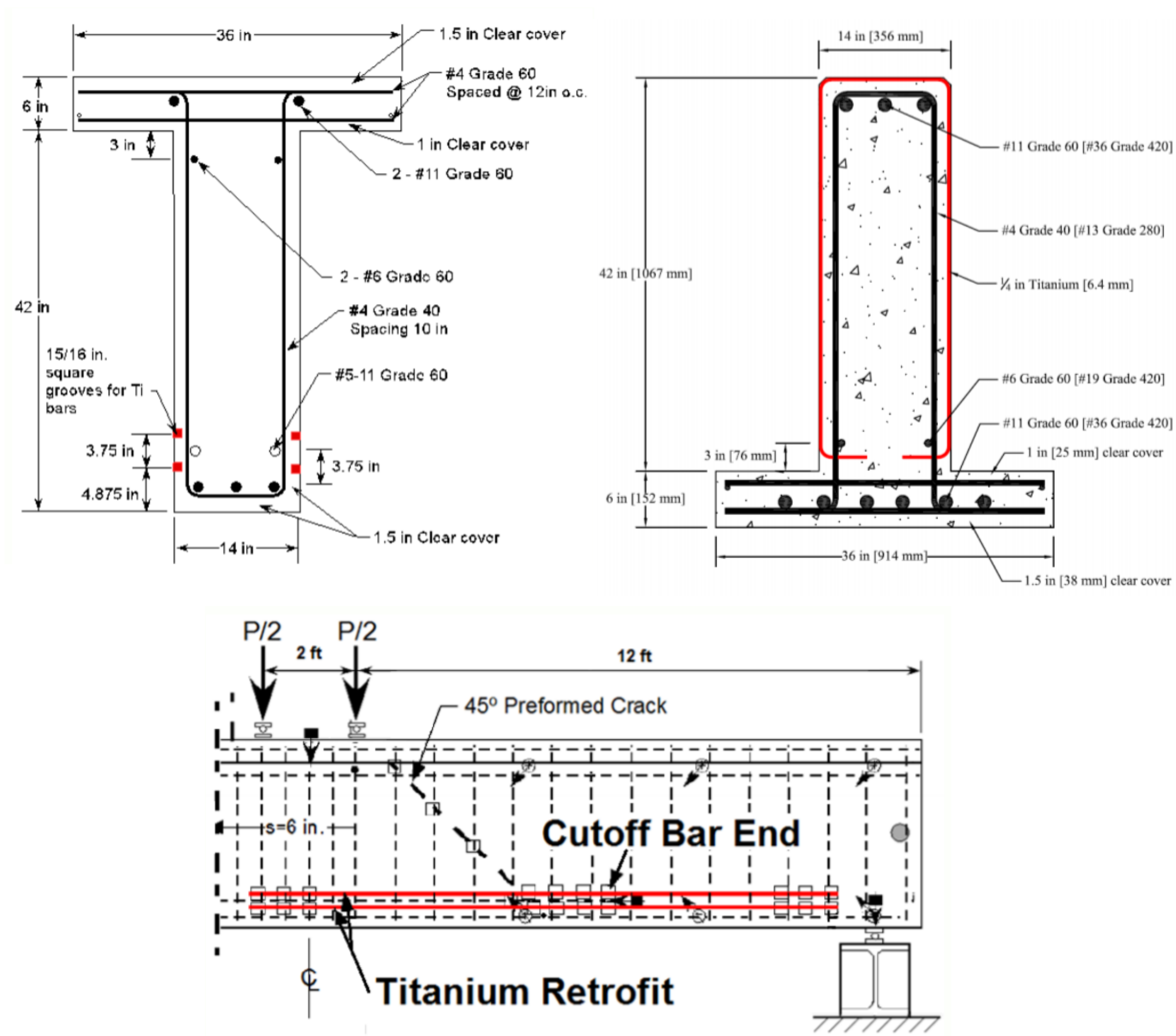

Figure 13. Strengthening Detail Using TiABs

Research at OSU has helped the Oregon Department of Transportation (ODOT) to successfully retrofit several bridges in the state of Oregon in the last 7 years. For instance, the bridge on Oregon's main East-West Route I-84, as shown in Figure 14, was retrofitted with TiABs. The retrofitting cost was less than 3% of the bridge replacement cost ($4.6 million), and 30% less than rehabilitation using FRP sheets or stainless-steel bars [9] [12]. Figure 14 clearly the bridge that was retrofitted using NSM technology in Oregon.

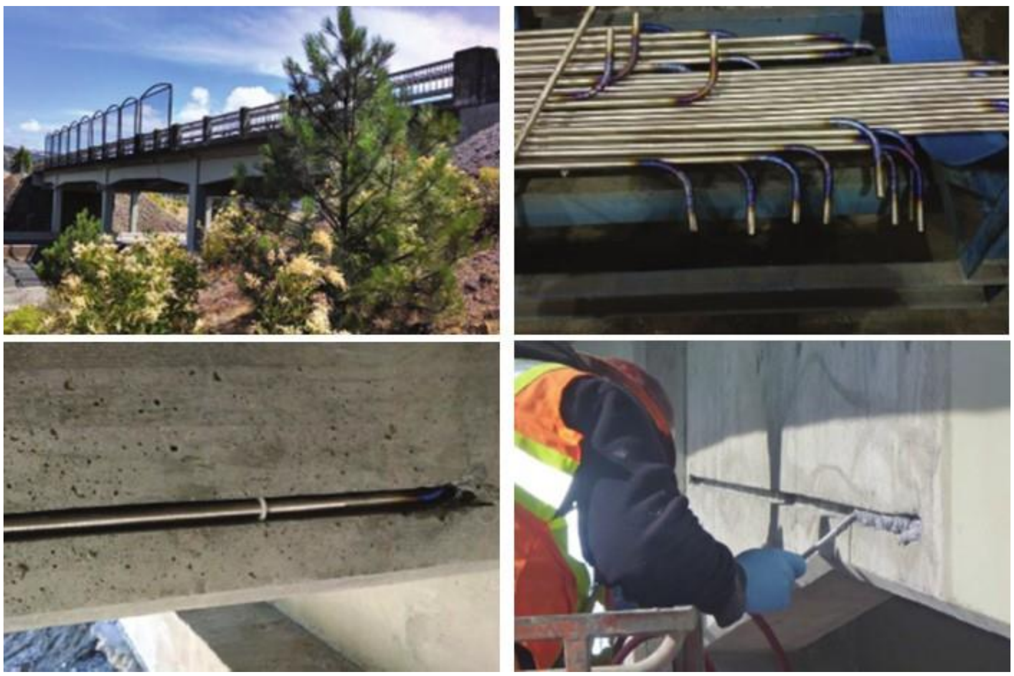

Figure 14. NSM TiABs technology used in Mosier Bridge by ODOT

2.1.4.3 Texas Department of Transportation (TxDOT)

Recently, the Texas Department of Transportation (TxDOT) utilized NSM techniques with TiABs in retrofitting of the San Jacinto River Bridge substructure on I-10 in the Houston District (Figure 15). The bridge was damaged during a tropical storm in 2019. TiABs were bent on-site and epoxied into saw-cut grooves and holes that were drilled at the surface of the bent-cap. This was intended to restore the capacity of the yielded reinforcing steel. TiABs provided increased strength across the cracks. Although TiABs are more expensive compared to normal steel rebars, however they offer 2 ½ times higher yield stress compared to grade 60-ksi steel rebars; this results in having few TiABs [10].

Past applications showed that the use of TiABs provides higher strength and durability at a lower cost and less construction time. The use of TiABs for retrofitting bridges offers cost savings for labor and materials, causes less traffic disruption, and provides durable and accelerated retrofitting process that is competitive to other conventional materials over service life of the structure.

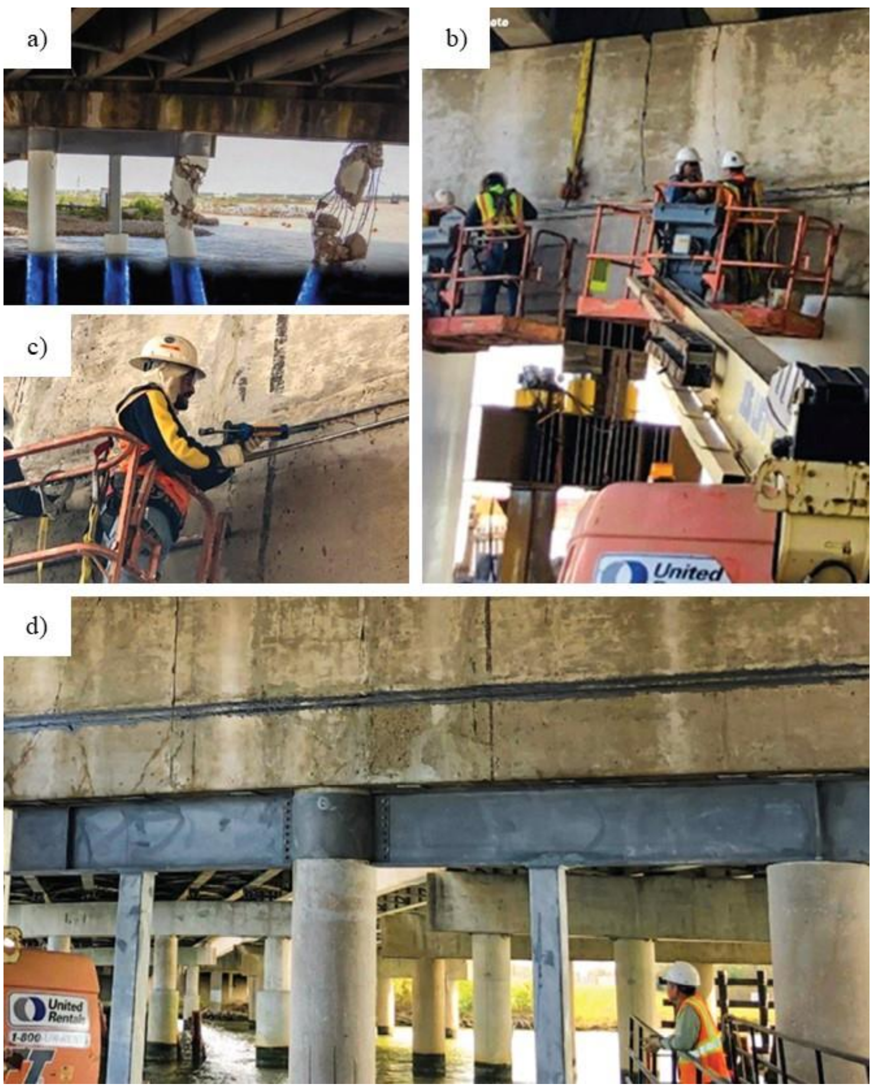

Figure 15. a) San Jacinto River Bridge, b) Making Grooves and Holes Drilled, c) Epoxied TiABs, d) Repaired Bridge using TiABs

2.2 Summary

In the last 25 years, researchers have invested considerable amount of effort to identify and introduce advanced materials in construction and retrofitting of civil infrastructure. Some of these advanced materials include Shape Memory Alloy (SMA), Fiber-Reinforced Polymer (FRP), Engineered Cementitious Composites (ECC) and Titanium Alloy Bars (TiABs). These novel materials have been demonstrated to improve structural performance and durability of bridge piers. Some of the material properties of TiABs such as excellent corrosion resistance, flexibility, low thermal conductivity, and high strength-to-weight ratio make them ideal for potential applications in bridge piers. Recently the Departments of Transportation in Oregon and Texas successfully used TiABs in retrofitting of several deficient and damaged concrete bridges. This marked the introduction of a new advanced material (TiABs) in civil infrastructure. In these projects, application of TiABs resulted in cost savings over other conventional materials such as steel rebars and FRP. TiABs require low maintenance and life-cycle cost. The AASHTO 1st edition of 'Guide for Design and Construction of Near-Surface Mounted Titanium Alloy Bars for Strengthening Concrete Structures' has provided first step for wider adoption of TiABs. Application of TiABs in construction of new structures, especially in bridge piers located in seismic zones, has not been investigated previously. The research in this thesis introduces TiABs as a potential advanced material in construction of seismic resilient and durable bridges that have much longer service life (e.g., 100 years or more) compared to the current practice (e.g., 50 years).

CHAPTER 3. PIER REINFORCED WITH TITANIUM ALLOY BARS

3.1 Introduction

This chapter presents the design, construction, and testing of a cast-in-place cantilever column reinforced with Grade 5, i.e., Ti6Al4V Titanium Alloy Bars (TiABs). The purpose of a cast-in-place pier reinforced with TiABs is to investigate seismic performance and then compare the results with a benchmark specimen, i.e., cast-in-place pier reinforced with normal steel rebars. The design of the cast-in-place pier follows the 2017 AASHTO LRFD Design Specifications to the extent possible [25].

3.2 Prototype Structure

South-East Idaho is considered to be the most seismic region in the entire Idaho. A typical bridge in South-East Idaho (Figure 16) is selected as the prototype. The bridge is 276 ft long with concrete girders and is located on SH-36 over Bear River in Franklin county.

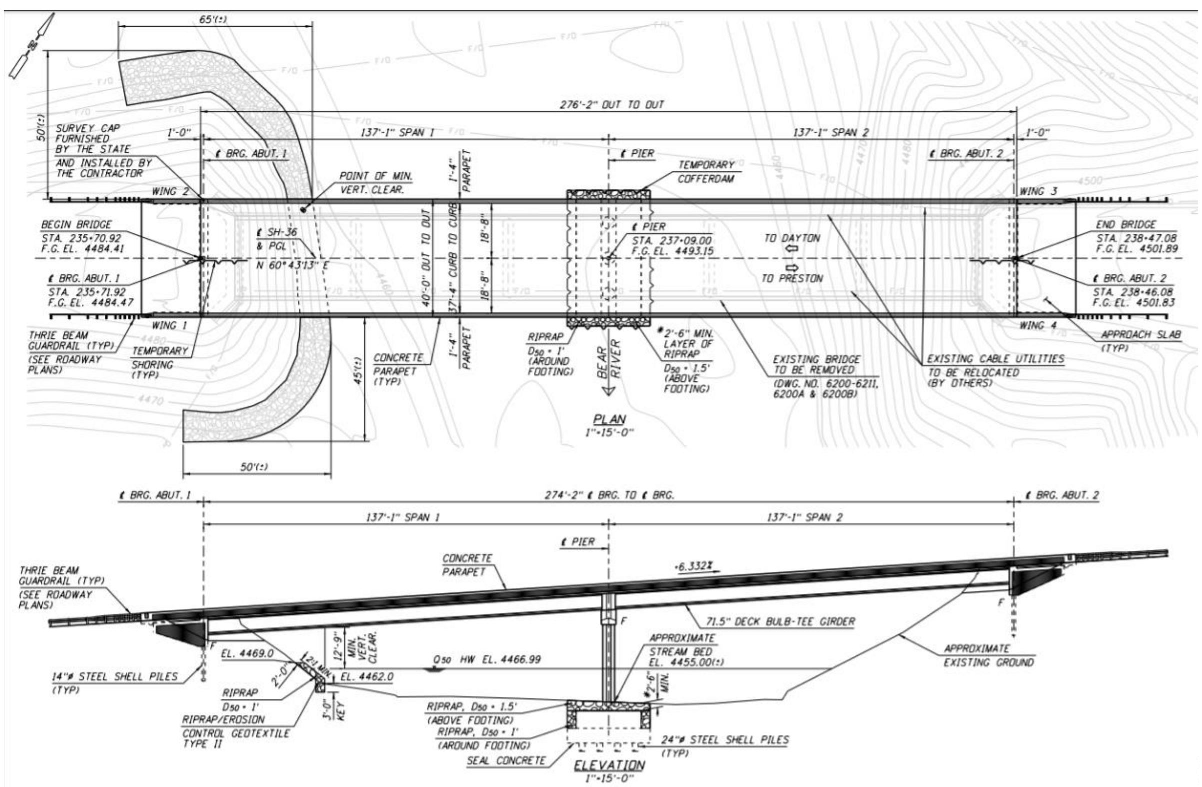

Figure 16. Plan View of the Prototype Bridge

One of the bridge piers shown in (Figure 16) is used to develop the specimens. The overall height and diameter of the pier is about 32 ft. and 4 ft., respectively. Due to height limitations in the Idaho State University's Structural Laboratory (SLAB), the pier is scaled down by a factor of 3 (e.g., 1/3 scale). Applying 1/3 scale to the original dimensions; the overall height and the diameter of the pier were obtained to be 10 ft-6 in. and 1 ft-6 in., respectively. The dimensions of the scaled pier is shown in Figure 17.

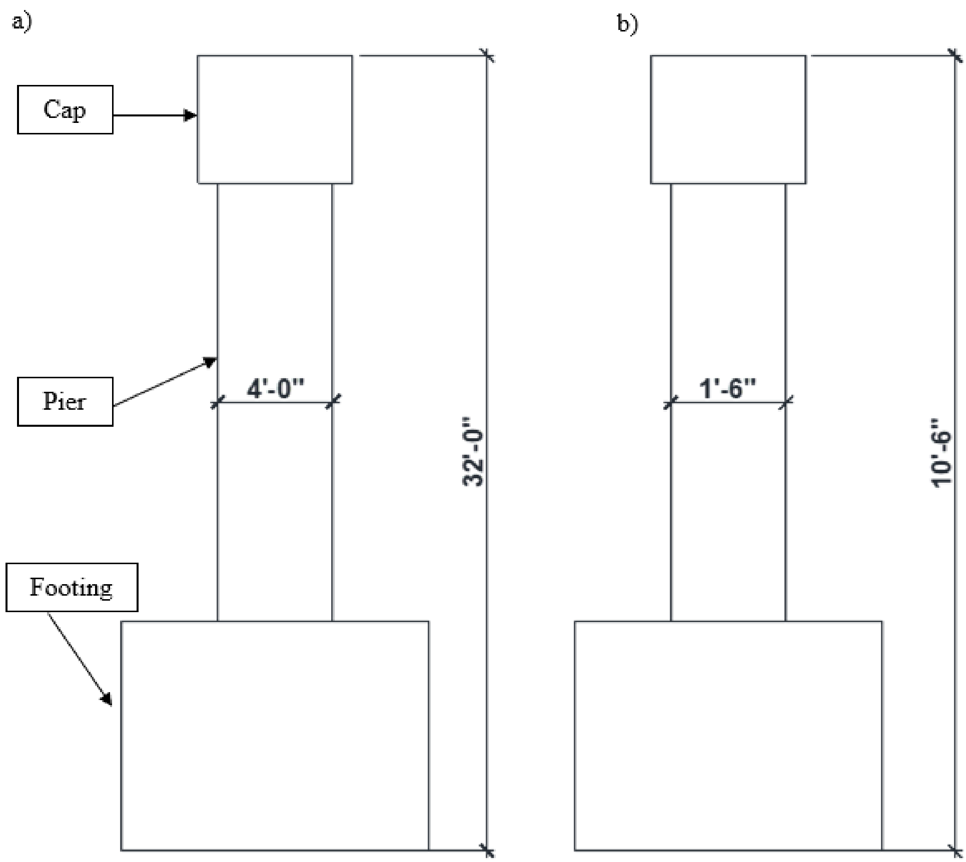

Figure 17. a) Full-Scale Bridge Pier, b) 1/3-Scale Bridge Pier

3.3 Testing Arrangement and Design Consideration

A 1/3rd-scale specimen reinforced with Titanium Alloy Bars (TiABs) is considered for experimental testing. The pier reinforced with TiABs has similar dimensions and capacity to the benchmark Cast-In-Place (CIP) pier reinforced with normal steel rebars (CHAPTER 4). The pier with TiABs was designed using basic reinforced concrete analysis and mechanics by targeting the moment capacity of the benchmark CIP pier. The number of TiABs required to match the capacity of the benchmark is almost half of the normal steel rebars. The calculation of the moment capacity to obtain the number of TiABs is presented in **Appendix A** and **Appendix B**. In order to enhance ductility, the use of an unbonded length of TiABs in the plastic hinge zone was investigated. The unbonded length for the TiABs was calculated using the PRESSS Design Handbook [15]. The unbonded length was obtained to be 0.646 in. to keep the strain in the bars lower than 2.5% at design level. However, in the construction of the pier, unbonded length was neglected and not implemented for better comparison with the pier reinforced with normal steel rebars.

3.3.1 Design of Cast-In-Place Pier Reinforced with TiABs

The dimensions of the CIP pier were identified from the prototype structure. The amount of TiABs or steel reinforcing to be used were identified from the 2017 AASHTO LRFD Design Specifications (AASHTO 2017). The diameter of the pier was 18 in. 50 kip (5% f'c Ag) was the assumed compression (axial load) on the pier. The moment capacity of the pier was calculated to be around 150 kip-ft for the pier reinforced with normal steel rebar. This was calculated by calculating the total compression in the concrete, total compression in the compression steel and the total tension in the tensile steel. So, keeping the moment capacity of 150 kip-ft, the number of TiABs required was back-calculated. The use of TiABs reduced the bars required to almost half to keep the same moment capacity in the column, i.e., 7 number 6 TiABs. The diameter of the longitudinal bars, i.e., #6 TiABs used was 0.75 in. Similarly, #3 (0.375 in.) TiABs spirals with 3 in. of pitch was used in the column to confine the concrete. Both the longitudinal and spiral TiABs were smooth and did not have any ribs on them. A 1.5 in. cover was used in calculations. The pier was in constructed octagonal in cross-section for the ease of construction. A cross-section of the pier reinforced with TiABs is presented in Figure 18.

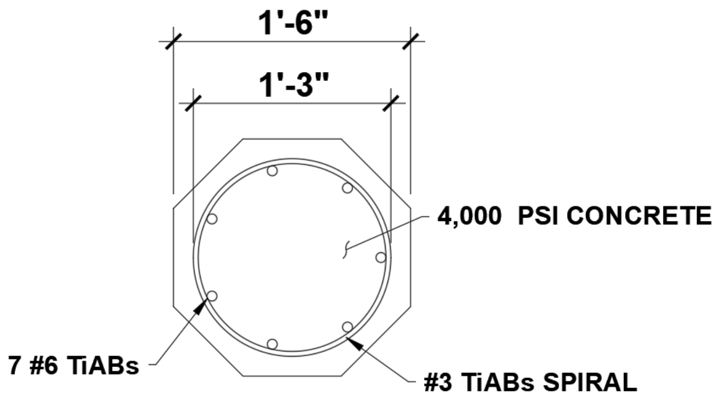

Figure 18. Column Detail: TiABs

The footing was designed as a capacity protected element with a moment capacity of 1,000 kip-ft so that pier reaches its ultimate capacity before the footing is yielded. The footing was designed using SAP2000, assuming 4,000 psi concrete and 60,000 psi steel rebar for the design of footing [17]. The overall dimension of the footing was 4 ft. × 4 ft. × 3 ft. with 2 in. cover, and 10 #6 bars on top and bottom in both directions. Similarly, eight hollow steel pipes of diameter 2 in. were installed in the footing. This was done to tie the footing to the strong floor during the testing of the pier. Details of the footing are presented in Figure 19.

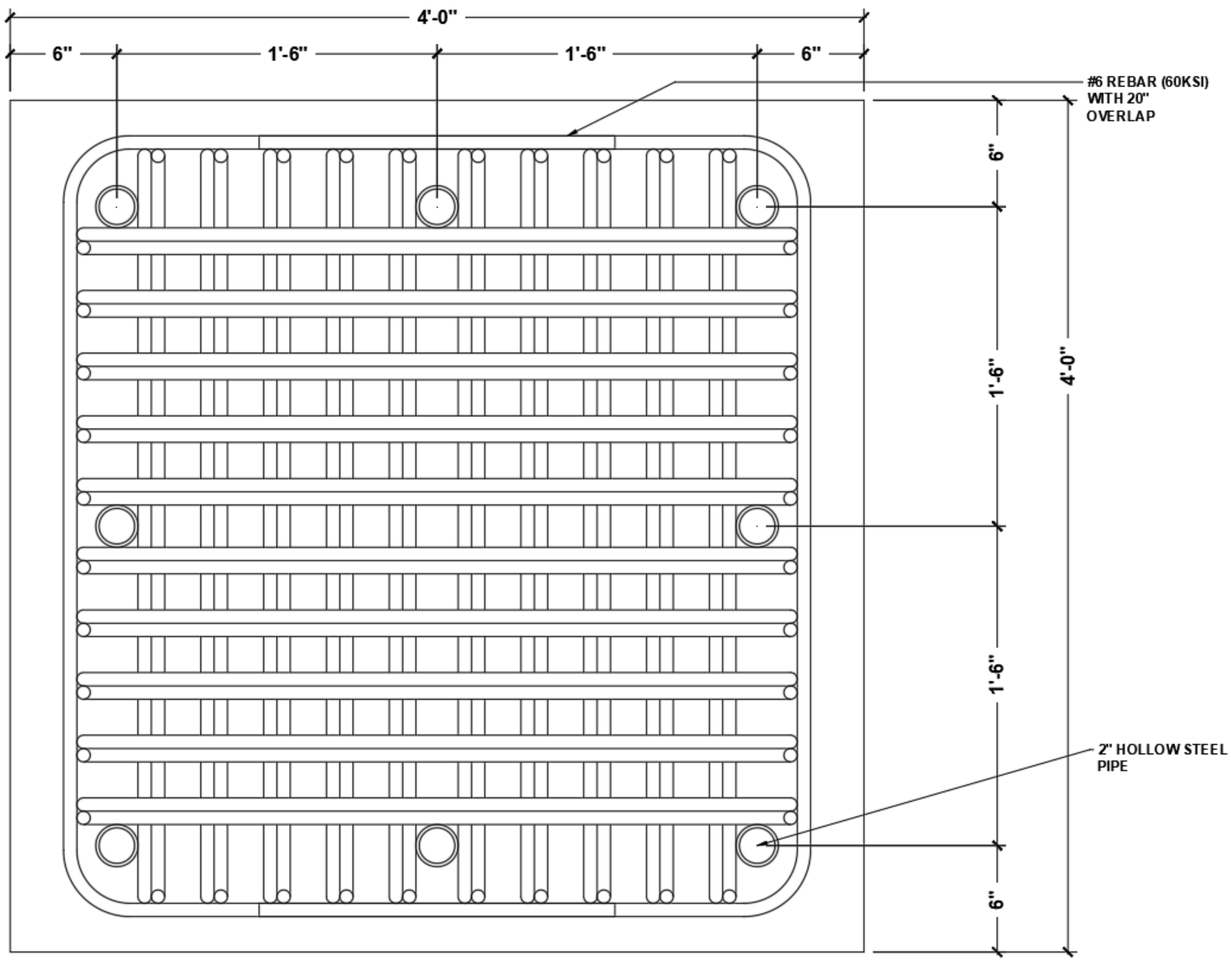

Figure 19. Footing Details

At the interface of the column and footing, the pitch of the spirals was set to 1.5 in. for better confinement in the plastic hinge zone. Also, the spirals had one and half extra turn at the column-to-footing interface and were tied together using the epoxy-coated mechanical splices. This was done on the spiral that went down from top of the pier to the footing, also the spiral that comes towards the column form the footing with the interface of spiral at column to footing being 2 in. The column-footing interface detail is shown in Figure 20.

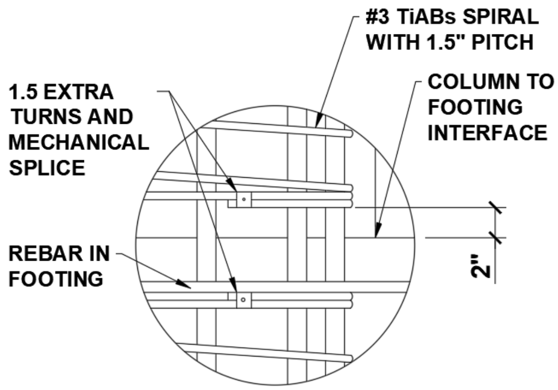

Figure 20. Column-Footing Interface Detail

A cubical cap was built on top of the column to provide a connection point to the horizontal actuator during testing. Four hollow metal pipes (1.5 in. diameter) were installed 9 in. apart from each other in the cap. Longitudinal TiABs were bent 90-degree at the cap in order to have enough development length. 4#6 steel rebars were used on top and bottom in both directions for the cap-reinforcing with 2 in. of cover. A circular recess of ½ in. was built at the center of the cap for the hydraulic jack that would exert gravity loads. Details of the cap is presented in Figure 21.

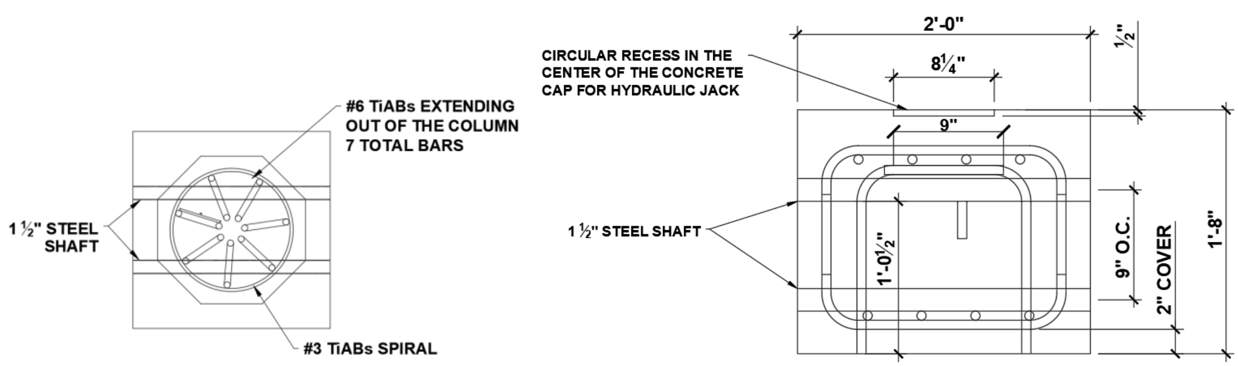

Figure 21. Cap Detail for the Pier Reinforced with TiABs

The full detail of the pier reinforced with TiABs is shown in Figure 22.

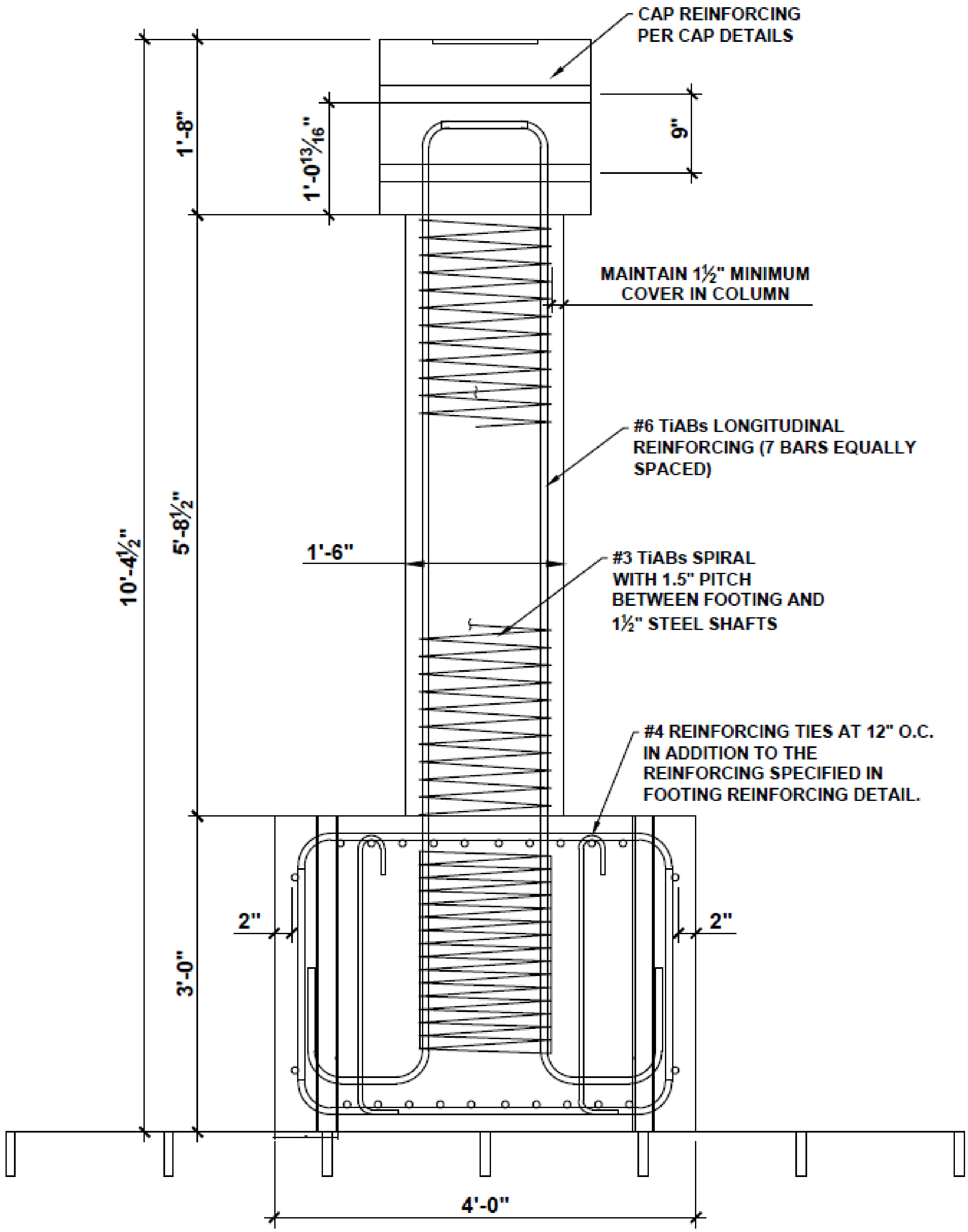

Figure 22. Details of the Pier Reinforced with TiABs

3.3.2 *Construction*

The cast-in-place pier reinforced with TiABs was constructed in-house in two stages. First, the footing cage was constructed, poured, and transported to testing site; then the column and cap cages were constructed. The formwork for the footing, column and cap were built using 2 in. × 4 in. and ½ in. Oriented Strand Boards (OSBs). Once the formwork was ready, the rebars needed were cut to length and bent. First the bottom reinforcing cage of the footing (Figure 23) was tied and placed on the bed with 2 in. tall rebar chairs. Before placing on the top cage for the footing, longitudinal reinforcing of the column had to be installed. #6 TiABs were cut to the required length in one-piece and bent at the ends. The spirals were tied together as shown in Figure 24 before installation in the footing cage. The spirals were tied to the longitudinal TiABs using the plastic ties (Figure 24).

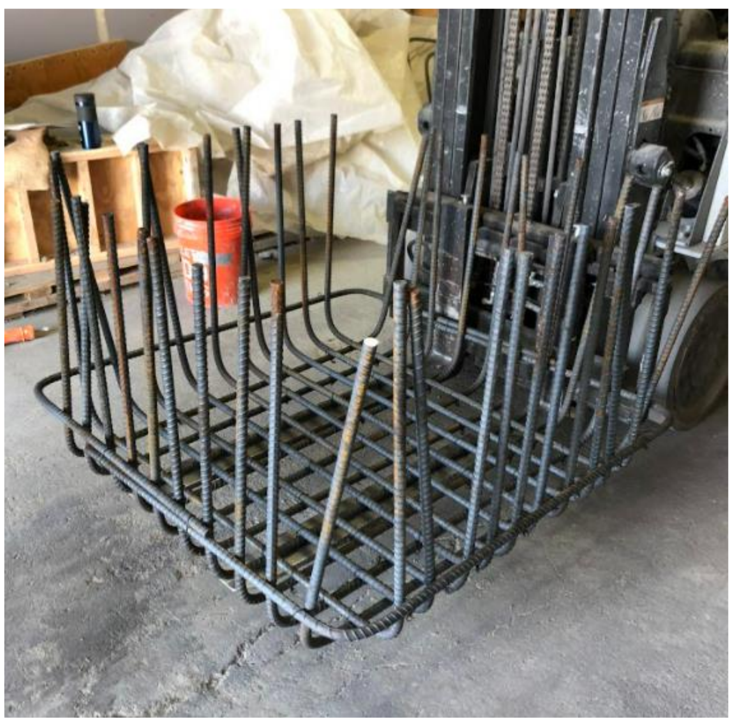

Figure 23. Bottom Reinforcing Cage of Footing

Figure 24. Tying TiABs Longitudinal Rebars and Spirals

Strain gages were installed on each longitudinal bar at the plastic hinge zone above the column-footing interface. The column cage was then placed on the footing bottom cage. The column cage was made of TiABs and the footing cage was made of normal steel rebars. In an actual bridge, it is important to ensure that TiABs do not contact normal rebars as it can cause galvanic corrosion. During construction of the pier reinforced with TiABs, plastic chairs and spacers were used to avoid contact of two different metals (Figure 25). The contact of TiABs and steel in long term can lead to the galvanic corrosion, which had to be avoided.

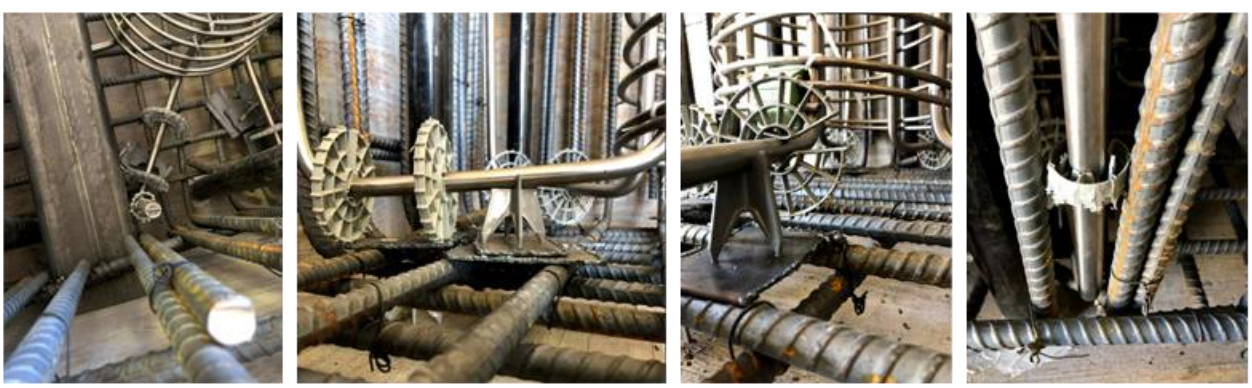

Figure 25. Use of Plastic Spacers and Chairs

After erecting the column cage, the metal pipes for anchoring of the footing (sleeves) were installed in the footing cage followed by placing the top cage. Figure 26 (a) shows the completed cage ready for concrete pour. The footing was cured for seven days in moist environment using burlaps and a plastic cover, it was then transported to the Structural Laboratory before pouring the column and cap as shown in Figure 26.

Figure 26. Footing a) Cage, b) Ready for Pour, c) Concrete Pour, d) Curing, e) Ready for Transportation, f) Transportation to the Structural Laboratory for Testing

Once the footing was transported to the testing site, the formwork for the column and cap were built and installed. A 1.5 in. hollow metal pipe was installed and used as a support to tie the reinforcing for the cap. Similarly, a ½ in. thick plywood (8.25 in. diameter) was cut and placed on the center of the cap with a threaded rod coupler inside. The ½ in. thick plywood was intended to provide a recess for the hollow hydraulic jack that would exert gravity loads during testing. The threaded rod coupler was added as a safety precaution to provide a tie between the hollow hydraulic jack and the column cap during the testing. Figure 27 shows construction photos of the cap reinforcing.

Figure 27. Construction of the Cap

The specimen was cured for 28 days in moist environment using burlaps and plastic wraps. After the pier was fully cured, it was painted in white and was ready for instrumentation and testing (Figure 28). The material properties of the pier reinforced with TiABs is discussed in detail in Section 3.3.3.

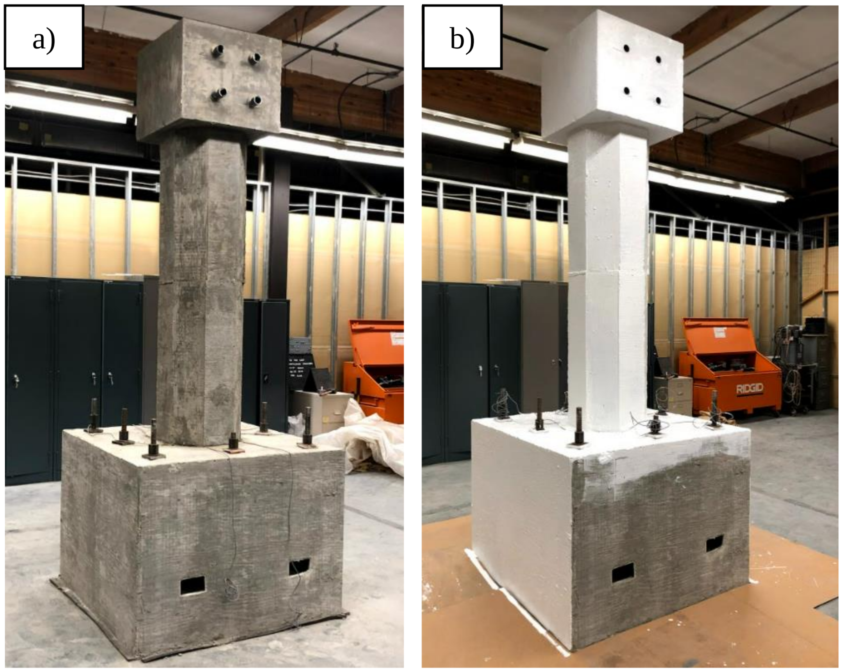

Figure 28. a) Fully Cured Pier, b) Painting the Pier

3.3.3 Material Properties

Materials used for construction of the pier were concrete, steel, TiABs and spirals. The design compressive strength of the concrete in both footing and column was 4,000 psi at 28 days. Six (4” × 8”) and Two (6” × 12”) cylinder samples were prepared in accordance with ASTM C192 during the pour of both footing and column [18]. WD-40 spray was used on the inside walls of cylinders so that the concrete mix does not adhere to the walls of the mold. Concrete mix was poured one third at a time and rodded 25 times per interval. The outside walls of the cylinders were cleaned, and the samples were kept in appropriate curing environment. The specimens were then finished smooth and dried for a day before being removed from their forms and submerged in a curing tank for 28 days. 4” × 8” cylindrical samples were used to obtain compressive strength of the concrete at 28 days and on the test-day. Similarly, 6” × 12” cylindrical samples were used to obtain tensile strength of the concrete. The compressive strength of the cylindrical concrete specimens was carried out in accordance with ASTM C39 [19] whereas the splitting tensile strength of the cylindrical concrete specimens were carried out in accordance with ASTM C496 [20]. The average experimental results are summarized in Table 3. The detail results of the compressive strength and split cylinder of the footing and column are presented in **Appendix C and D,** respectively.

Table 3. Average Compressive and Split Tensile Strength in (psi) for the Footing and Pier

FOOTING				**PIER**			
Compressive Strength		**Tensile Strength**		**Compressive Strength**		**Tensile Strength**	
28 Days	**Test-Day**	**28 Days**	**Test-Day**	**28 Days**	**Test-Day**	**28 Days**	**Test-Day**
5613.76	6892.79	289.58	425.49	4928.1	5898.37	294.07	331.25

The failure of the cylindrical concrete specimen after testing for both column and footing is shown in Figure 29 to Figure 32.

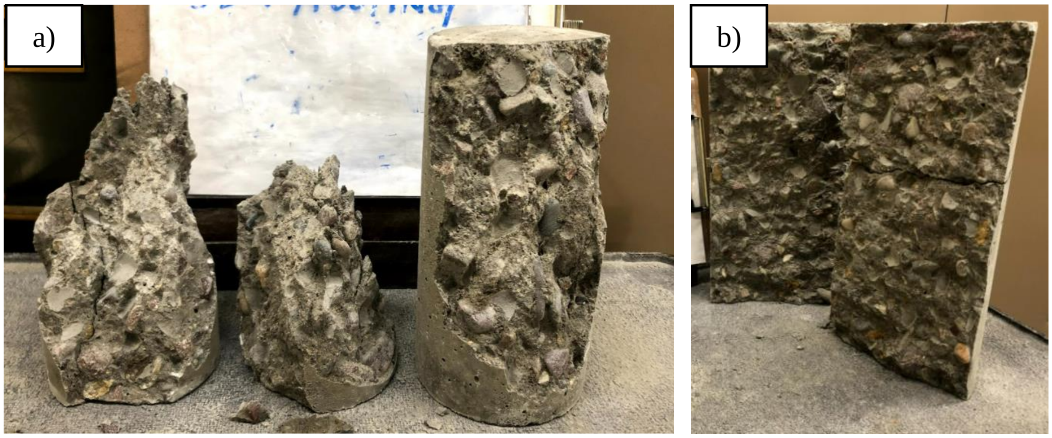

Figure 29. Footing: Failure of Cylindrical Specimen at 28-Days a) Compressive Strength, b) Split Tensile Strength

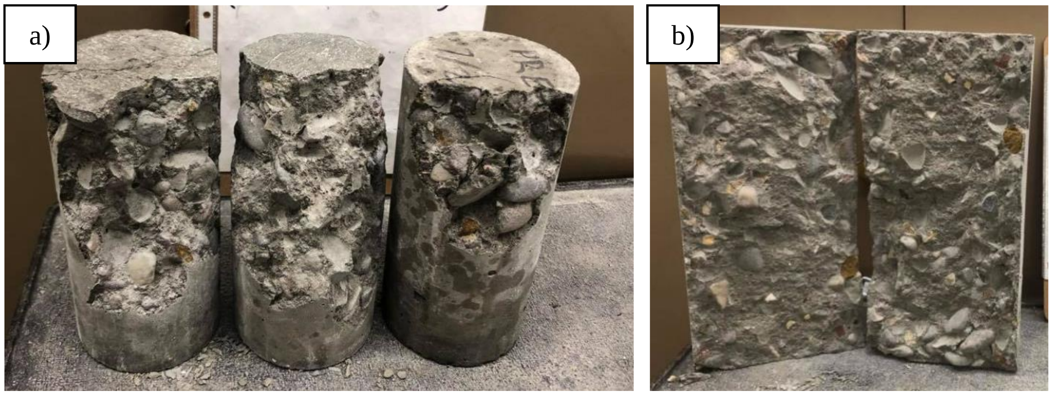

Figure 30. Column: Failure of Cylindrical Specimen at 28-Days a) Compressive Strength, b) Split Tensile Strength

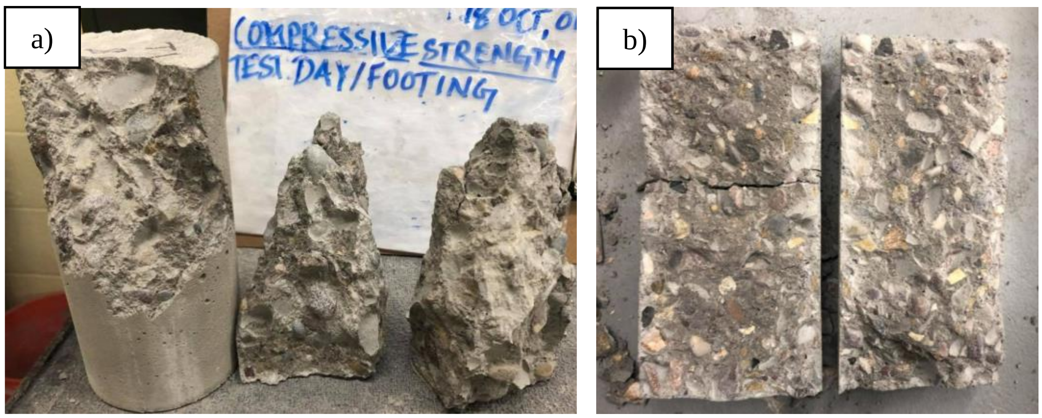

Figure 31. Footing: Failure of Cylindrical Specimen at Test-Day a) Compressive Strength, b) Split Tensile Strength

Figure 32. Column: Failure of Cylindrical Specimen at Test-Day a) Compressive Strength, b) Split Tensile Strength

Grade-60 steel rebars were used in the construction of footing and pier cap. Minimum yield strength and the ultimate strength of grade-60 steel rebars are 60 ksi and 90 ksi respectively.

Grade 5 TiABs were used for the longitudinal and transverse reinforcing of the pier. Only smooth TiABs were available for this research. The minimum yield strength and the ultimate strength of TiABs bars were 140 ksi and 150 ksi respectively [8]. The modulus of elasticity for TiABs was 15 ksi [8]. The material properties for TiABs were based on previous research at Idaho State University.

3.4 Test Setup

3.4.1 Setup and Instrumentation

Following construction of the pier with TiABs, it was transported to a designated spot in the Structural Laboratory for experimental testing. Preparation of the test-setup started with erection of a demountable reaction frame which was tied down to the strong floor using high strength threaded rods. A displacement-controlled servo-hydraulic actuator was used to apply lateral in-plane loads to the specimen. The actuator was placed against the reaction frame. The head of the actuator was mounted to the cap of the pier using high-strength threaded rods and a 1.5 in. bearing plate on both ends. The pier was tied to the actuator in-order-to achieve both push and pull loading intervals. High-strength anchor rods were used to tie down the footing to the strong floor.

To exert gravity (axial loads) on the column, a hydraulic ram was placed on top of the pier. Two externally attached high strength threaded rods were used to transfer axial loads on the column using a steel cross on top of the pier. The magnitude of the axial load was set to 50 kip and was kept constant with ±5% tolerance throughout the testing.

Details of the test-setup is presented in Figure 33. Similarly, actual test setup of the pier reinforced with TiABs is presented in Figure 34.

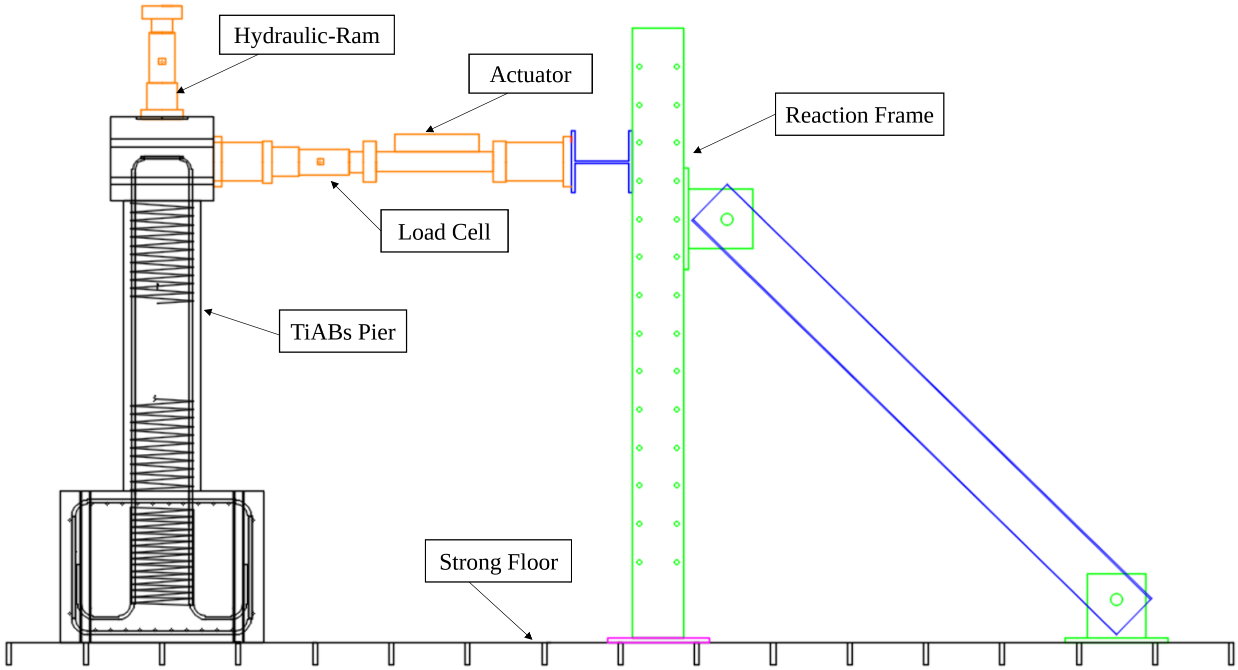

Figure 33. Schematic for the Test-Setup

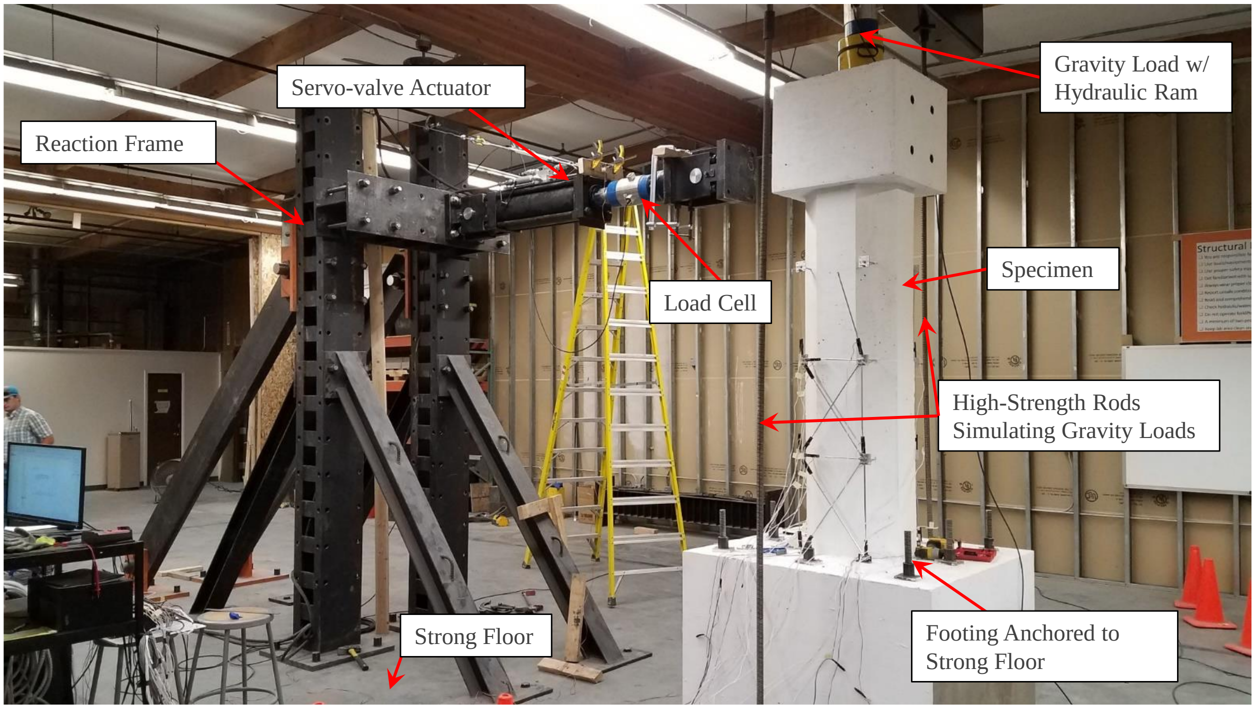

Figure 34. Actual Test-Setup

Instrumentation included strain gages attached to TiABs inside the pier and located in the plastic hinge zone, externally mounted potentiometers, and load cells as shown in the previous figures. A Campbell Scientific data acquisition system was used to record and collect data from the loadcells, strain gauges, linear string potentiometers and stroke potentiometers during testing. There were two tension/compression load cells, each with ±225-kip capacity. One of the loadcells was mounted in front of the lateral actuator. The second load cell was mounted between the ram and the steel cross beam to measure axial loads.

The in-plane displacement of the pier was measured using a string potentiometer. The string potentiometer was mounted independent of the testing setup to measure the actual displacement during testing. Flexural and shear deformation of the pier was measured using an array of vertical, horizontal, and diagonal potentiometers with 2-4 in. stroke. These potentiometers were attached up height of the pier in three segments, measured 18 in., 36 in., and 54 in. from the top of the footing. The footing was also instrumented to measure any sliding or rocking that might occur during testing of the specimen. Table 4 presents a summary of the instrumentation for the pier. Figure 35 shows the schematics for the locations of the instruments.

Table 4. Instrumentation Description and Function for Column Specimens

Label	Description	Function
IPC	string potentiometer	In-plane displacement of column
OPC	string potentiometer	Out-of-plane displacement of column
ASP	string potentiometer	Actuator displacement
FHI	4-inch stroke potentiometer	Footing horizontal in-plane
FHO	4-inch stroke potentiometer	Footing horizontal out-of-plane
FVN	4-inch stroke potentiometer	Footing vertical on north-end
FVS	4-inch stroke potentiometer	Footing vertical on south end
A (1-7)	2-inch stroke potentiometer	Deformation of the column up to 18” from base of footing
B (1-7)	2-inch stroke potentiometer	Deformation of the column from 18” to 36” from base of footing
C (1-4)	2-inch stroke potentiometer	Deformation of the column from 36” to 54” from base of footing

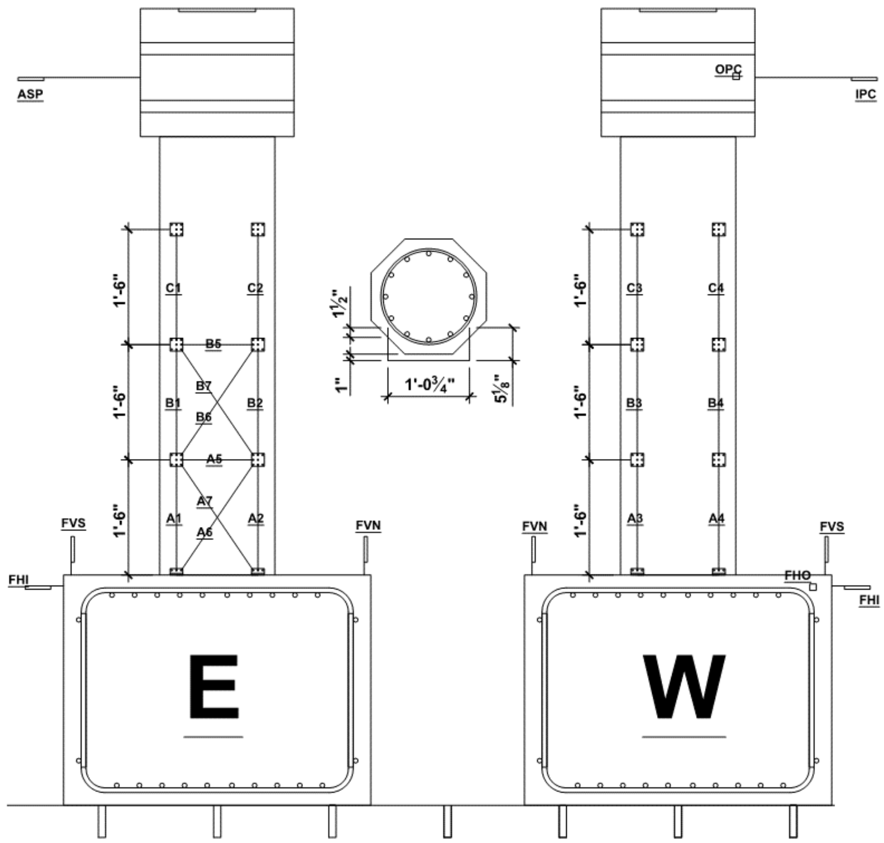

Figure 35. Schematics for Instrumentation of the Cantilever Pier

3.4.2 Loading Protocol

A uniaxial lateral loading protocol was used for testing of the pier. The load protocol was quasi-static and cyclic. The specimen was subjected to push and pull cycles with increasing displacements/drifts. The load protocol was developed in accordance with "Guide for Testing Reinforced Concrete Structural Elements under Slowly Applied Simulated Seismic Loads" (ACI 374.2R-13). Drift ratios are calculated by dividing the in-place displacements of the pier by the cantilever height of the specimen. In accordance with ACI 374.2R-13, the initial applied displacement is equal to half of the yield drift ratio for the pier.

The yield displacement is calculated using **Equation 1** derived from Priestley et. al. [23] Since, the loading protocol for pier reinforced with TiABs was kept identical to the benchmark pier; calculation for the yield displacement was carried out for the pier reinforced with normal steel rebar. Yield displacement was calculated to be 0.692 in.

$$\Delta_y = \frac{\varphi_y (H+L_{SP})^2}{3} \qquad \text{Equation 1}$$

Where, Δ_y = Yield displacement (in.)

φ_y = Yield curvature (calculated using **Equation 2**)

H = Height of the pier (in.)

L_{SP} = Strain penetration length (in.) (calculated using **Equation 3**)

$$\varphi_y = \frac{2.25\ (1.1\ F_y)}{E_s D} \qquad \text{Equation 2}$$

Where, F_y = Yield strength of the rebar (ksi)

E_s = Modulus of elasticity of the longitudinal rebar (ksi)

D = Diameter of the pier (in.)

$$L_{SP} = 0.15\ (1.1\ F_y) d_{bl} \qquad \text{Equation 3}$$

Where, d_{bl} = Diameter of the longitudinal rebars (in.)

The displacement is increased at certain interval until failure of the element as shown in Figure 36. The actuator displacement rate was set to be 0.1 mm/sec. A plot of the loading protocol from ACI 374.2R-13 is presented in Figure 37 [17].

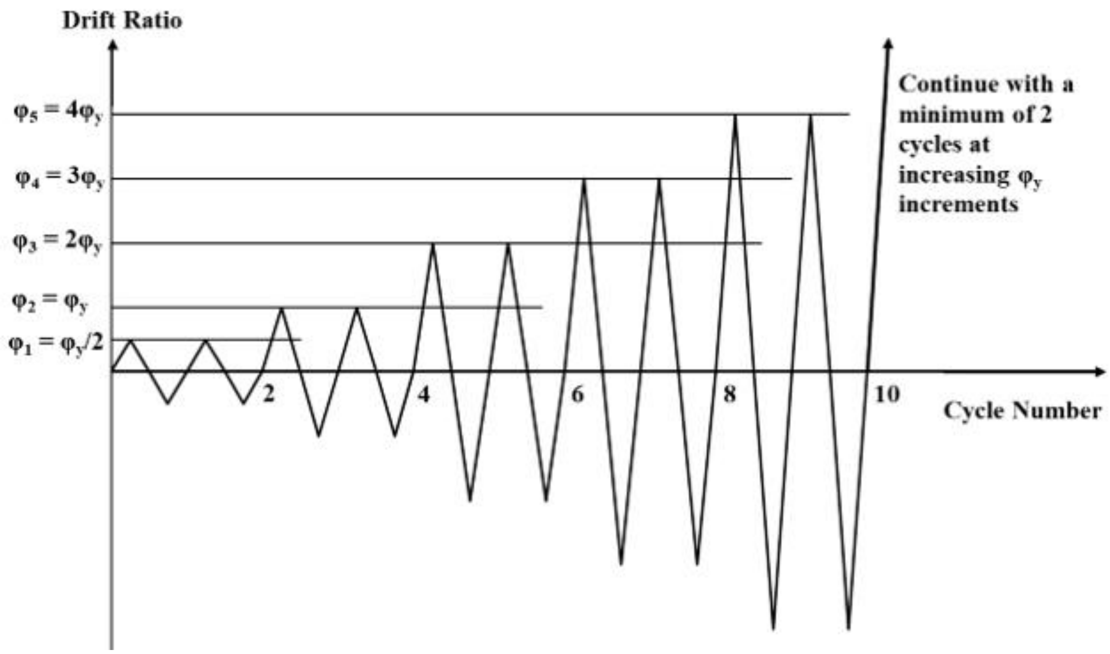

Figure 36. Loading Protocol as per ACI 374.2R

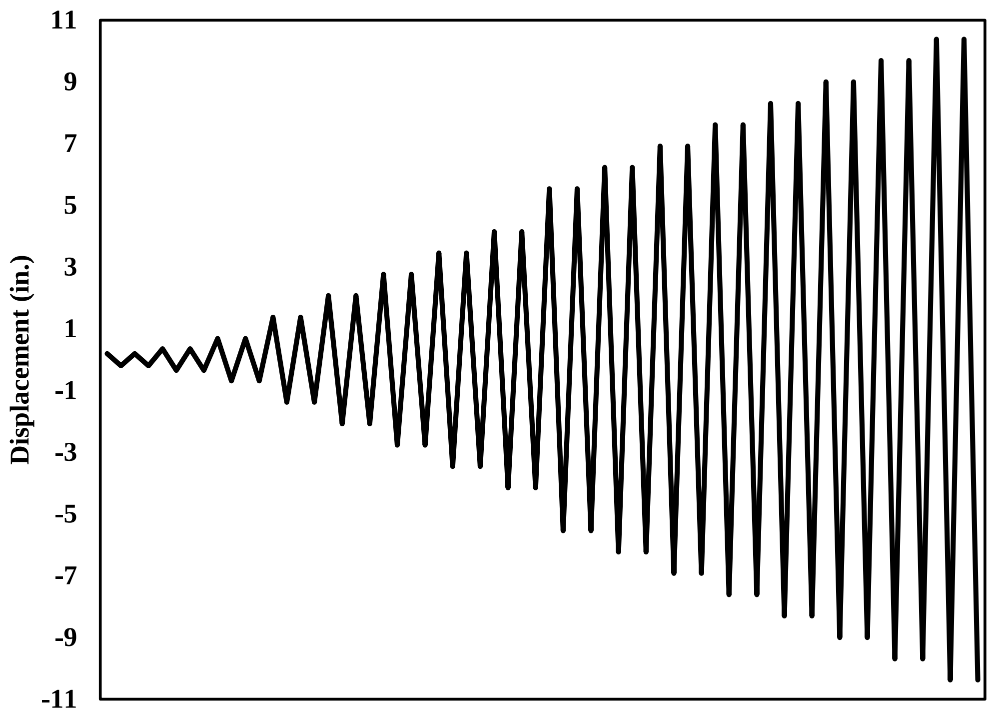

Figure 37. Quasi-Static Loading Protocol [17]

During testing, the actual displacement or drift ratio was not same as the targeted displacement and drift ratio. This was due to deflection of reaction frame and some minor sliding of the footing. Table 5 shows a comparison of both the targeted drift and the actual drift achieved during testing. Testing continued until there was a 50% drop in the ultimate lateral capacity of the pier.

Table 5. Lateral Loading Protocol for Cantilever Column: TiABs

	Targeted Values		**Actual Values**	
Cycle	**Δ (inch)**	**Drift (%)**	**Δ (inch)**	**Drift (%)**
1	0.20	0.26	0.13	0.17
2	0.35	0.45	0.23	0.29
3	0.69	0.88	0.50	0.64
4	1.38	1.77	1.09	1.40
5	2.08	2.67	1.74	2.23
6	2.77	3.55	2.39	3.06
7	3.46	4.44	3.02	3.87
8	4.15	5.32	3.65	4.68
9	5.54	7.10	4.97	6.37
10	6.23	7.99	5.66	7.26
11	6.92	8.87	6.34	8.13
12	7.61	9.76	7.04	9.03
13	8.30	10.64	7.75	9.94
14	8.97	11.50	8.48	10.87
15	9.66	12.38	9.29	11.91
16	10.35	13.27	10.14	13.00

3.5 Testing Results

The pier reinforced with TiABs were tested up to failure point. The failure point was assumed to be fracture of two to three longitudinal TiABs. During testing, no visible cracks were observed during the first cycle of 0.26 % drift ratio. Hairline cracks started to appear at second cycle of 0.45% drift ratio. The cracks were measured and marked on the pier at each drift ratio throughout the test.

During the third cycle, i.e., 0.88 % drift ratio, more cracks were observed in between the 0 in. and 18 in. (0 mm and 457.2 mm) region above the footing (plastic hinge zone). Also, the hairline cracks at the base opened up to 1.5 mm in width. Width of the cracks increased at increasing cycles and drift ratios. At the drift ratio of 1.77 %, i.e., fourth cycle, the cracks opened up to 4 mm in the plastic hinge region of the pier.

Some hairline cracks appeared at 36 in. (914.4 mm) and above region up height of the pier. The cracks in the plastic hinge became wider and measured to be greater than 5 mm after fifth cycle (2.67 % drift ratio). As the drift ratio increased, more opening of the crack at the pier-to-footing interface was observed. There was no spalling of the cover concrete until the ninth cycle (drift ratio of 7.10 %). There were signs of spalling of concrete in the first cycle at this drift which increased in the second cycle and more rocking of column was seen. Gap opening at the base of the pier became larger at the tenth cycle (drift ratio of 7.99 %). At the same time, strength loss was noticed at the tenth cycle (drift ratio of 7.99 %). This was thought to be due to bond-slip as smooth TiABs were used. The rocking/gap opening was also influenced by the bond-slip. The column was rocking more from the base opening and bar slide also observed.

Failure and buckling of the longitudinal bars occurred during the second cycle of the 9.76 % drift ratio (12th cycle). The breaking of the longitudinal bars could be identified either by large or small pop sounds or by peaking from the gap opening to inside. Significant strength loss and rupture of TiABs initiated at the fifteenth cycle (12.38 % drift ratio). Similarly, the slip of the smooth TiABs was also observed. As the longitudinal bars started buckling, the spirals were effective to confine them, however it is possible that the spirals in the plastic hinge zones were yielded during cycles of the larger drift ratios. The spirals performed well and there was no rupture or opening of the spiral clip in the plastic hinge zone.

Figure 38 through Figure 41 present the damage progression in the plastic hinge region of the pier reinforced with TiABs. There was no damage to the footing which was designed as a capacity protected element. The footing remained intact and elastic.

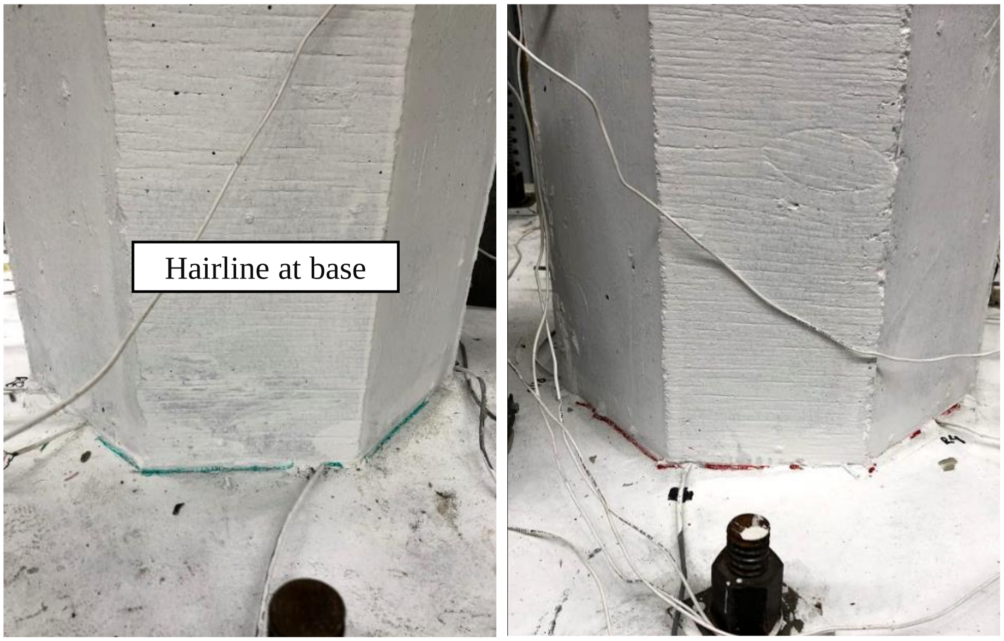

Figure 38. 1st Cycle (Drift Ratio of 0.44%)

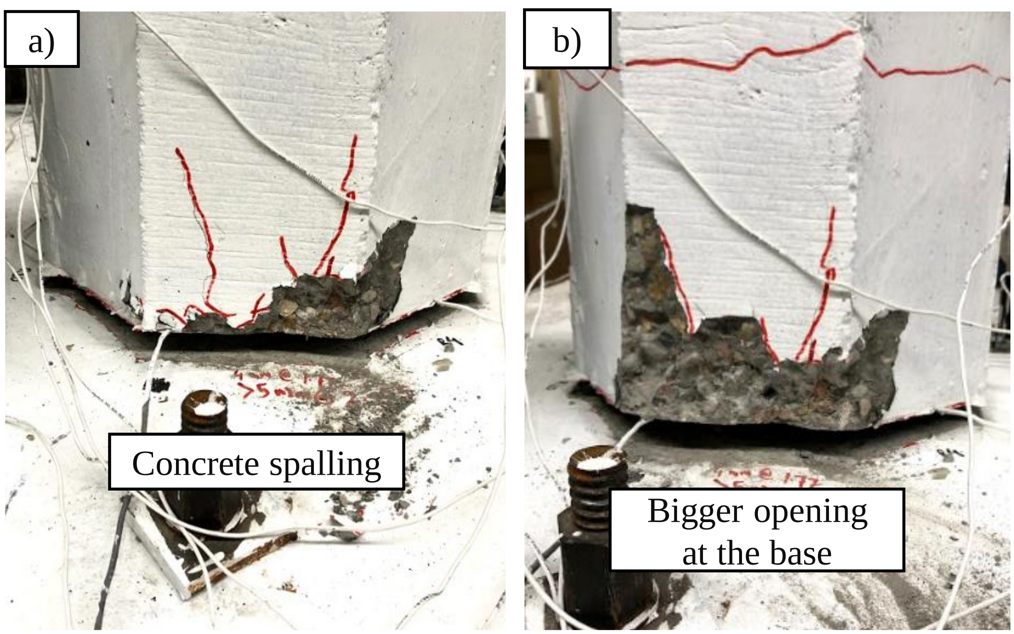

Figure 39. a) 9th Cycle (Drift Ratio of 7.10%), b) 10th Cycle (Drift Ratio of 7.99%)

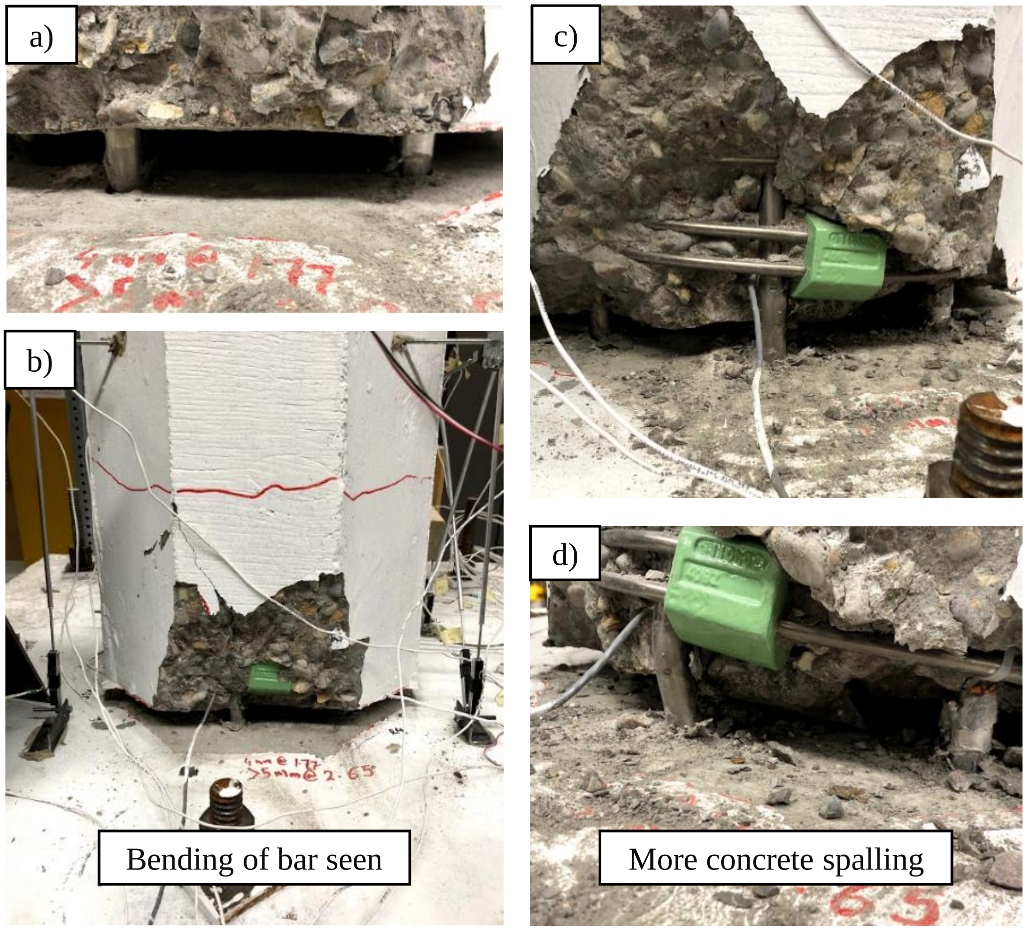

Figure 40. a), b) 13th Cycle (Drift Ratio of 10.64%), c), d) 14th Cycle (Drift Ratio of 11.50%)

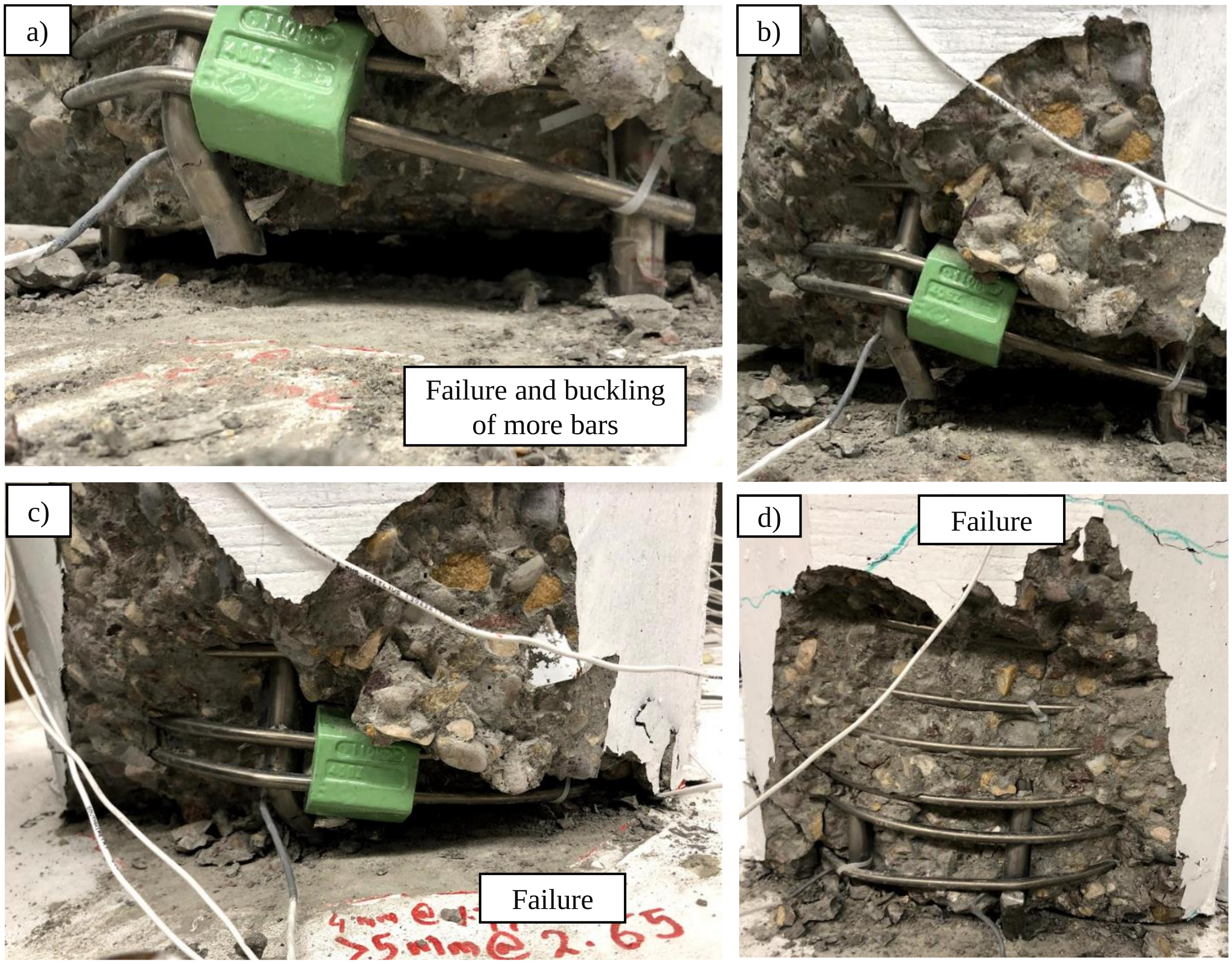

Figure 41. a), b) 15th Cycle (Drift Ratio of 12.38%), c), d) 16th Cycle (Drift Ratio of 13.27%)

Upon completion of the test, data from the instruments were processed in the form of tables and plots. Figure 42and Figure 43 show experimental plots for the Force-vs-Displacement and Force-vs-Drift. In these plots, the force represents the base shear, and the displacement/drift represents the actual deflection at the top of the pier. As it can be observed, the hysteresis for the pier with TiABs is pinched, but stable in push and pull cycles. The sudden reduction in base shear on the plots during the cycles of large drifts represent longitudinal bar fracture. The ultimate capacity of the pier was 21.42 kips at 4.97 in. displacement (6.38% drift ratio). The maximum displacement of the pier was 10.13 in. which corresponded to 13% drift ratio.

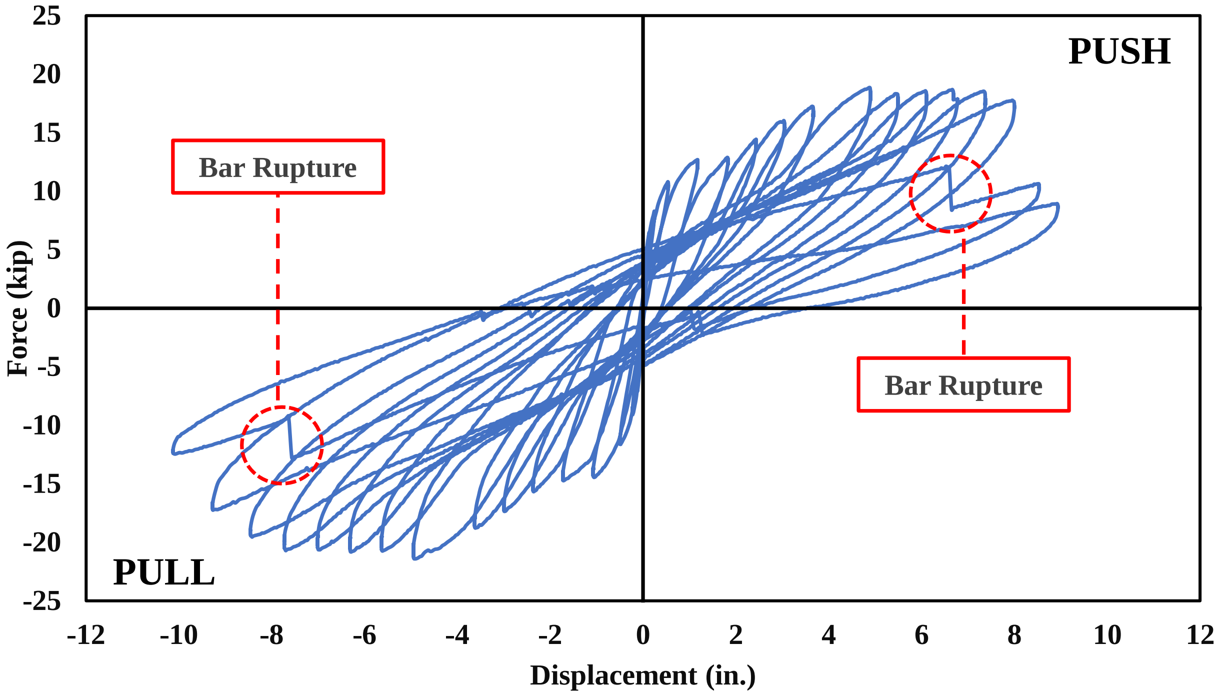

Figure 42. Force-Displacement Hysteresis: Pier Reinforced with TiABs

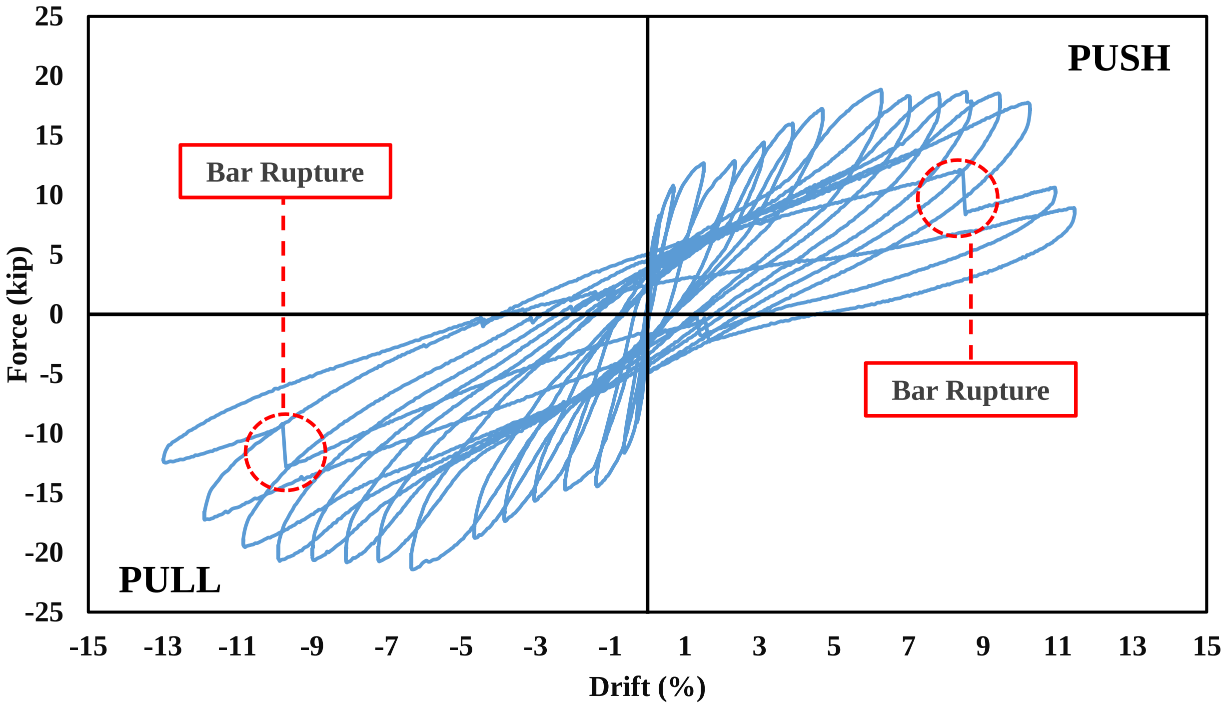

Figure 43. Force-Drift Hysteresis: Pier Reinforced with TiABs

The peak points for each loop of the hysteresis plot were picked for both push-pull cycle and plotted against drift to obtain the backbone cure. Figure 44 shows the backbone curve.

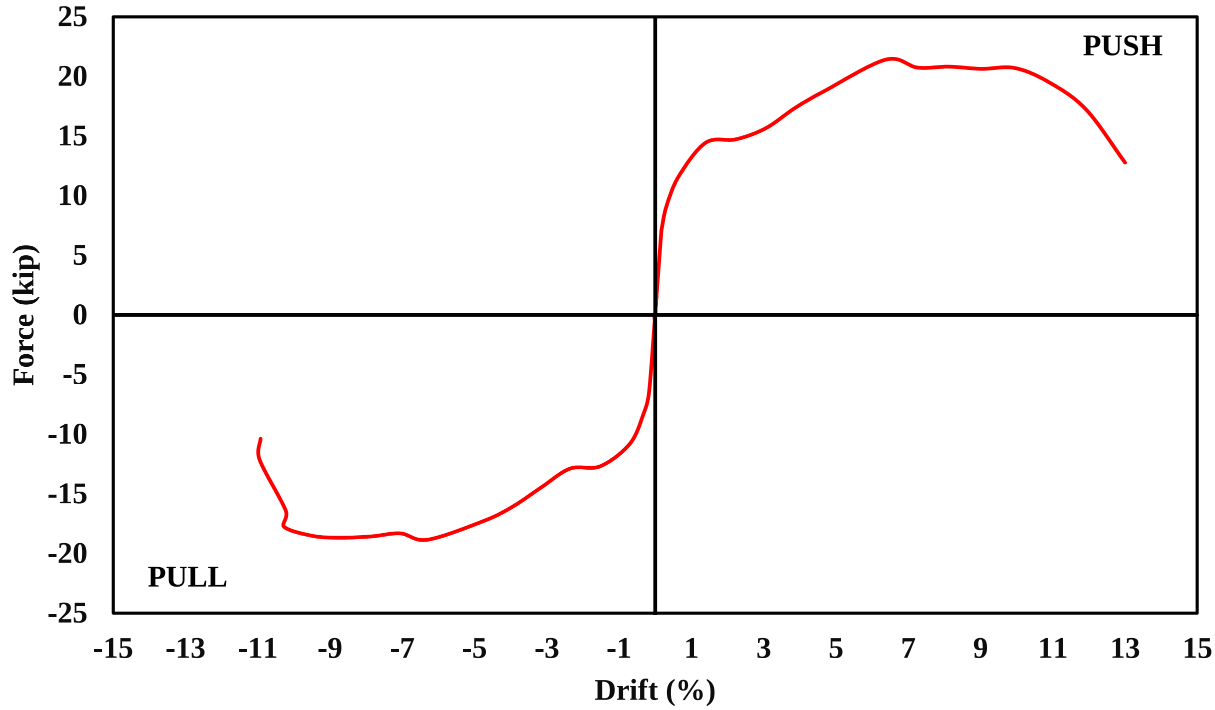

Figure 44. Backbone Curve: Pier Reinforced with TiABs

The Moment-Curvature curve (Figure 46) is plotted and is utilized to obtain the experimental yield curvature and yield moment using Moment-Curvature (M-ϕ) analysis. Caltrans Idealized Model of an elastic-perfectly plastic moment-curvature relationship was considered to obtain the global yield values [22]. The moment capacity can be obtained by balancing the areas between the actual and idealized M- ϕ plot as modeled by Caltrans in Figure 45 [22]. The global yield curvature and yield moment was found to be 7.32E-03 radians and 104.9 kip-ft.

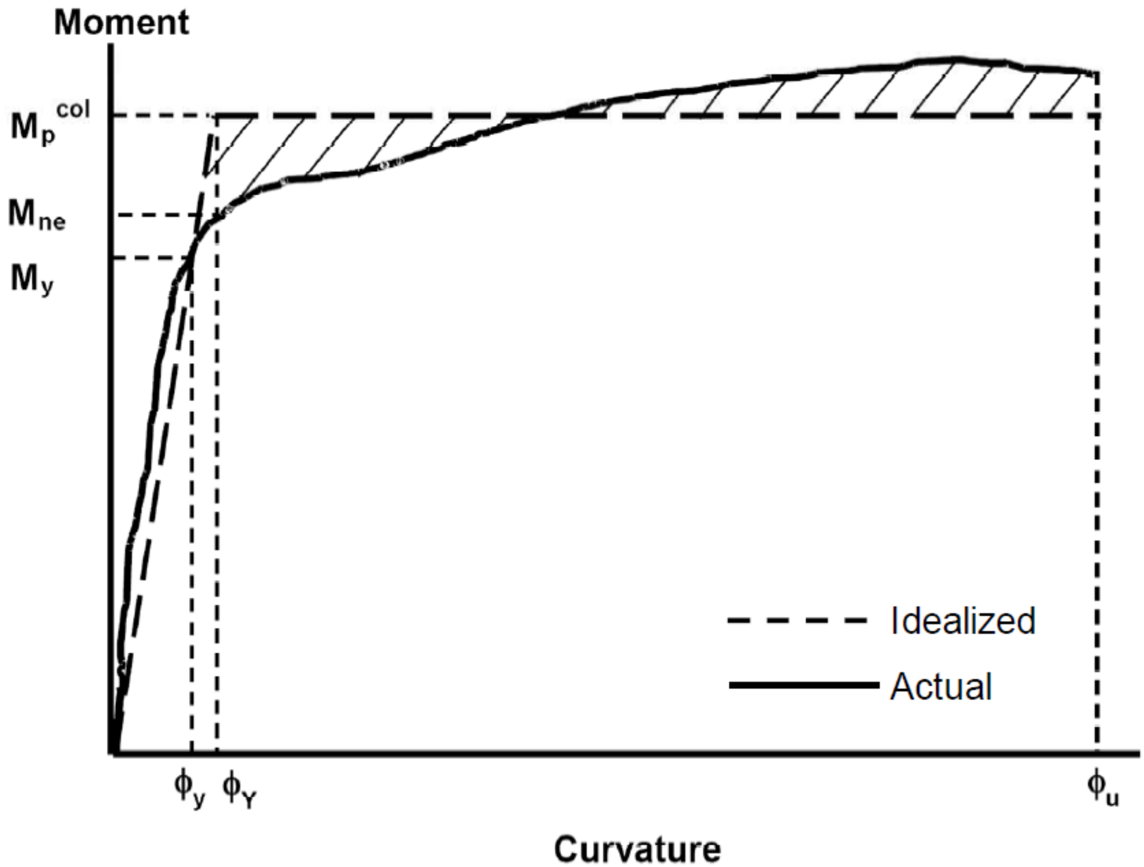

Figure 45. Caltrans Idealized Model for *M*- ϕ Analysis [22]

In the Caltrans Idealized Model for *M*- ϕ Analysis (Figure 45),

ϕ_y = Curvature at the first bar yield point (mm^{-1})

ϕ_Y = Curvature at the global yield point (mm^{-1})

ϕ_u = Ultimate curvature at the failure point (mm^{-1})

M_y = Moment capacity at the first bar yield point (kNm)

M_P = Plastic moment capacity (kNm)

The global yield moment capacity from experimental results was used to obtain the base shear at yield 16.19 kip which corresponded to a yield displacement of 1.09 in. The ultimate base shear was found from the backbone curve 21.42 kip at displacement of 4.97 in. Table 6 presents a summary of the performance points for the pier.

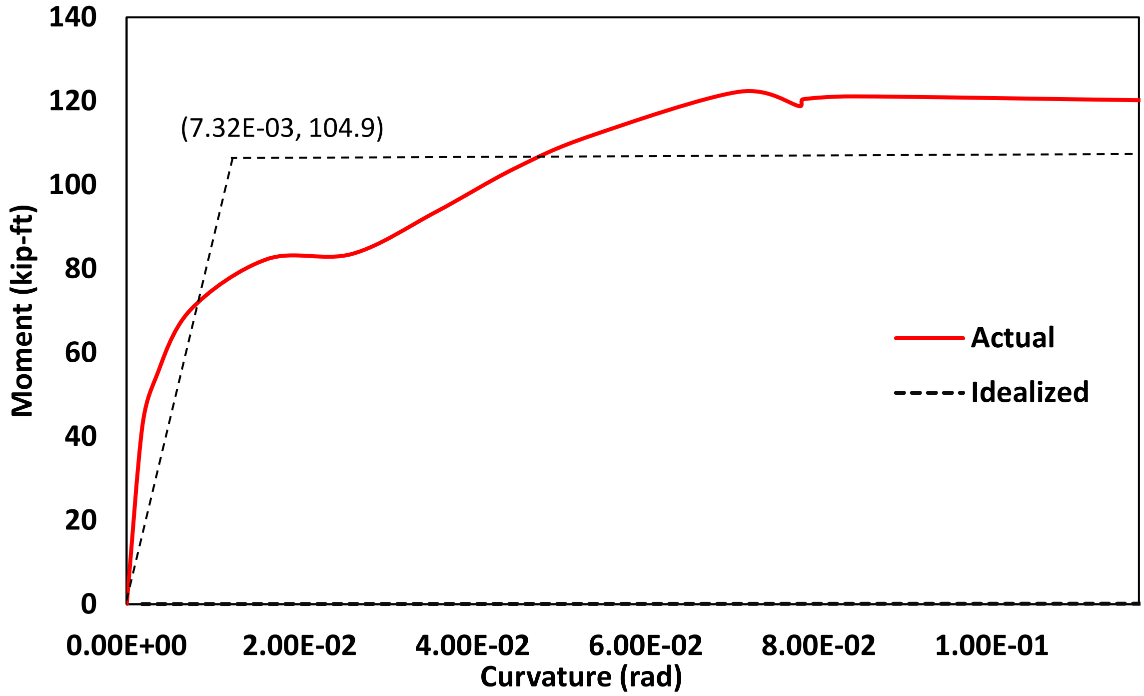

Figure 46. Moment-Curvature: Pier Reinforced with TiABs

Table 6. Summary of Performance Points

Yielding			**Ultimate**		
Displacement (in.)	**Drift (%)**	**Base Shear (kip)**	**Displacement (in.)**	**Drift (%)**	**Base Shear (kip)**
1.09	1.39	16.19	4.97	6.38	21.42

Experimental results are utilized to define some important seismic parameters, the overstrength factor (Ω_0) and the displacement ductility at ultimate base shear and failure points (μ) for the pier. The failure point for the pier is defined as the point where 20% reduction in the base shear capacity occurred. This was done in accordance with guidelines in FEMA P-695 "Quantification of Building Seismic Performance Factors: Component Equivalency Methodology" [21]. The overstrength factor is calculated using **Equation 4** and is presented in Table 7. The lower overstrength factor (1.32) is due to elastic perfectly plastic behavior of the TiABs.

$\Omega_0 = \frac{V_{ultimate}}{V_{yield}}$ Equation 4

Where, Ω_0 = Overstrength Factor,

$V_{ultimate}$ = Ultimate base shear capacity (kip),

V_{yield} = Base shear at yield (kip)

Table 7. Overstrength Factor: Pier Reinforced with TiABs

Base Shear		***Overstrength Factor (Ω_0)**
V_{yield} = Base Shear at Yield (kip)	**$V_{ultimate}$ = Base Shear at Ultimate (kip)**	
16.19	21.42	1.32
*Overstrength Factor (Ω_0) from Equation		

Similarly, the displacement ductility is calculated using **Equation 5** and is presented in Table 8.

$\mu = \frac{\delta}{\delta_y}$ Equation 5

Where, μ = Displacement ductility,

δ = Displacement at the ultimate base shear point on the backbone plot (in.) for the displacement ductility at the ultimate base shear capacity,

δ = Deflection at $0.8V_{ultimate}$ in the backbone plot (in.) for the ultimate displacement ductility,

δ_y = Deflection at yield (in.)

Table 8. Displacement Ductility: Pier Reinforced with TiABs

Deflection		***Displacement Ductility (μ)**
δ_y = Deflection at Yield (in.)	**δ (in.)**	
1.09	4.97	4.56 (Ultimate Base Shear)
1.09	9.29	8.52 (Failure Point)
*Displacement Ductility (μ) from Equation 5		

The amount of energy dissipated per cycle for the pier with TiABs is plotted in Figure 47. The energy dissipated by the pier reinforced with TiABs is evaluated using the Force-

Displacement hysteresis loop and is simply the envelope areas inside the loop. The dissipated energy was calculated using the numerical integration of the area enclosed inside the hysteresis loop for each of first two cycles at each drift ratio. MATLAB (MATLAB R2020b) was used to obtain the area of each loop. The cumulative dissipated energy is the sum of the energy dissipated in the first two cycles at each drift ratio. For each drift cycle, the first loop of cycle dissipated more energy than the second loop of cycle. The result showed that for lower drift ratios, lower energy is dissipated for both loop of cycle. For higher drift ratios, more energy is dissipated with increasing drift ratios; however, first loop of cycle dissipated more energy than second loop of cycle which indicates the strength degradation of the pier. The total energy dissipated for the pier reinforced with TiABs was 210.29 kJ.

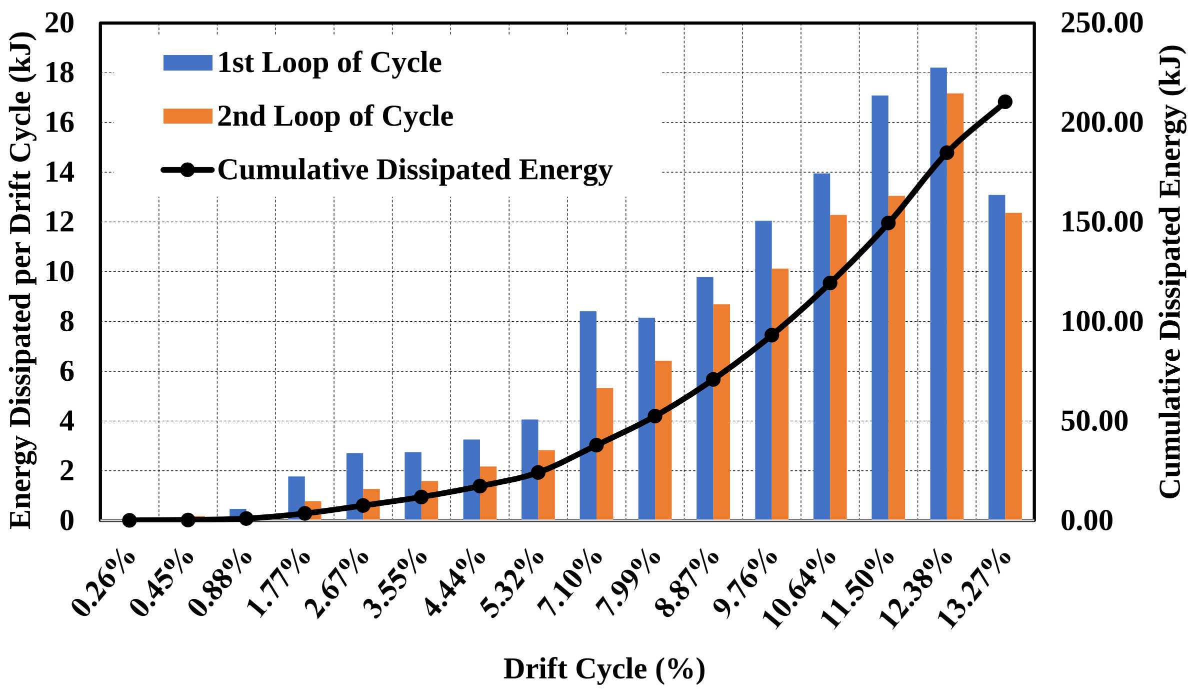

Figure 47. Energy Dissipation Plot: Pier Reinforced with TiABs

The distribution of curvature along the height of the pier at peak of each drift ratio was evaluated and is presented in Figure 48. The pier yielded and failed within the plastic hinge region. The procedure proposed by Priestley et al. was used to calculate the length of plastic hinge and to analyze the distribution of curvature along the height of the pier [23]. A summary of the calculation for the plastic hinge length is presented in **Appendix E**. The plastic hinge length was calculated to be 23.57 in. The distribution of curvature along the height showed that yielding was concentrated in the base of the pier, i.e., 0-18 in. height of the pier. The height above 18 in. in the pier approached the yielding and remained elastic throughout the testing. The cracks in the pier, spalling of the concrete and non-linear deformation occurred mainly at the pier-to-footing interface which is located in the plastic hinge region, i.e., between 0 in. and 23.57 in. from the bottom of the pier.

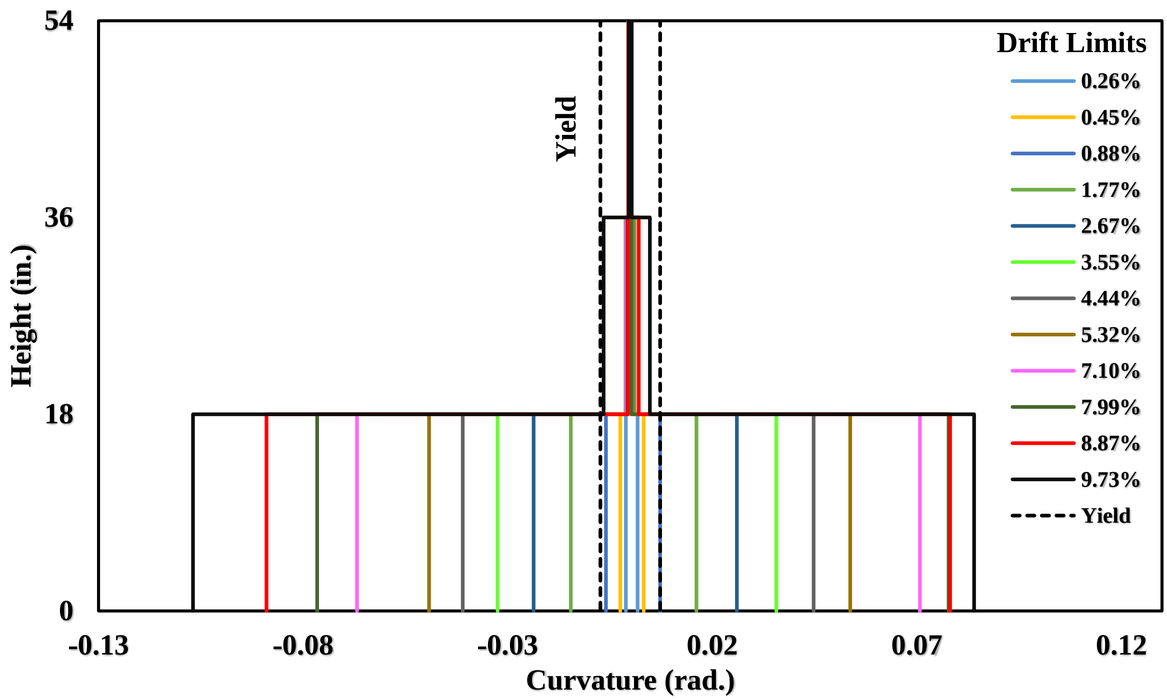

Figure 48. Distribution of Curvature Up: Pier Reinforced with TiABs

The residual drift for the pier reinforced with TiABs is obtained and plotted against the drift ratio as in Figure 49. Residual drift is the permanent deformation of the pier after each cycle or drift.

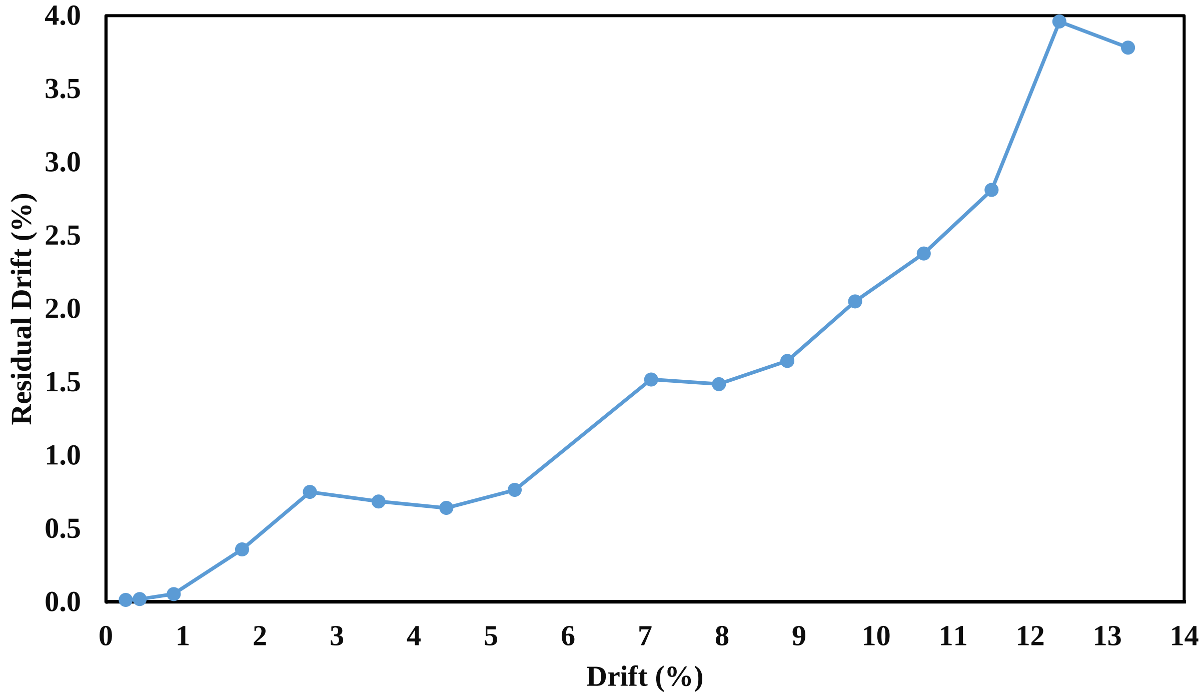

Figure 49. Residual Drift: Pier Reinforced with TiABs

3.6 Summary

- The design of the cast-in-place pier reinforced with TiABs followed the 2017 AASHTO LRFD Design Specifications (AASHTO 2017) to the extent possible.
- Guide for Testing Reinforced Concrete Structural Elements under Slowly Applied Simulated Seismic Loads (ACI 374.2R-13) was used to obtain the quasi-static cyclic loading protocol for the experiment testing of the pier reinforced with TiABs.
- The pier reinforced with TiABs was tested up to the failure point.
- Average 28 days compressive strengths of the footing and the pier concrete was found to be 5,614 psi and 4,928 psi, respectively.
- Observations from testing showed rocking and bond-slip of TiABs at the pier-to-footing interface. This was mainly due to application of smooth TiABs. Spirals made of TiABs and spliced using mechanical clips in the plastic hinge were very effective to provide confinement

and prevent buckling of the longitudinal bars. During larger drift ratios, buckling of longitudinal TiABs occurred. It is possible that some of the spirals were yielded, however there was no fracture or splice failure of TiABs spirals throughout the testing.

- The failure mechanism for the pier was fracture of longitudinal rebars during cycles of large drifts (e.g., nearly 10%).
- The hysteresis loop from the testing was pinched but stable in push and pull cycles.
- The ultimate load applied to the pier during the testing was 21.42 kip and the displacement of pier at maximum load was 4.97 in. which corresponds to 6.38% drift ratio.
- Caltrans Moment-Curvature (M-ϕ) analysis was carried out to obtain the global yield curvature and yield moment from the experimental results. The yield point was found to be at 7.32E-03 radians curvature corresponding to 104.9 kip-ft moment capacity.
- The base shear at yield was found to be 16.19 kips with displacement of 1.09 in. (1.39% drift ratio).
- The overstrength factor (Ω_0) of the pier was 1.32; the displacement ductility at the ultimate base shear and failure points were 4.56 and 8.52, respectively.
- More energy was dissipated with increasing drift ratios; however, first loop of cycle dissipated more energy than second loop of cycle which indicates strength degradation of the pier under cyclic loads. The total energy dissipated for the pier reinforced with TiABs was 210.29 kJ.
- The plastic hinge length was obtained to be 23.57 in. The distribution of curvature along the height showed that yielding occurred in plastic hinge region of the pier, and height above it approached, but never reached the yield point.
- Overall, the pier reinforced with TiABs performed well and achieved higher values of ductility before failure.

CHAPTER 4. CIP PIER REINFORCED WITH NORMAL STEEL REBARS

4.1 Introduction

This chapter presents the design, construction, and testing of the cast-in-place (CIP) cantilever pier reinforced with normal steel rebars. The purpose of the CIP pier reinforced with normal steel bars is to have a benchmark specimen to compare results against the pier reinforced with TiABs. The design of the benchmark strictly followed the 2017 AASHTO LRFD Design Specifications [25].

4.2 Testing Arrangement and Design Consideration

A large-scale specimen reinforced with normal steel rebars and spiral was considered for the large-scale experimental testing. This specimen was supposed to act as the benchmark specimen for comparison with the pier reinforced with TiABs. The pier was designed using basic reinforced concrete analysis. The moment capacity for the pier was obtained and number of longitudinal rebars required was calculated. The calculation of the moment capacity to obtain the number of normal steel rebars is presented in **Appendix A.**

4.2.1 Design of CIP Pier Reinforced with Normal Steel Rebar

The dimensions of the CIP pier were identified from the prototype structure discussed in the earlier chapters; however, the amount of steel reinforcing to be used were designed from the 2017 AASHTO LRFD Design Specifications (AASHTO 2017). The diameter of the pier used was 18 in. The moment capacity of the pier was calculated to be around 150 kip-ft under a 50-kip axial load for the pier reinforced with normal steel rebar. This was calculated by calculating the total compression in the concrete, total compression in the compression steel and the total tension in the tensile steel. To meet the moment capacity, the number of 60 ksi steel rebar was found to be 12 number 6 rebars. The diameter of the longitudinal bars, i.e., #6 rebar used was 0.75 in. Similarly, #3 (0.375 in.) steel spirals with 1.5 in. of pitch were used in the column to confine the concrete. A

1.5 in. cover was used for calculation. The column was constructed octagonal in shape for the ease of construction. The column detail for the pier reinforced with steel bars and spirals is presented in Figure 50.

The detail of the footing for pier reinforced with normal rebar was kept identical to the footing used for pier reinforced with TiABs. The design of footing is discussed in Section 3.3.1. The footing details for the benchmark pier is presented in Figure 19. Similarly, at the interface of the column and footing, the pitch of the spirals was set to be 1.5 in. to provide more confinement. Also, the spirals had one and half extra turn and were tied together using mechanical splices. This was identical to what presented for the pier with TiABs in the previous chapter. The pier-to-footing interface detail is shown in Figure 50.

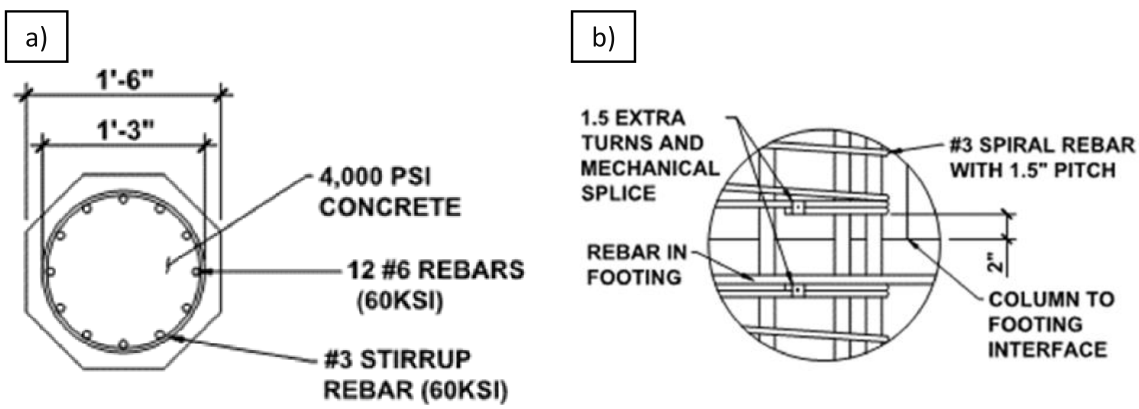

Figure 50. Pier Reinforced with Normal Steel Rebar: a) Column Detail, b) Column-Footing Interface

The details of the cap for mounting of the actuator to the pier was identical to the pier with TiABs. The reinforcing details of the pier reinforced with normal steel rebars are presented in Figure 51.

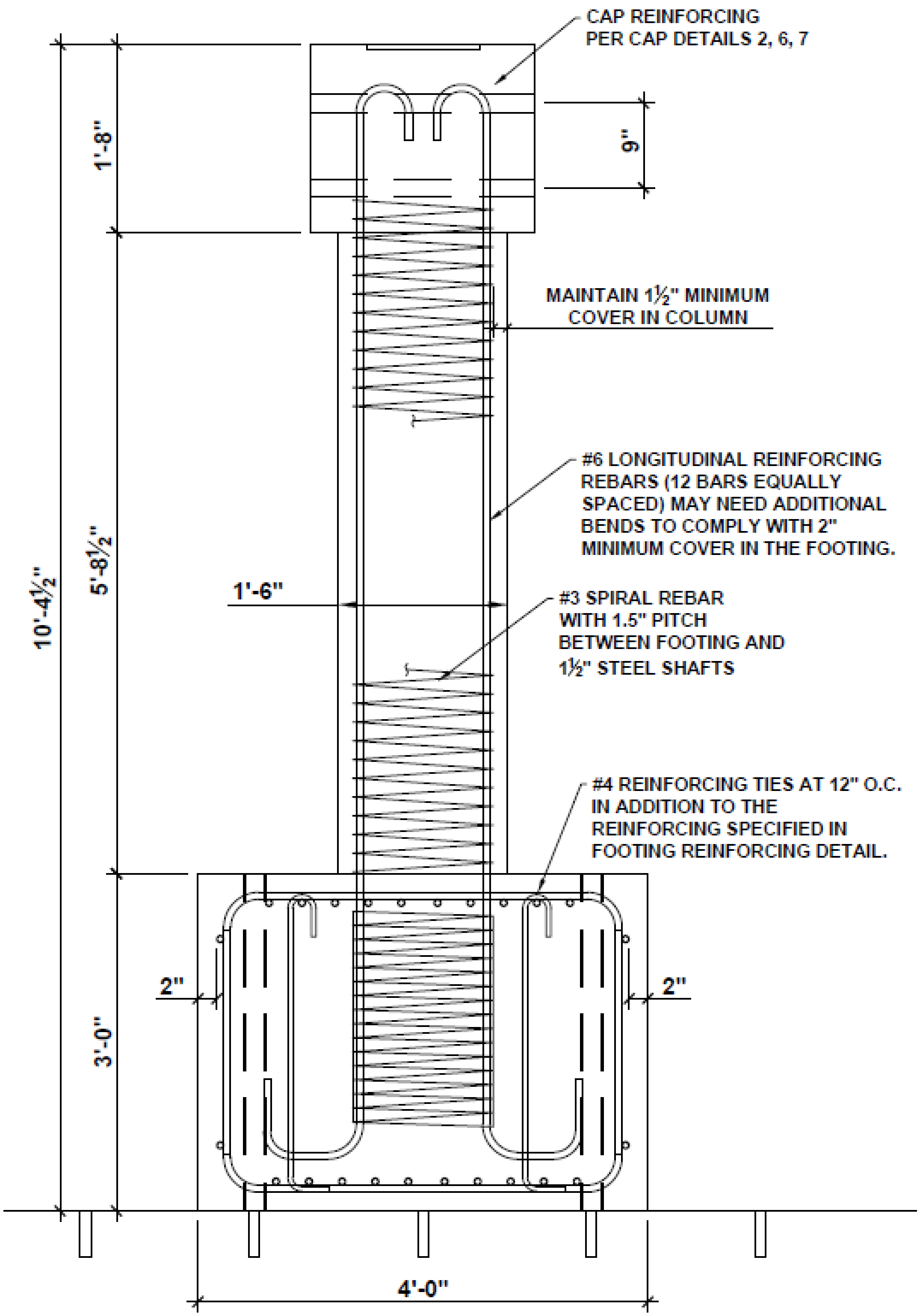

Figure 51. Details of the Pier Reinforced with Normal Steel Rebars (Benchmark Specimen)

4.2.2 Construction

Construction sequence for the benchmark pier was identical to the sequence discussed in Chapter 3.3.2 for the pier reinforced with TiABs. However, for the benchmark specimen, there was no need of using rebar chairs/spacers as the whole specimen was made of the same grade of reinforcing bars and materials (refer to Figure 52 and Figure 53).

a) Footing ready for Pour

b) Pour of Footing

d) Curing of Footing

c) Footing after Pour

e) Footing Transportation

Figure 52. Construction Sequence of Footing: Pier Reinforced with Normal Steel Rebar

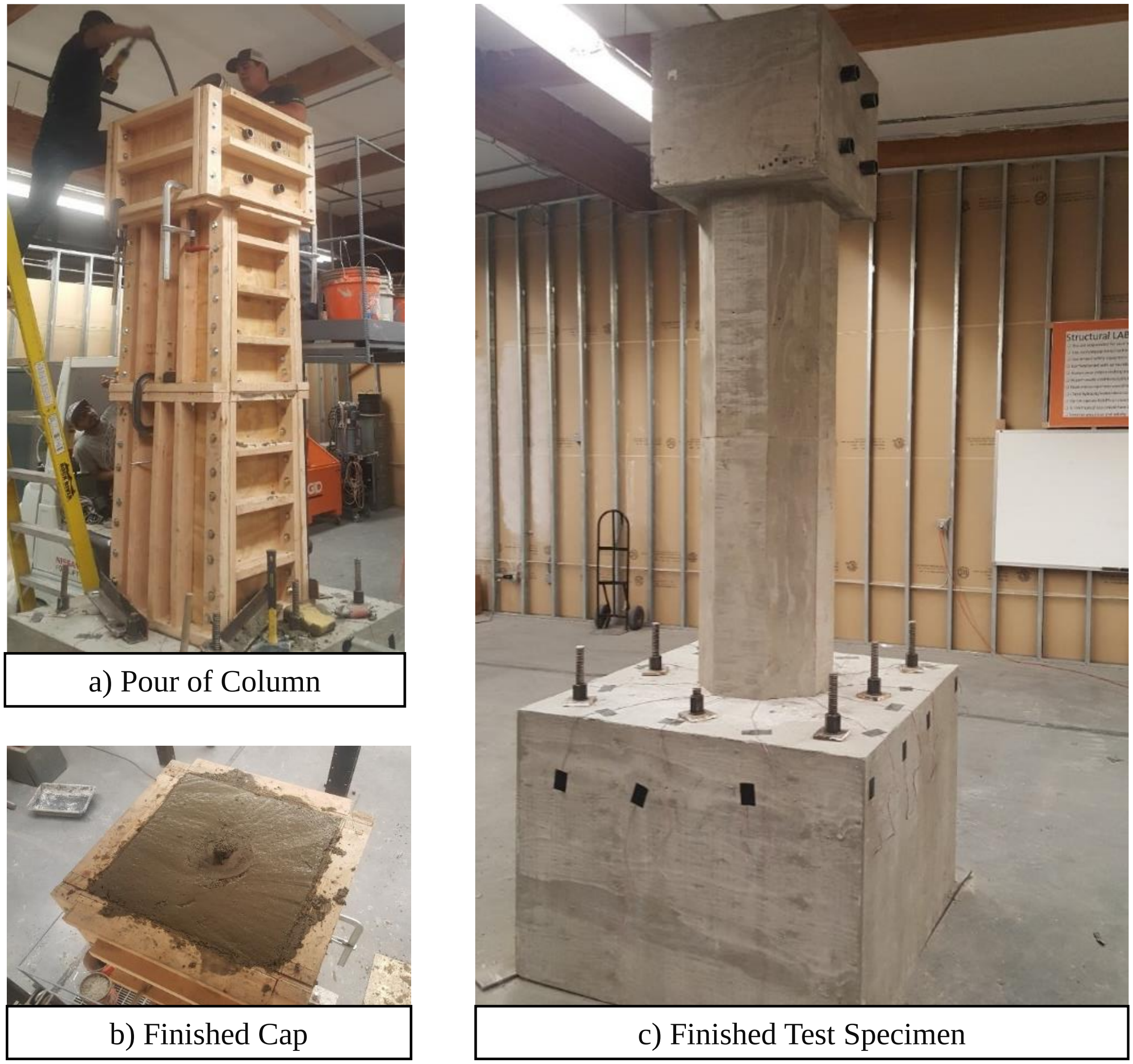

a) Pour of Column

b) Finished Cap

c) Finished Test Specimen

Figure 53. Construction Images: Pier Reinforced with Normal Steel Rebar

4.2.3 Material Properties

Materials used for the construction of the pier were normal weight concrete and grade 60 rebars. Both longitudinal and transverse reinforcement of the pier were made of grade-60 steel rebars with a modulus of elasticity 29,000 ksi. Minimum yield strength and the ultimate strength for grade-60 rebars were 60 ksi and 90 ksi respectively.

The design compressive strength of the concrete for the pier and footing was 4,000 psi. The average 28-day compressive strength (f'c) of the pier and footing were 4,850 psi and 4,630 psi respectively. The summary of the compressive strength is shown in Table 9.

Table 9. f'c Values for Footing and Pier in (psi) [17]

	Test 1	Test 2	Test 3	Test 4	Average
Footing	3,980	4,740	4,450	5,330	4,630
Pier	5,280	4,680	4,97-	4,460	4,850

4.3 Test Setup

The schematics for the test setup of the pier reinforced with normal steel rebars is presented in Figure 54. This was identical to the pier reinforced with TiABs (Figure 34).

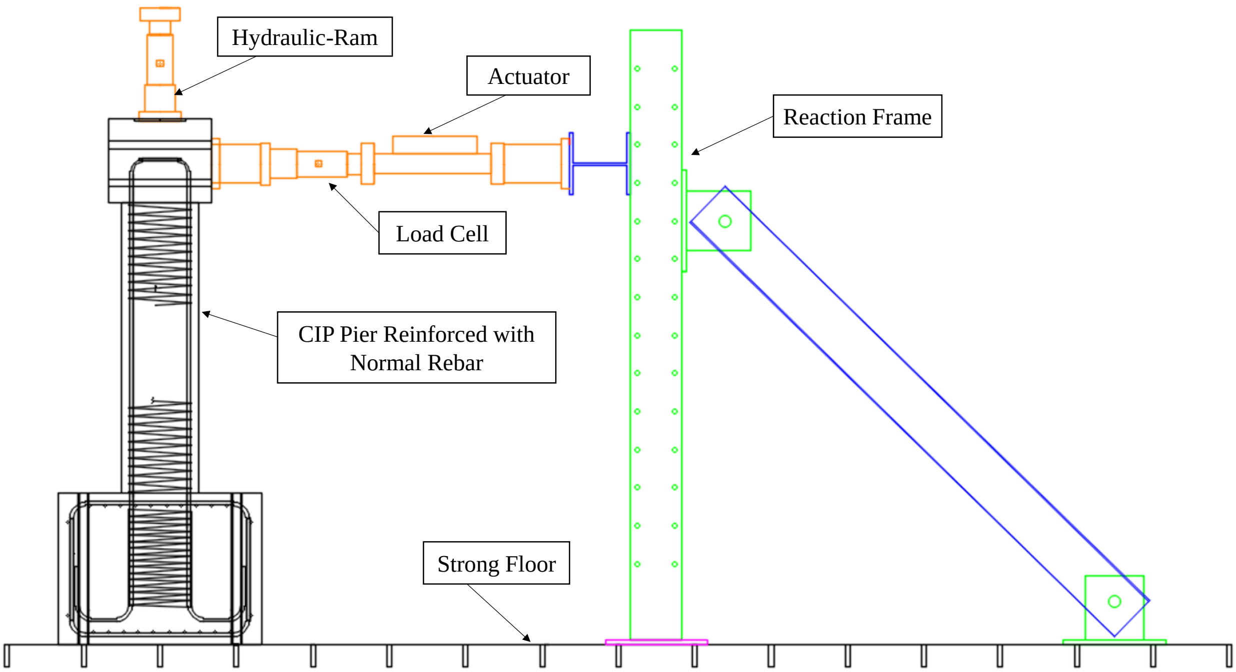

Figure 54. Schematic of Test-Setup: Pier Reinforced with Normal Steel Rebars

The instrumentation plan, axial load, and loading protocol for the benchmark pier were identical to those presented in the previous chapter for the pier reinforced with TiABs.

The targeted values of drift and the actual values of the drift were slightly different from each other. This was due to deflection of the reaction frame. A summary of the targeted values and actual values of drift is presented in Table 10.

Table 10. Lateral Loading Protocol for Cantilever Column: Normal Steel Rebar [17]

	Targeted Values		**Actual Values**	
Cycle	**Δ (inch)**	**Drift (%)**	**Δ (inch)**	**Drift (%)**
1	0.20	0.26	0.16	0.20
2	0.35	0.45	0.26	0.33
3	0.69	0.88	0.46	0.59
4	1.38	1.77	0.86	1.10
5	2.08	2.67	1.50	1.93
6	2.77	3.55	2.15	2.76
7	3.46	4.44	2.84	3.64
8	4.15	5.32	3.50	4.49
9	5.54	7.10	4.86	6.23
10	6.23	7.99	5.54	7.10
11	6.92	8.87	6.23	7.99
12	7.61	9.76	6.94	8.90
13	8.30	10.64	7.71	9.89

4.4 Testing Results

Hairline cracks were observed at bottom section of the pier during the first cycle (0.26 % drift ratio). The cracks were measured and marked on the pier at each drift ratio throughout the testing.

During the second cycle, i.e., 0.45 % drift ratio, more cracks were observed in between the 18 in and 36 in (457.2 mm and 914.4 mm) region above the footing. Also, the hairline cracks at the base opened to 1 mm in width. Width of the cracks increased at increasing cycles and drift ratio. At the drift ratio of 2.67 %, i.e., fifth cycle, the cracks opened up-to 4 mm and concrete began to spall at the plastic hinge region of the pier. Also, more cracks showed up at the height of 36 in. (914.4 mm) and above from the top of the footing. As the drift ratio increased, opening of the cracks got bigger and more cracks appeared right above the opening. The breaking of the longitudinal bars could be identified either by large or small pop sounds or by peaking from the opening to inside. Failure and buckling of the longitudinal bars occurred during the 9.76 % drift ratio (12th cycle). At the same time, significant strength loss was noticed at thirteen cycle (drift ratio of 10.64 %) with rupture of two additional rebars which marked the end of the test. There was no rocking or significant bond-slip observed in the plastic hinge zone of the pier. Figure 55 presents the damage progression in the plastic hinge region of the pier reinforced with normal rebar. There was no damage to the footing which was designed to remain elastic throughout the testing.

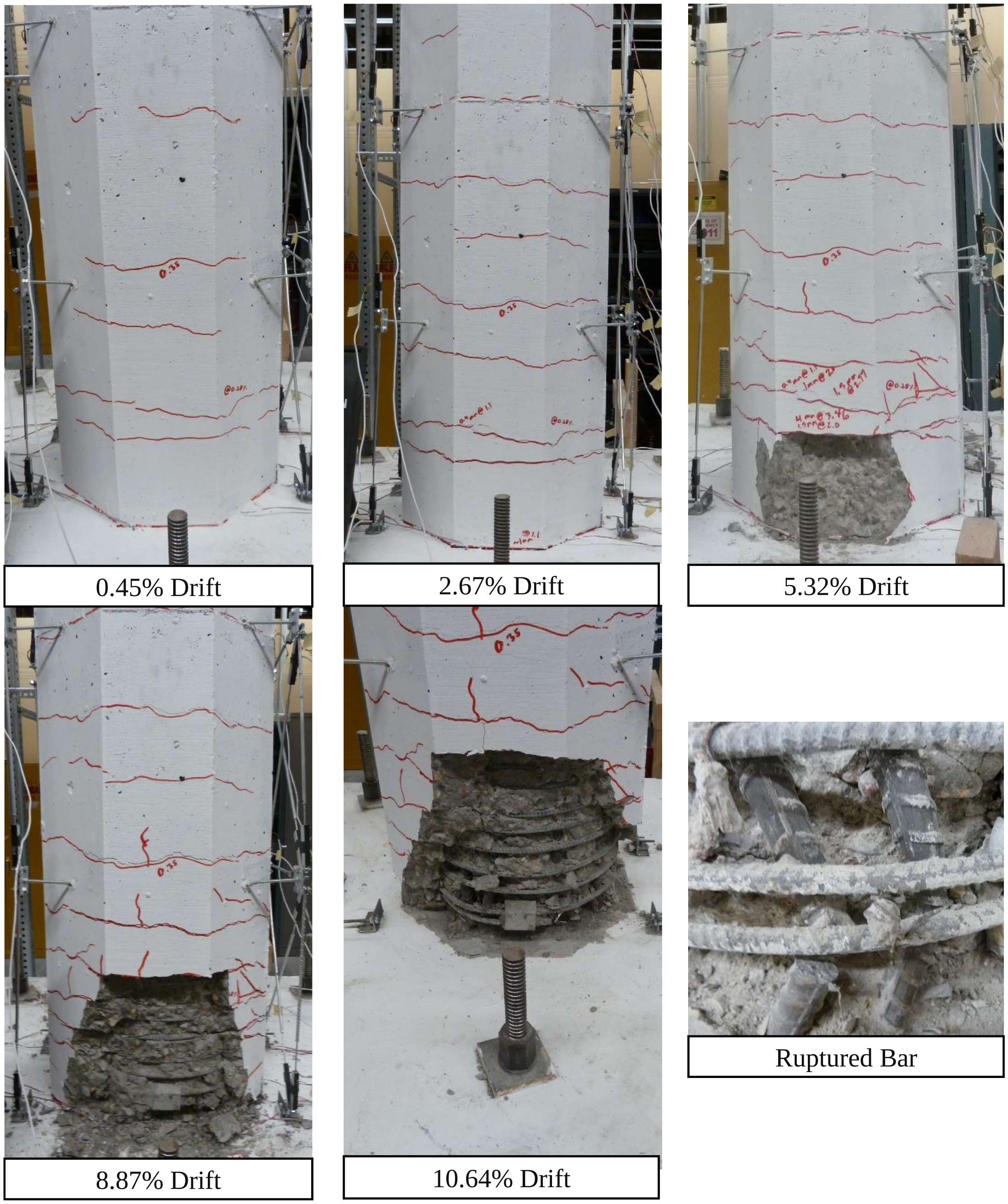

Figure 55. Damage Progression: CIP Pier Reinforced with Normal Steel Rebars [17]

Figure 56 and Figure 57 present the Force-vs-Drift and backbone plots for the benchmark pier. The maximum load applied to the pier during the testing was 37.89 kip at 1.71 in. displacement (2.19% drift ratio). The maximum displacement of the pier during the testing procedure was 7.7 inch which corresponded to 9.89 % drift ratio.

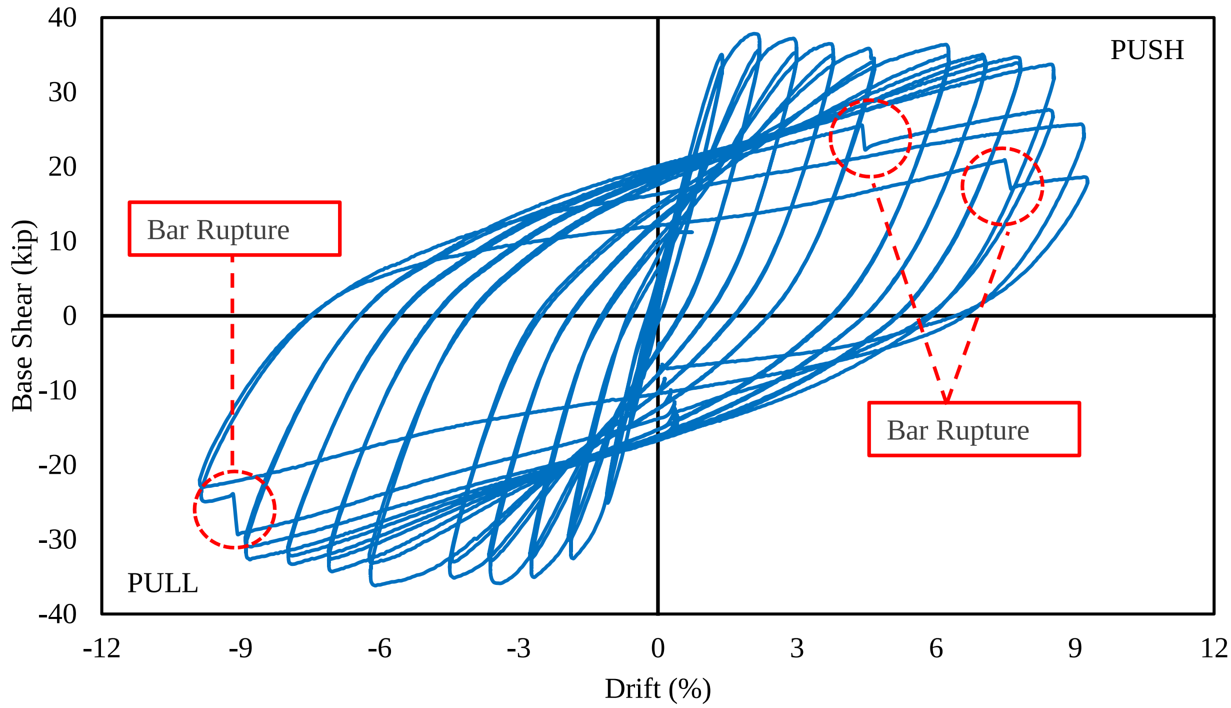

Figure 56. Force-Drift Hysteresis: Pier Reinforced with Normal Steel Rebars (Benchmark)

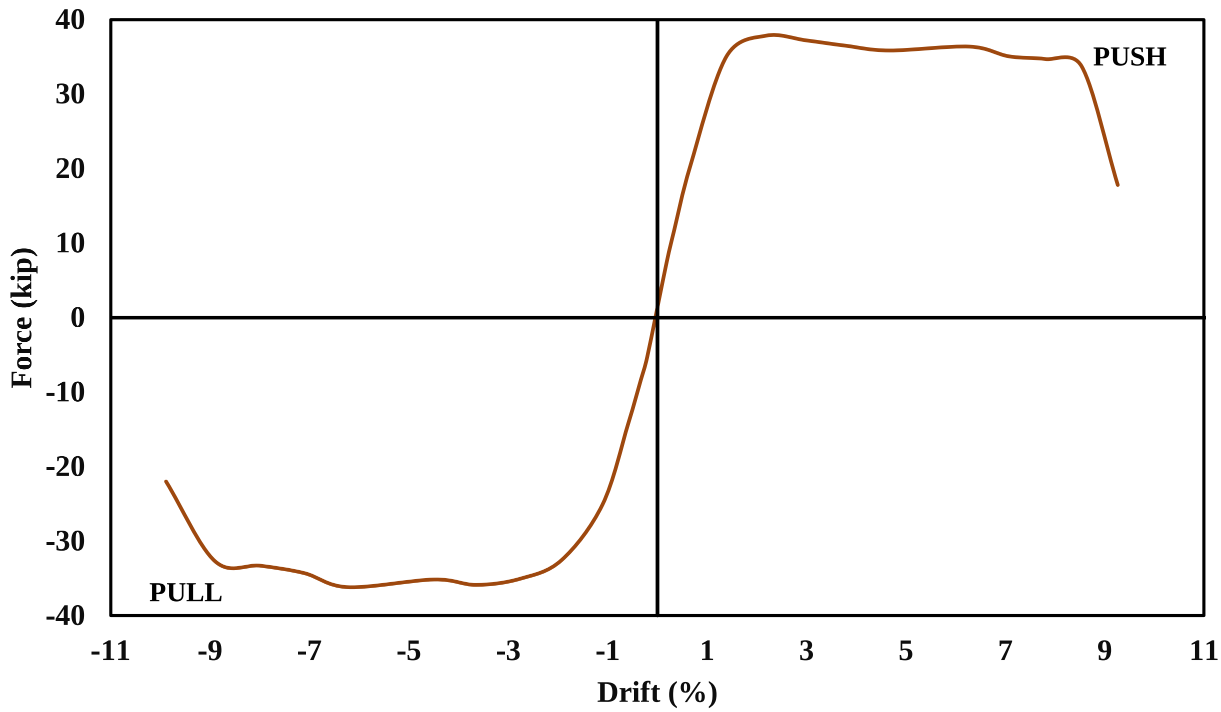

Figure 57. Backbone Curve: Pier Reinforced with Normal Steel Rebars (Benchmark)

Table 11 presents a summary of the performance points for the benchmark specimen.

Table 11. Summary of Performance Points: Pier Reinforced with Normal Steel Rebars

Yielding			Ultimate		
Displacement (in.)	**Drift (%)**	**Base Shear (kip)**	**Displacement (in.)**	**Drift (%)**	**Base Shear (kips)**
0.31*	0.40*	25.58*	1.71**	2.19**	37.8**
*Design capacity and yield displacement/drift from analytical calculations **Experimental results					

The amount of energy dissipated per cycle for the pier with normal steel rebar is plotted in Figure 58. The total energy dissipated for the pier reinforced with normal steel rebar was 455.7 kJ.

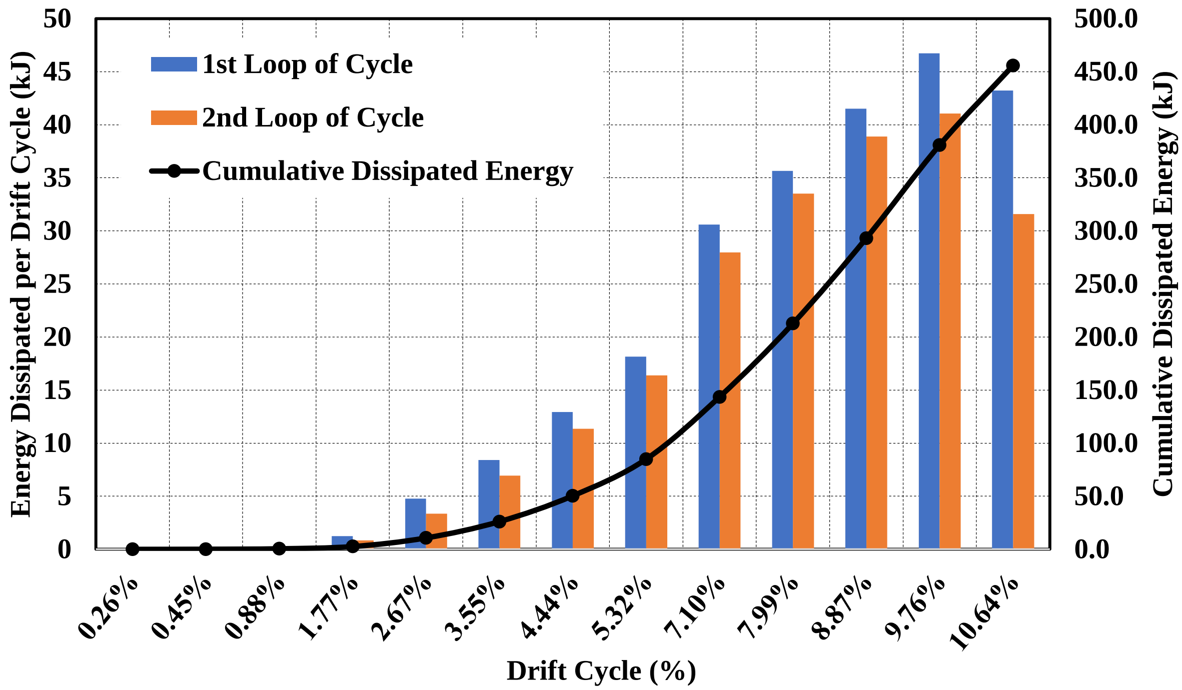

Figure 58. Energy Dissipation Plot: Pier Reinforced with Normal Steel Rebars (Benchmark)

The distribution of curvature along the height of the pier at peak of each drift ratio is evaluated and is presented in Figure 59. The pier yielded and failed within the plastic hinge region. According to Priestley et al. [23], the plastic hinge length was calculated to be 13.67 in. (refer to **Appendix E**). The distribution of curvature along the height showed that yielding occurred in the base of the pier, i.e., 0-18 in. of the pier. The height above 18 in. approached yielding but remained elastic throughout the testing.

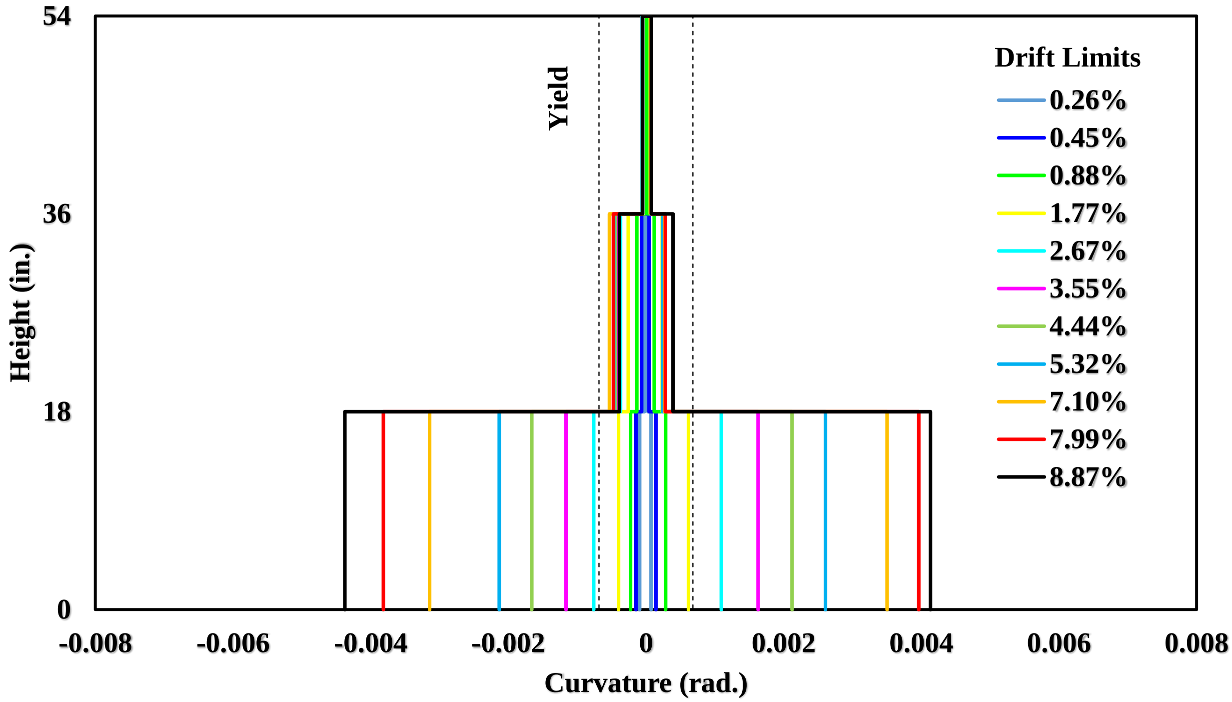

Figure 59. Height-Curvature: Pier Reinforced with Normal Steel Rebars (Benchmark)

The residual drift for the pier reinforced with normal rebars is plotted against the drift ratio in Figure 60.

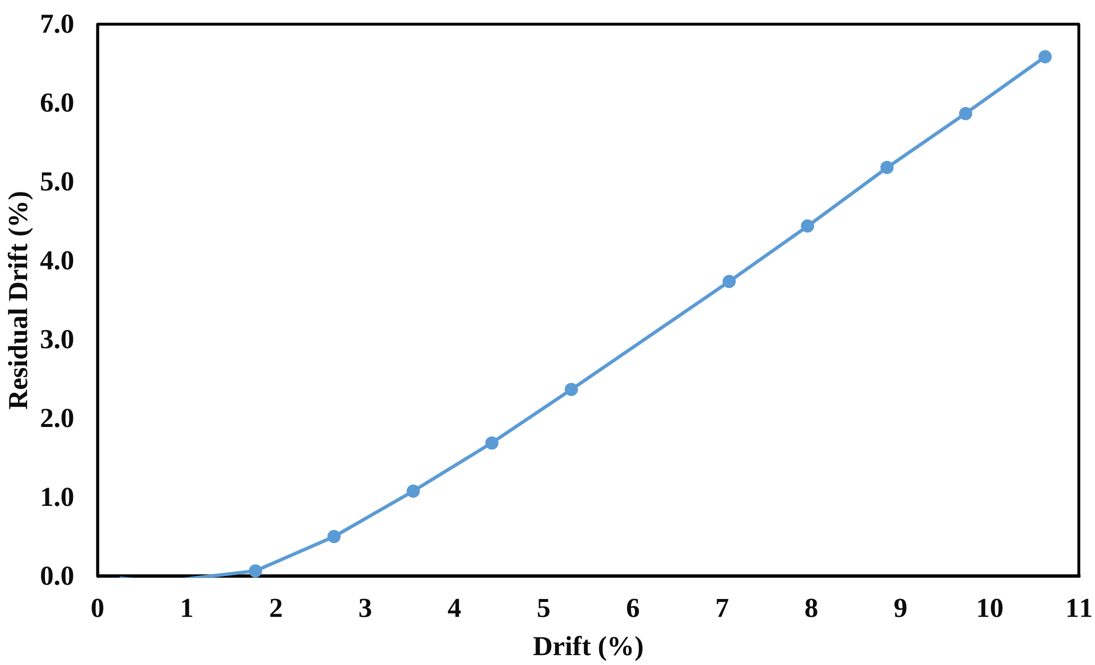

Figure 60. Residual Drift: Pier Reinforced with Normal Steel Rebar

4.5 Summary

- A benchmark pier reinforced with normal steel rebars was tested up to failure point.
- The instrumentation plans, test setup, and load protocol were identical to the pier reinforced with TiABs in the previous chapter.
- Average 28 days compressive strengths of the footing and the pier were found to be 4,630 psi and 4,850 psi, respectively.
- Observations from testing were similar to what can be expected from testing of a well-detailed cast-in-place pier. There were several large cracks in the plastic hinge zone. The pier achieved good levels of ductility and capacity. There was no rocking or significant bond-slip observed in the plastic hinge zone of the pier
- The ultimate base shear capacity of the pier was 37.8 kip at the displacement of 1.71 in. (2.19% drift ratio).
- The base shear at yield was found to be 35.1 kip at the displacement of 0.90 in. (1.15% drift ratio).
- More energy was dissipated with increasing drift ratios; however, first loop of cycle dissipated more energy than second loop of cycle which indicates the strength degradation of the pier. The total energy dissipated for the pier reinforced with normal steel rebar was 455.7 kJ.
- The plastic hinge length was calculated to be 13.67 in. The distribution of curvature along the height showed that yielding was concentrated in plastic hinge region of the pier, and height above it approached, but never reached the yield point.

CHAPTER 5. COMPARISION OF CIP PIER REINFORCED WITH NORMAL STEEL REBARS AND TITANIUM ALLOY BARS

This chapter presents a comparison of testing results between the cast-in-place cantilever piers reinforced with TiABs and normal steel rebars (benchmark). Both cantilever piers were designed in accordance with 2017 AASHTO LRFD Design Specifications [25]. The design moment capacity for both piers was 150 kip-ft. The piers had an octagonal section with a diameter of 18 in. and a height of 88 in. The height from top of footing to center of actuator is 78 in. The test setup and construction procedure were identical for both cantilever piers.

5.1 Hysteresis and Backbone Plot Comparison

Table 12 shows the comparison of the performance points for both CIP cantilever piers. The table shows the base shear at yield and the maximum base shear obtained during the testing. The displacement and drift at yielding and ultimate are the corresponding values of the base shear.

Table 12. Comparison of Performance Points

CIP Pier Reinforced with	Yielding			Ultimate		
	Displacement (in.)	**Drift (%)**	**Base Shear (kip)**	**Displacement (in.)**	**Drift (%)**	**Base Shear (kip)**
TiABs	1.09**	1.39**	16.19**	4.97**	6.38**	21.42**
Steel Rebar	0.31*	0.40*	25.58*	1.71**	2.19**	37.80**
Difference (%)	71.6	71.2	-58.0	65.6	65.7	-76.5
*Design capacity and yield displacement/drift from analytical calculations **Experimental results						

Figure 61 and Figure 62 shows a comparison of the hysteresis loops and the backbone plots for two piers. The hysteresis plot indicates that the benchmark pier had more energy dissipation (e.g., fatter loops) compared to the pier reinforced with TiABs. The elastic stiffness of the pier reinforced with TiABs was 13.4 kip/in which was 63% lower compared to the stiffness of the benchmark specimen (36.7 kip/in). The pier with TiABs also had a lower overstrength factor (1.32) compared to the benchmark (1.48). A lower overstrength factor for the pier with TiABs would result in smaller cross sections and less reinforcing for the cap beam and footings in an actual pier. The pier reinforced with TiABs achieved a higher drift ratio before failure compared to the benchmark specimen.

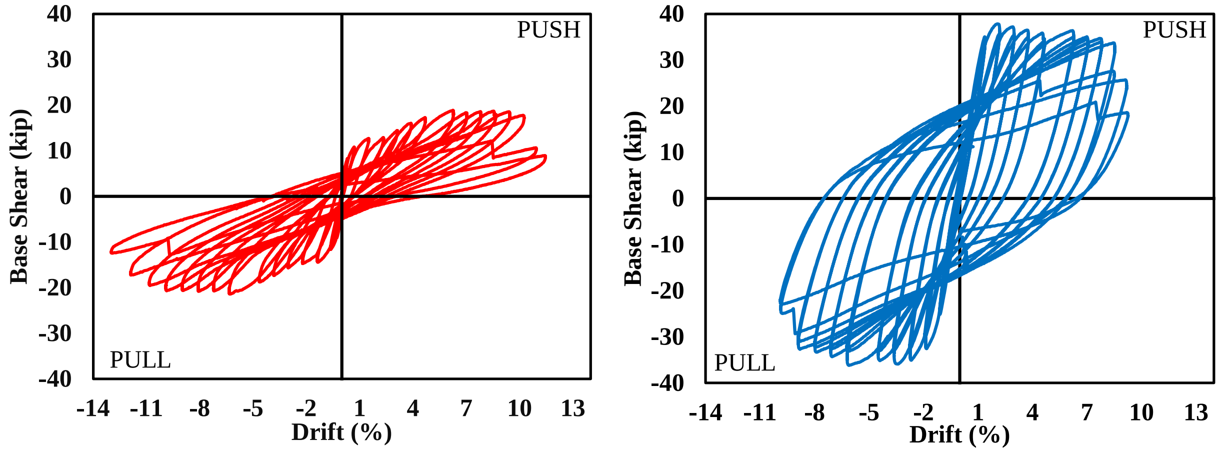

Figure 61. Base Shear Vs. Drift for CIP Pier Reinforced with a) TiABs, b) Normal Steel Rebars

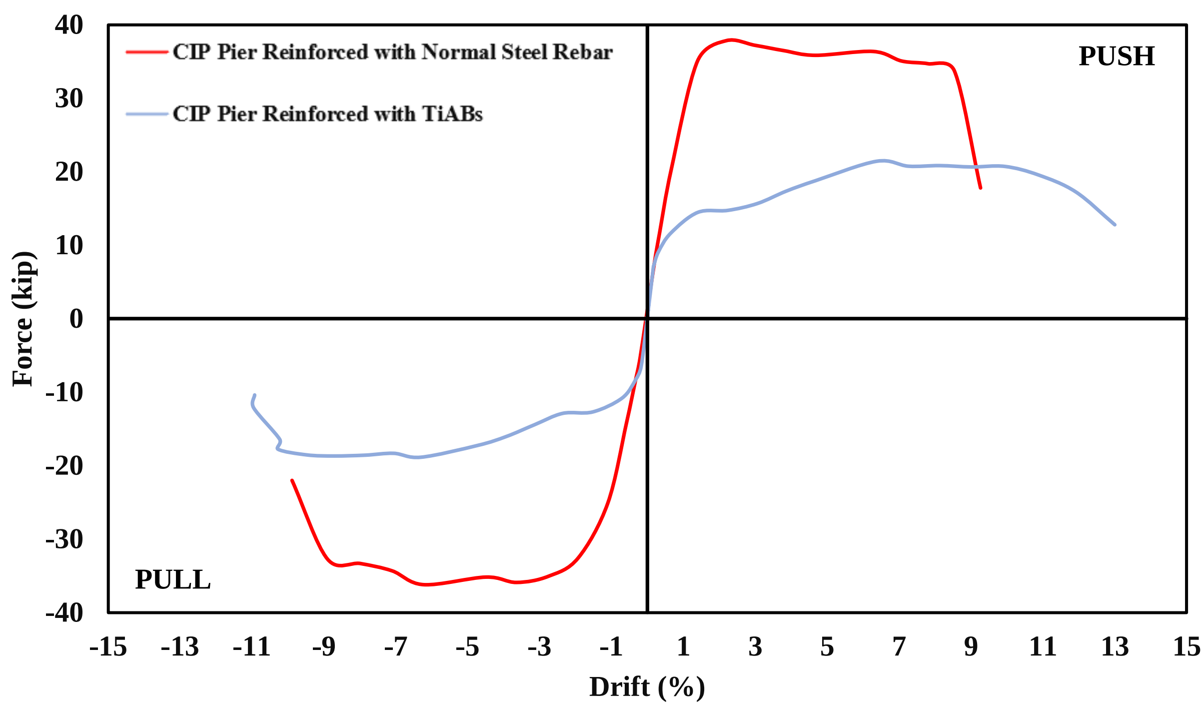

Figure 62. Comparison of Backbone Curves

5.2 Energy Dissipation Comparison

The amount of energy dissipated per cycle for the pier with TiABs is compared against the pier with normal steel rebars (benchmark) and plotted in Figure 63. As it can be observed the benchmark had higher level of energy dissipation compared to the pier with TiABs. The total energy dissipated for the pier reinforced with TiABs and pier reinforced with steel rebar were 210.29 kJ and 455.7 kJ, respectively. The cumulative dissipated energy for the benchmark pier was 54% higher than the pier reinforced with TiABs; however, the pier reinforced with TiABs achieved larger number of cycles before failure.

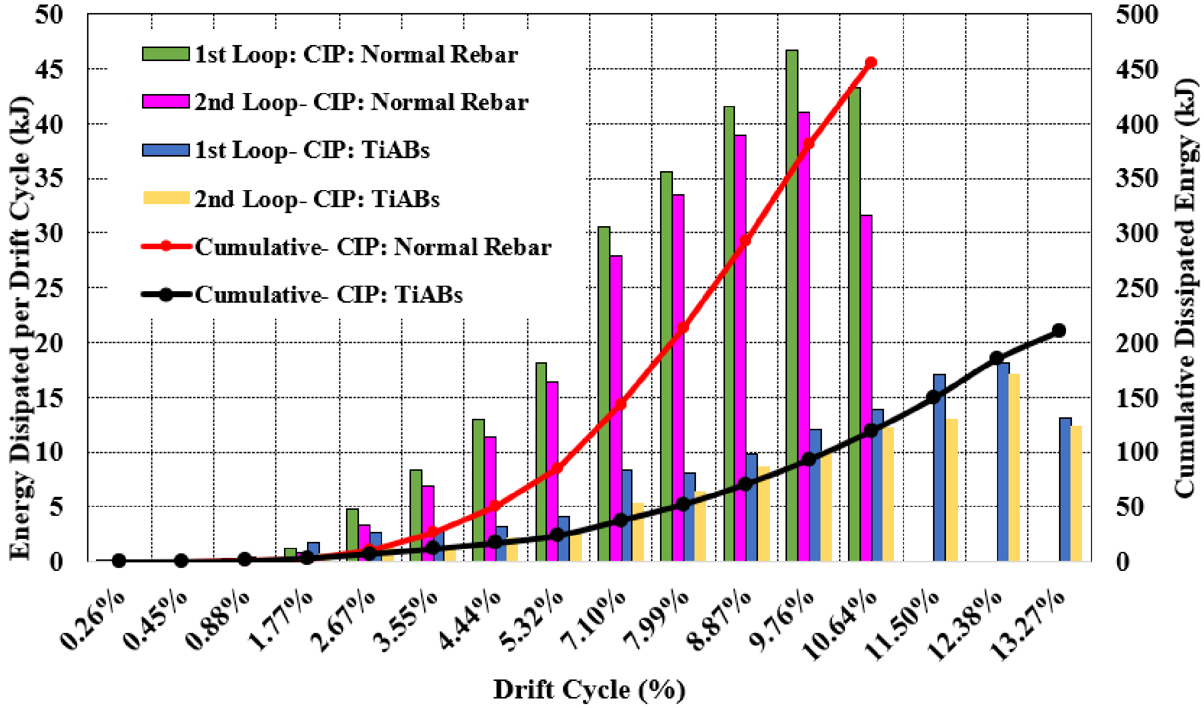

Figure 63. Comparison of Energy Dissipation

5.3 Distribution of Curvature

Figure 48 and Figure 59 show the distribution of curvature along the height of the pier at peak of each drift ratio. The plastic hinge lengths were calculated to be 23.57 in. (1.3 times diameter of the pier) and 12.67 in. (0.67 times diameter of the pier) for the piers reinforced with TiABs and normal steel rebars, respectively. For both cantilever column, the distribution of curvature along the height showed that yielding occurred in the bottom of the pier, i.e., 0-18 in. from top of the footing. The height above 18 in. in the pier approached the yield but remained essentially elastic throughout the testing. The curvature at yield for the pier reinforced with TiABs was 7.32E -03 radians compared to 6.84E-04 radians for the benchmark specimen.

5.4 Residual Drift Comparison

Residual drift is defined as the permanent deformation of the structure after a design level earthquake. Excess residual drift would limit post-earthquake functionality and repair options. Bridges with excessive residual drift may require full replacement. Residual drift was obtained at each drift ratio for both piers. Testing results showed lesser residual drifts of the pier reinforced with TiABs compared to the benchmark with normal steel rebars. At large drifts, the pier reinforced with TiABs had almost half of the residual drift of the benchmark that can be observed in Figure 64. In countries such as Japan, the bridge design code requires evaluation of residual drift for the bridge at the design stage.

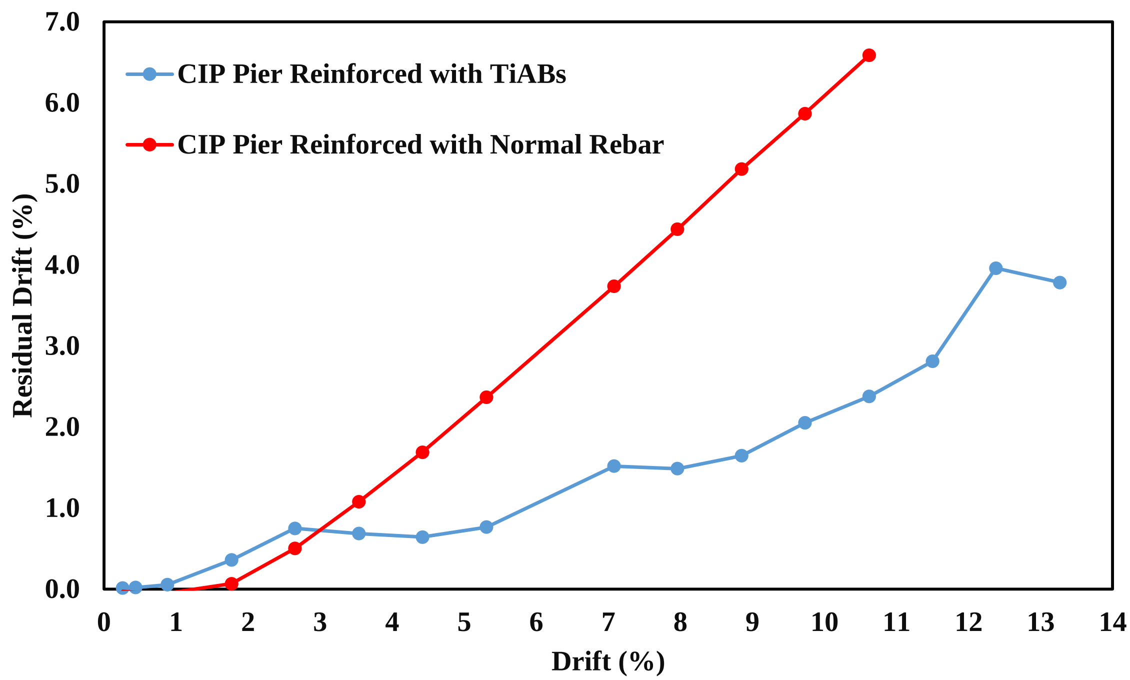

Figure 64. Comparison of Residual Drift

5.5 Displacement Ductility

Displacement ductility values at ultimate and failure for both piers are summarized and presented in Table 13.

Table 13. Displacement Ductility Comparison

	*Displacement Ductility (μ)		
	TiABs pier	**Normal Steel Pier**	**% Difference**
Ultimate Base Shear	4.6	5.5	16
Failure Point	8.5	7.4	15
*Calculated using **Equation 5**			

5.6 Summary

- Observations from testing and experimental results for the piers reinforced with TiABs and normal rebars (benchmark) were compared. The specimens had identical dimensions, instrumentation, test setup, and were subjected to similar loading protocols.
- The cracks, spalling of the concrete and non-linear deformation occurred mostly at the plastic hinge region for both piers. However, in testing of the pier with TiABs, significant rocking (gap opening) and bond-slip were observed at the pier-to-footing interface. This was due to presence of smooth TiABs. In testing of the benchmark, there was no noticeable rocking (gap opening) or bond-slip. The benchmark pier had several large cracks concentrated in the plastic hinge zone.
- Overall, the pier reinforced with TiABs appeared to have a better low-cycle fatigue performance compared to the benchmark and was able to sustain more cycles of inelastic deformation at large drift ratio.
- Presence of flexural cracks in the plastic hinge zone of a pier reinforced with TiABs should not compromise durability as TiABs have excellent corrosion resistance. This is not true for a pier reinforced with normal rebars. This advantage of TiABs would reduce post-earthquake

repairs and costs compared to a benchmark/conventional construction. For a pier reinforced with TiABs, it is important to ensure that the risk of galvanic corrosion is eliminated (e.g., no direct contact) if there are two metals present in the plastic hinge zone.

- The yield displacement for TiABs reinforced pier was 71.6% higher compared to the benchmark, however, the base shear at yield was 58% lower compared to the benchmark.
- The pier with TiABs had 63% lower elastic stiffness compared to the benchmark.
- The displacement ductility at the ultimate base shear and failure points, were 4.56 and 8.82 for the pier with TiABs, and 5.52 and 7.40 for the benchmark pier, respectively.
- The ultimate displacement for TiABs reinforced pier was 66% higher compared to the benchmark pier.
- The total energy dissipated for the pier reinforced with TiABs and the benchmark were 210.29 kJ and 455.7 kJ, respectively. The dissipated energy for benchmark pier was 54% higher compared to the pier with TiABs.
- The plastic hinge lengths for the pier with TiABs and the benchmark were calculated to be 23.57 in. (1.3 diameter of the pier) and 13.67 in. (0.76 times diameter of the pier), respectively.
- The curvature at yield for pier reinforced with TiABs was 7.32E -03 radians, this was 6.84E-04 radians for the benchmark.
- Testing results showed lesser residual drifts of the pier with TiABs. At large drifts, TiABs reinforced pier had almost half of the residual drift of that with steel reinforced pier.

CHAPTER 6. MECHANICAL SPLICES FOR TITANIUM ALLOY BARS

This chapter presents some preliminary investigation for identifying appropriate and commercially available mechanical couplers for splicing of TiABs. Since TiABs are more expensive compared to normal rebars, it is necessary to limit their quantity and use in bridge piers (e.g., plastic hinge zone only). Products from a well-known producer of mechanical couplers in the United States was considered for this research. A few mechanical couplers were investigated for splicing of #5 and #6 smooth and pseudo-threaded TiABs (grade 5). Tensile testing was carried out in accordance with ASTM A1034 to address the 2017 AASHTO LRFD requirements [24],[25]and a suitable coupler was identified.

6.1 Introduction

To splice two pieces of TiABs, the bars must be joined together so that the force is effectively transferred from one bar to another without any premature failure or damage to the coupler. Mechanical splice is a common method of splicing rebars where a coupler or a sleeve is used to splice two bars. The major advantage of using mechanical splice is to avoid congestion and have greater flexibility for designers and engineers. Mechanical couplers are more cost-effective compared to lap-splices, especially for materials such as TiABs. There are various types of mechanical couplers for normal and high strength rebars. In this research, three types of mechanical splices produced by Producer 'X' in the United States are investigated for splicing of TiABs.

Tensile testing is carried out to investigate the adequacy of the couplers/splices. The tensile test is to determine stress-strain relationships. It is a simple uniaxial test that consists of slowly pulling a sample of a material in tension until it breaks. The typical testing procedure is to deform or 'stretch' the material at a constant speed. The load and displacement in the specimen are monitored throughout the testing

6.2 Testing Arrangement and Design Consideration

No. 5 and No. 6 TiABs with and without pseudo threads were considered for splicing (Figure 65).

Figure 65. Smooth and Pseudo-Threaded Titanium Alloy Bars

A tension test of a TiAB was also carried out to obtain some of the important mechanical properties for #5 (0.625 in. diameter) and #6 (0.750 in. diameter) bars. The testing matrix for the bar itself is presented in Table 14. The specimens were loaded in a universal testing machine and slowly pulled in tension until they ruptured. The specimens were tested in accordance with ASTM E8 and A370 [26],[27]. The grip length for each specimen was kept at 8 in. The length of each specimen was 30 in. which provided 14 in. bar length between the grips due to gripping requirements of the testing.

Table 14. Tension Test Matrix: Pure Bar

Specimen ID	Bar No.	Diameter (in.)	Description
T1	#5	0.625	Tension Test
T2	#6	0.750	Tension Test

Mechanical splices produced by Producer ‘X’ were considered for TiABs. Three different mechanical splices were selected. The bars were #5 and #6 with and without pseudo-threads. The three mechanical splice systems were as follows:

1) Coupler with Shear Screw (Specimen ID: Coupler ‘A’)

2) Coupler with Gripping Technology (Specimen ID: Coupler ‘B’)

3) Coupler with Taper-Threaded and Gripping Technology (Specimen ID: Coupler ‘C’)

6.2.1 Splicing of TiABs with Coupler ‘A’

Coupler ‘A’ produced by Producer ‘X’ uses a shear screw to splice the bars. They can be either epoxy-coated or uncoated. The bars are inserted through the two ends until they touch the positive center inside the coupler. Next, the twist-off screws of the coupler are tightened using an impact wrench and a socket on both sides of the coupler. The coupler ‘A’ and a sample spliced TiAB is shown in Figure 66. The datasheet for Coupler ‘A’ is attached in **Appendix F.**

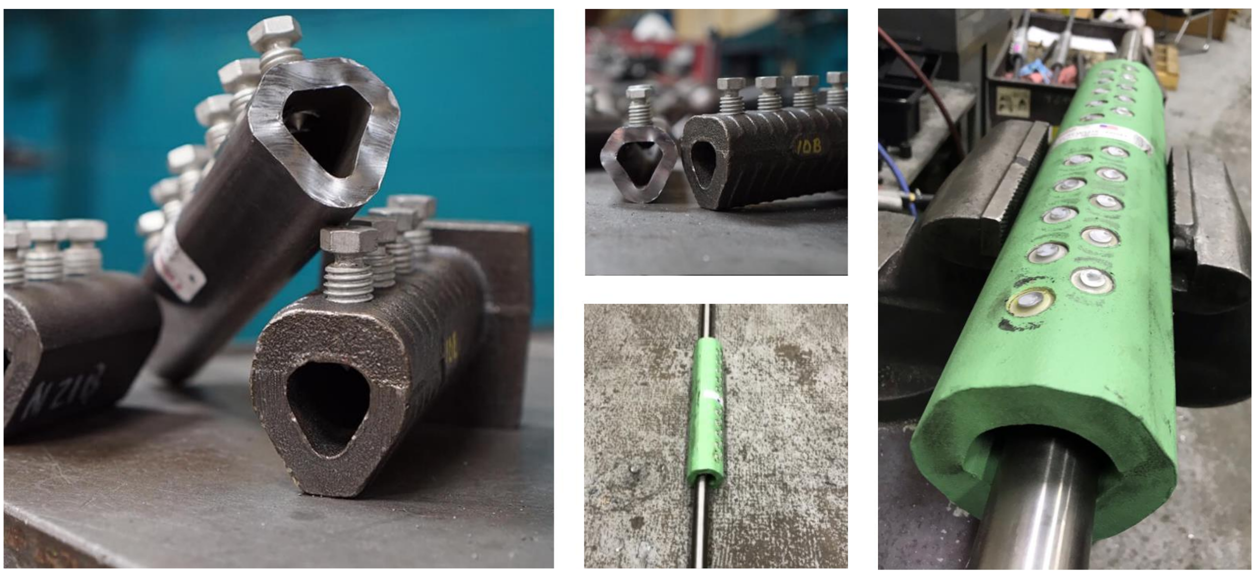

Figure 66. Coupler ‘A’

Three tests were carried out using coupler ‘A’. The testing matrix is presented in Table 15. Specimen A1 (#5) and A2 (#6) were made of pseudo-threaded TiABs whereas specimen A3 was smooth and much larger in diameter (#14). The specimens were subjected to tensile loading in a universal testing machine in accordance with ASTM A1034 [24]

Table 15. Tension Test Matrix: Coupler 'A'

Specimen ID	Diameter (in.)	Product Code	Number of Tests	Description
A1	0.625	05ZBA	1	#5 pseudo-threaded bar
A2	0.750	06ZBA	1	#6 pseudo-threaded bar
A3	1.750	14ZBA	1	#14 smooth bar

6.2.2 Splicing of TiABs with Coupler 'B'

Coupler 'B' produced by Producer 'X' uses a cold swaged steel sleeve and is installed in situ with overlapping bites. Each bar is inserted from one end. Once the bars are inserted inside the coupler, the coupler is squished using a portable press. Coupler 'B' is shown in Figure 67 and the datasheet is attached in **Appendix G**. In Figure 67, the spliced deformed bars are just indicative. In this research Coupler 'B' was used for splicing of TiABs with pseudo threads.

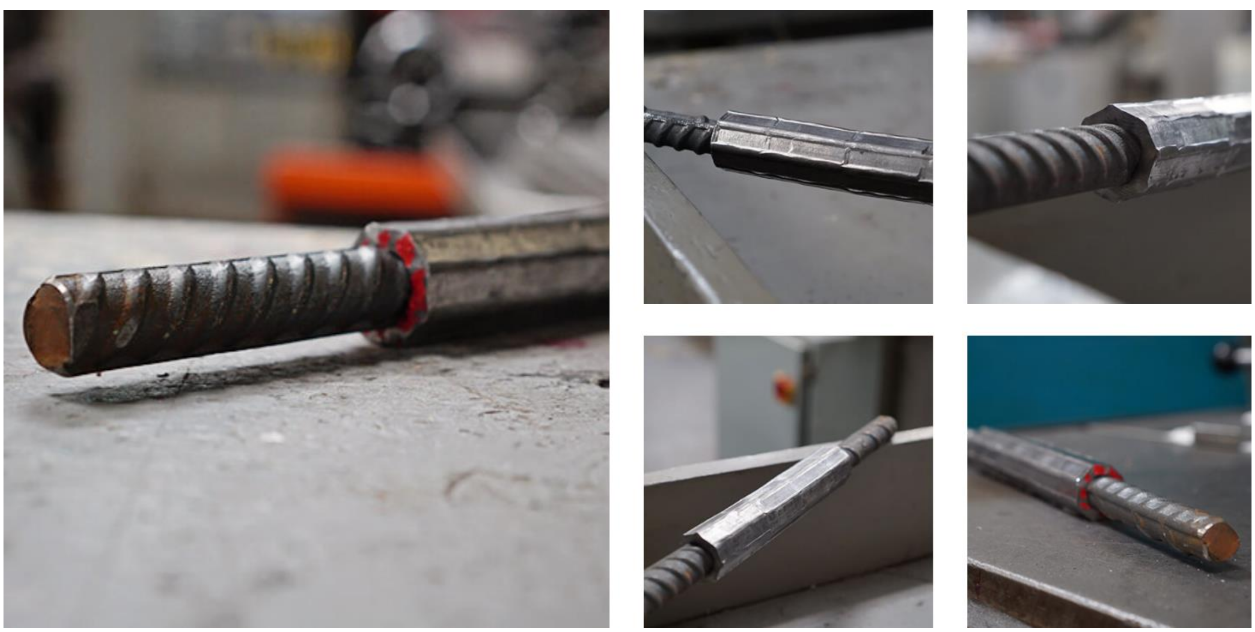

Figure 67. Coupler 'B'

Two tests were carried out using a Coupler 'B'. The testing matrix is presented in Table 16.

Table 16. Tension Test Matrix: Coupler 'B'

Specimen ID	Diameter (in.)	Product Code	Number of Tests	Description
B1	0.625	05XL	1	#5 pseudo-threaded bar
B2	0.750	06XL	1	#6 pseudo-threaded bar

6.2.3 Splicing of TiABs with Coupler 'C'

Coupler 'C' produced by Producer 'X' uses a cold swaged steel sleeve and is thicker and designed specifically for use with high-strength bars. The male and female taper threaded coupler components maintain the full cross-sectional area of the reinforcing bar. The concept of the Coupler 'C' is shown in Figure 67 and the datasheet is attached in **Appendix H**.

Six tests were carried out using Coupler 'C'. The testing matrix is presented in Table 17.

Table 17. Tension Test Matrix: Coupler 'C'

Specimen ID	**Diameter (in.)**	**Product Code**	**Number of Tests**	**Description**
C1, C2, C3	0.625	XT05F and XT05M	3	#5 pseudo-threaded bar
C4, C5, C6	0.750	XT06F and XT06M	3	#6 pseudo-threaded bar

Figure 68. Coupler 'C'

6.3 Test Setup

Tensile testing was performed in accordance with ASTM A1034 [24]. Once the specimen was prepared, a series of measurements were made prior to start of the test. Table 18 shows the description of the important parameters used in the testing.

Table 18. Initial Measurements for Tensile Test of Couplers

ID	Description
$D_{Initial}$	Initial diameter of the titanium alloy bars
$L_{Initial}$	Total length of specimen after installation of the mechanical coupler
L_{Final}	Final length of each bar after fracture
D_{Final}	Diameter of bar at the point of fracture (3 measurements for precision)

All tests were uniaxial that consisted of slowly pulling a sample in tension until it ruptured. Figure 69 illustrates a typical tensile test setup for the samples. Figure 70 presents a photo from testing of one of the samples.

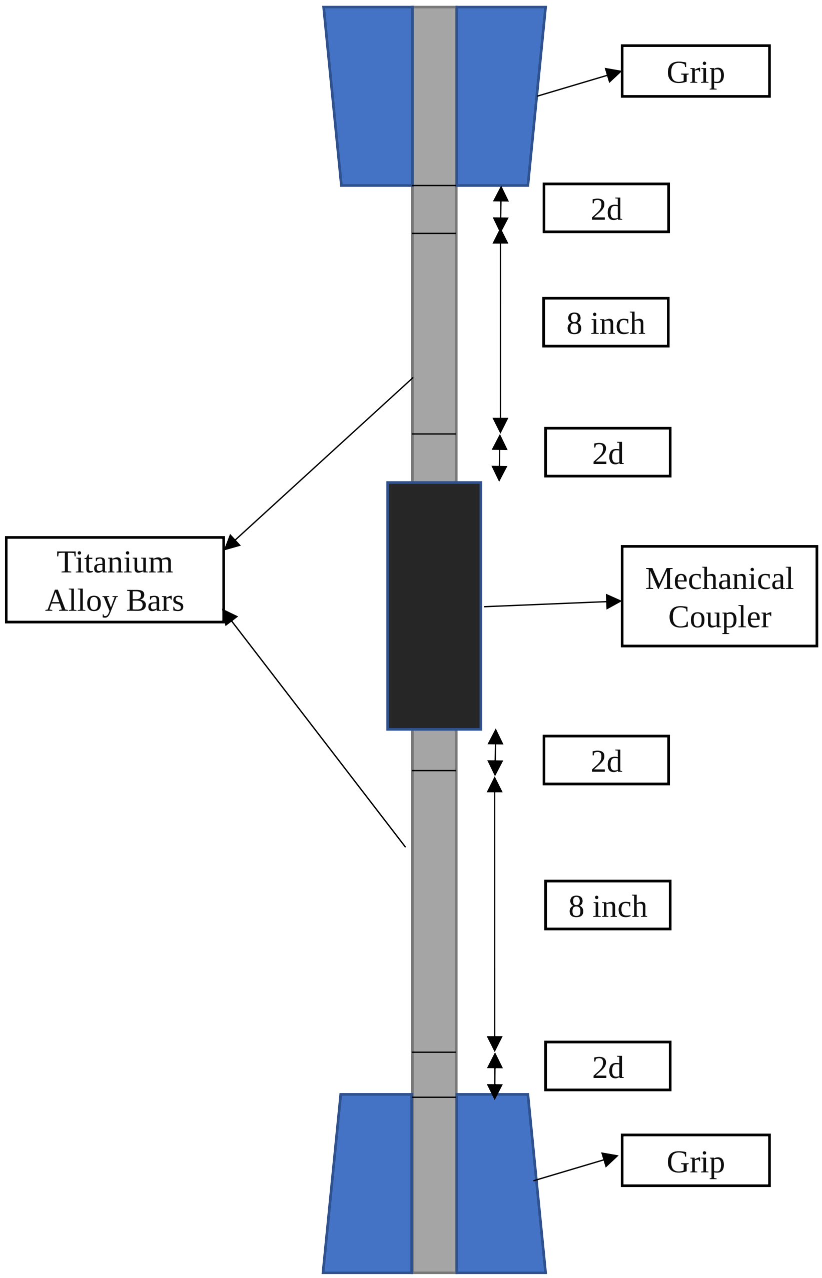

Figure 69. Tensile Test Setup for the Samples

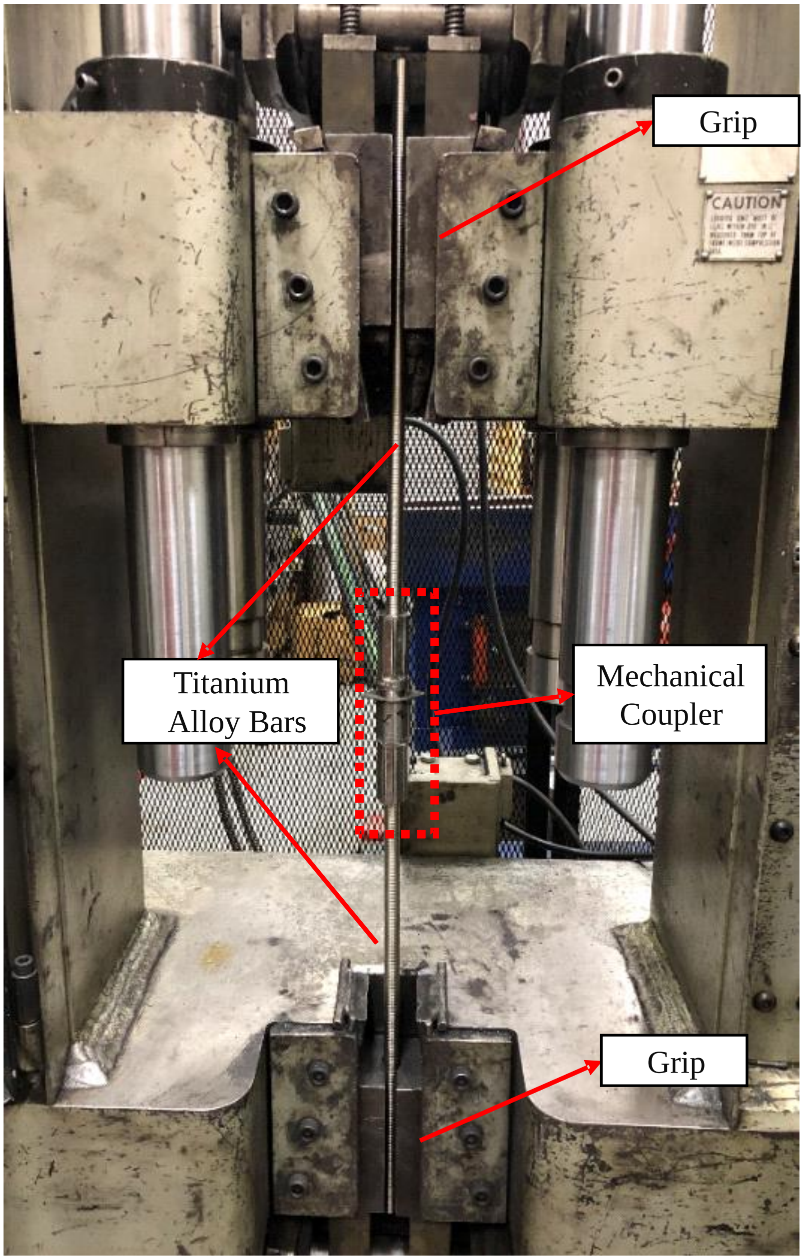

Figure 70. Tensile Testing of a Mechanically Spliced TiAB

6.4 Testing Results

This section presents observations and results from tensile testing of TiABs with different mechanical couplers.

6.4.1 Without Coupler

Table 19 presents a summary of the dimension's measurements for specimens T1 and T2 before and after testing. These specimens were pseudo-threaded and tested in tension without any mechanical couplers. In this table, the final diameter is measured at the point of fracture. The changes in diameter of the specimens after the test were found to be 11.8% and 11.3% for specimens T1 and T2, respectively. The length change was 3.96% for T1 and 5.21% for T2. Table 20 presents a summary of the results from tensile testing. The Stress-Displacement plots are presented in Figure 71 and Figure 72.

Table 19. Dimension Measurements: Pseudo-Threaded TiABs without a Coupler

Specimen	$D_{Initial}$ (in.)	$L_{Initial}$ (in.)	L_{Final} (in.)	D_{final} (in.)			
				D_{final_1}	D_{final_2}	D_{final_3}	$D_{final\_average}$
T1	0.625	30	31.188	0.564	0.550	0.540	0.551
T2	0.750	30	31.563	0.674	0.667	0.655	0.665

Table 20. Tensile Test Results: Pseudo Threaded TiABs without a Coupler

Specimen	Diameter (in.)	Max Load (lbf)	Stress Value (psi)	Failure Mode
T1	0.625	47,880	154,452	Bar Rupture in Tension
T2	0.750	66,670	151,323	Bar Rupture in Tension

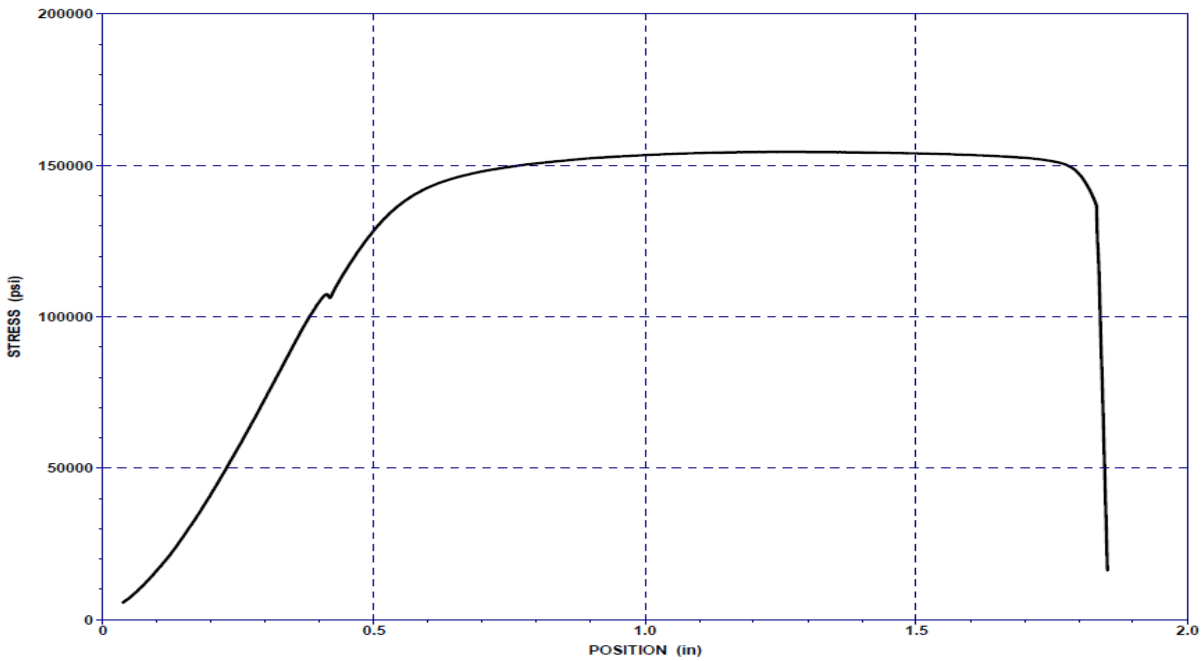

Figure 71. Stress-Displacement Plot for T1

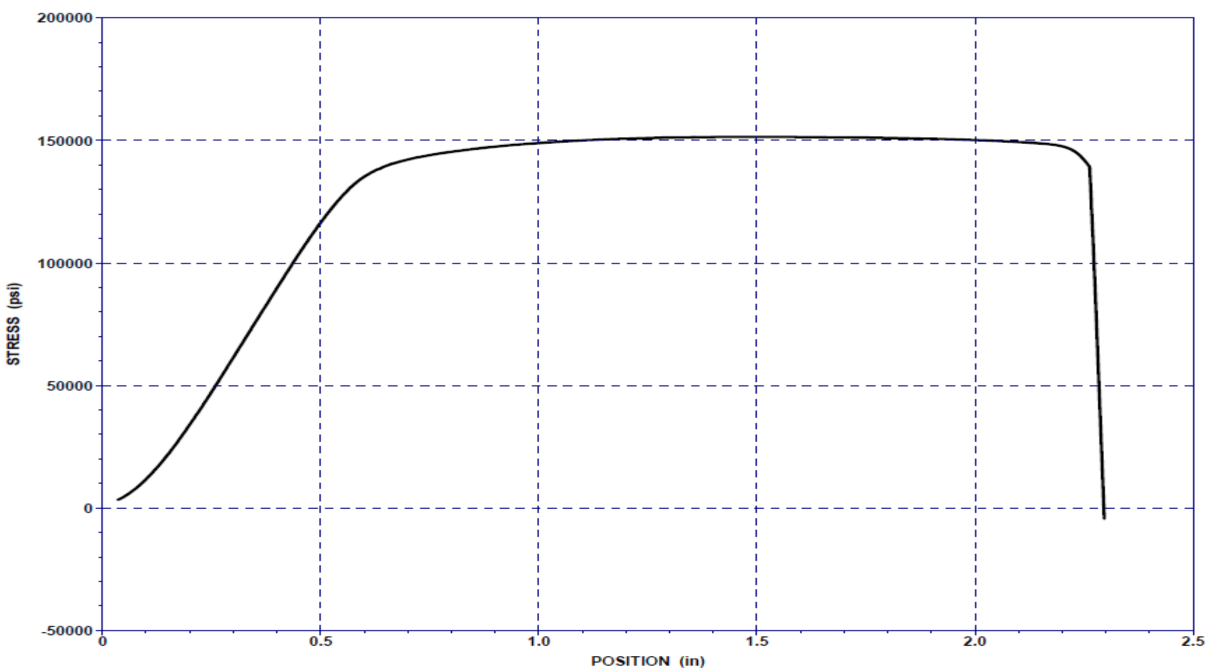

Figure 72. Stress-Displacement Plot for T2

6.4.2 Coupler 'A'

All three samples with and without pseudo-threads had premature failure. The failure was in the form of pullout. Observations from testing showed that the screws in the coupler were unable to develop the capacity of the bars and sliding/pullout occurred as can be observed in Figure 73.

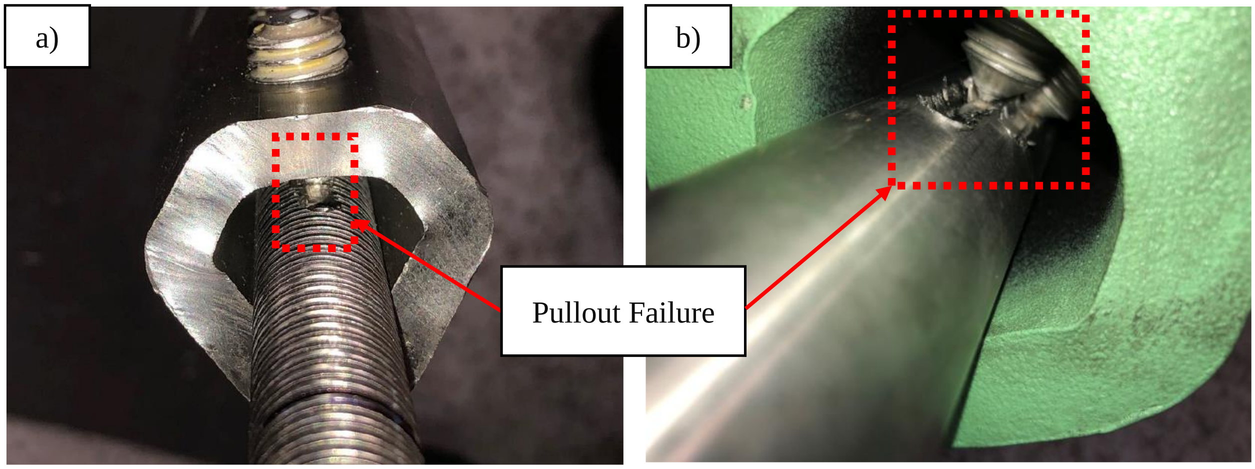

Figure 73. Pullout Failure of TiABs with Coupler 'A': a) A1, b) A3

The length and diameter measurements for the three samples are presented in Table 21. Length is the overall length of the specimen after coupler is installed, whereas final diameter is measured at the point of failure which is on pullout side of the specimen.

The change in diameter of the specimen after the test was found to be 0.48%, 1.6% and 0% for specimen A1, A2, and A3, respectively. The change in length of the specimen after the test was found to be 1.0%, 2.2% and 1.0% for specimen A1, A2, and A3, respectively. The tensile stress for A1 was close to the yield strength of the bar (e.g., 140 ksi) and it is possible that this specimen experienced some inelastic deformation. The stress values for the other two samples (A2 and A3) were lower than the yield strength. Therefore, specimens A2 and A3 would have essentially remained elastic during testing

Table 21. Dimension Measurements: TiABs with Coupler 'A'

Specimen	$D_{Initial}$ (in.)	$L_{Initial}$ (in.)	L_{Final} (in.)	D_{final} (in.)			
				D_{final_1}	D_{final_2}	D_{final_3}	$D_{final\_average}$
A1	0.625	50.250	50.750	0.620	0.622	0.623	0.622
A2	0.750	50.188	51.250	0.736	0.738	0.741	0.738
A3	1.500	51.375	51.750	1.500	1.500	1.500	1.500

Table 22. Tensile Test Results: TiABs with Coupler 'A'

Specimen	Diameter (in.)	Max Load (lbf)	Stress Value (psi)	Failure Mode
A1	0.625	44,040	142,065	Pullout
A2	0.750	58,020	131,864	Pullout
A3	1.500	160,485	90,823	Pullout

The Stress-Displacement plots are presented in Figure 74 through Figure 76. Coupler 'A' was not able to withstand the full tensile capacity of the rebar due to premature failure (e.g., pullout).

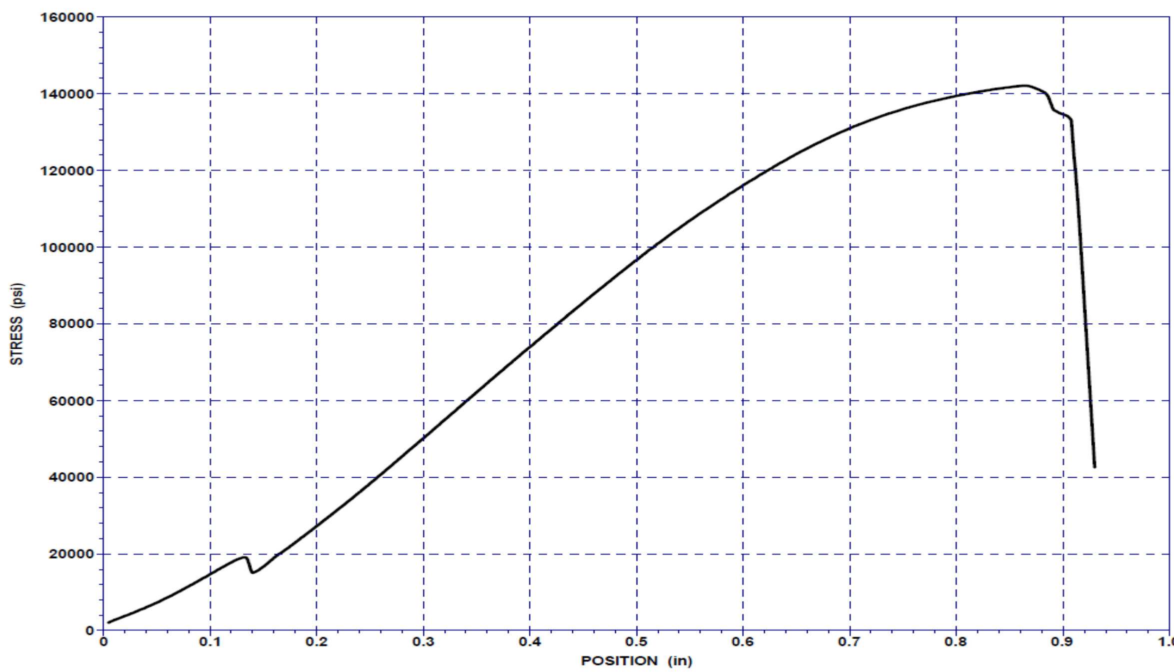

Figure 74. Stress-Displacement Plot for A1

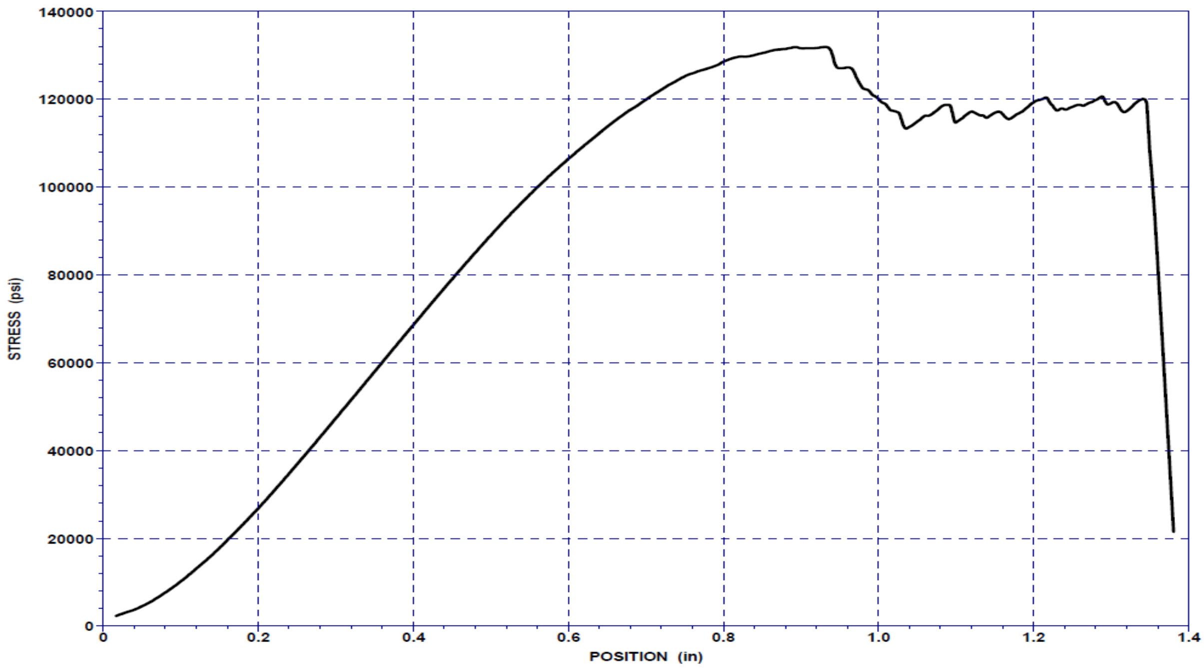

Figure 75. Stress-Displacement Plot for A2

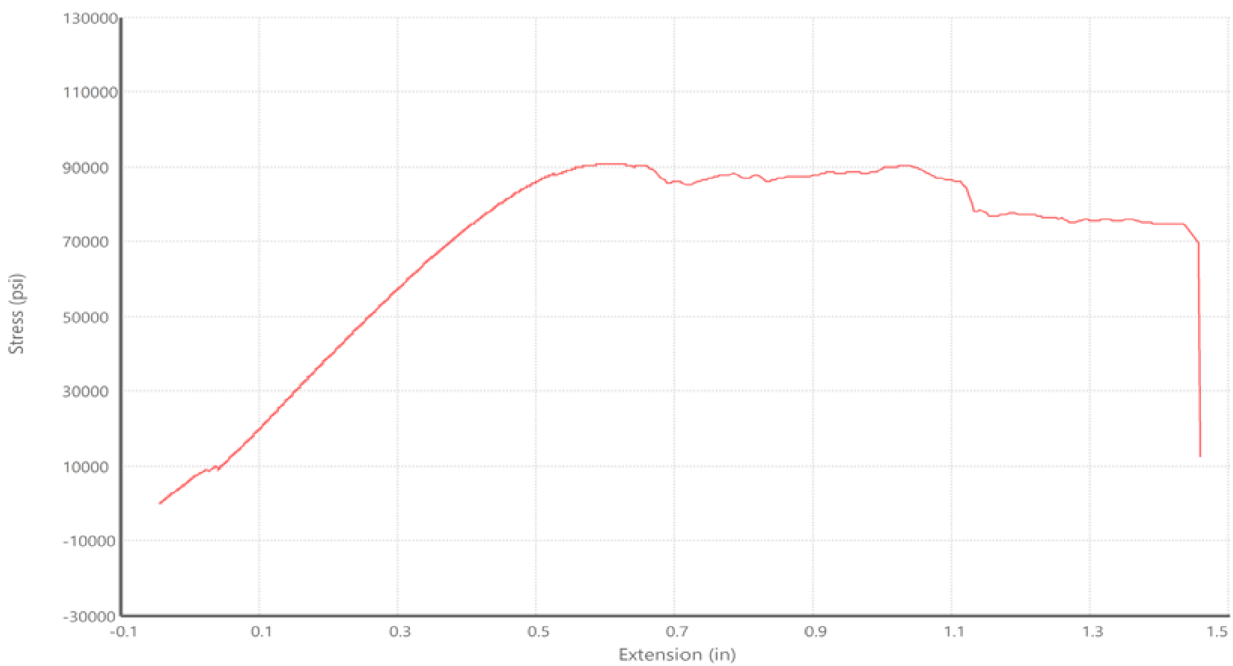

Figure 76. Stress-Displacement Plot for A3

6.4.3 *Coupler 'B'*

Testing showed that both spliced specimens were not able to withstand the full tensile capacity of TiABs and the coupler failed instead of TiABs. However, Coupler 'B' was successful in gripping the pseudo-threaded TiABs which avoided a pullout failure. Both specimens fractured in the middle of the coupler (Figure 77), where the stress was the highest as the load was transferred from one TiABs to the other. The coupler failure showed that the swaged portions were effective in gripping the pseudo-threaded TiABs. The coupler material was able to form around the machined deformations well during the swaging process. If this was not the case, the failure mode would have been a pullout failure.

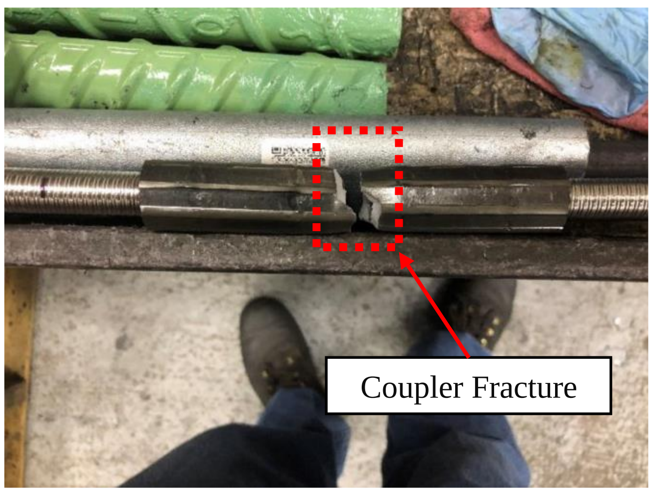

Figure 77. Coupler Fracture for TiABs with Coupler 'B'

Results from testing of TiABs spliced with Coupler 'B' are presented in Table 23 and Table 24. The change in diameter of the specimen after the test was found to be 0.2% and 0.4% for specimen B1 and B2, respectively. The change in diameter for both specimens is minimal because of the fracture of the coupler prior to bar yielding. The change in length of the specimen after the test was found to be 0.2% and 1.2% for specimen B1 and B2, respectively. As it can be observed, specimen B1 failed very close to the yield point of a TiAB. It is likely that specimen B2 yielded as it experienced a stress value (e.g., 145 ksi) which is in excess of the minimum yield strength for a typical TiAB (140 ksi)

Table 23. Dimension Measurements: TiABs with Coupler 'B'

Specimen	$D_{Initial}$ (in.)	$L_{Initial}$ (in.)	L_{Final} (in.)	D_{final} (in.)			
				D_{final_1}	D_{final_2}	D_{final_3}	$D_{final\_average}$
B1	0.625	50.125	50.250	0.622	0.623	0.626	0.624
B2	0.750	50.313	50.938	0.745	0.748	0.748	0.747

Table 24. Tensile Test Results: TiABs with Coupler 'B'

Specimen	Diameter (in.)	Max Load (lb.)	Stress Value (psi)	Failure Mode
B1	0.625	43,190	139,323	Coupler Fracture
B2	0.750	63,860	145,136	Coupler Fracture

Figure 78 and Figure 79 present the stress-displacement plots for specimens B1 and B2, respectively.

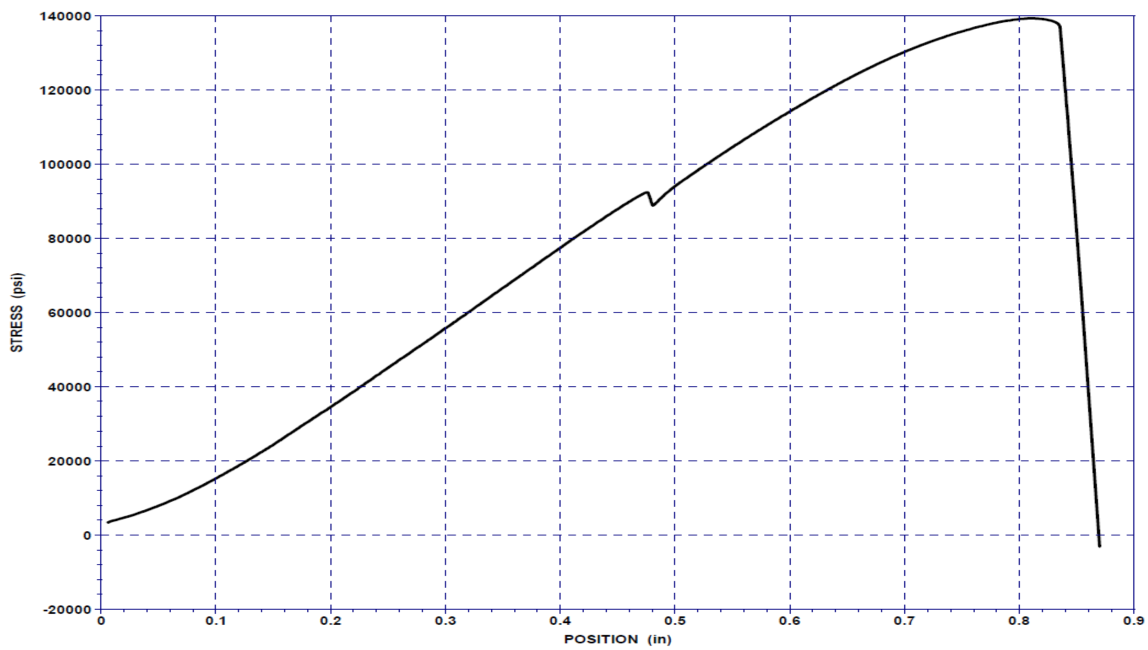

Figure 78. Stress-Displacement Plot for B1

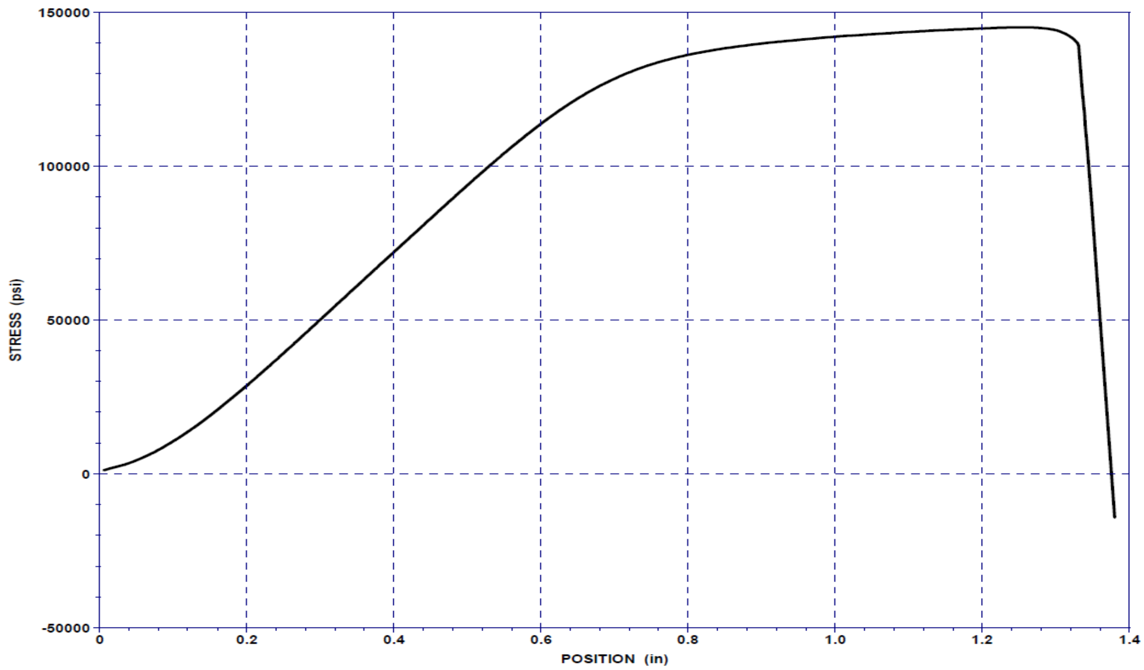

Figure 79. Stress-Displacement Plot for B2

6.4.4 *Coupler 'C'*

The specimens spliced with Coupler 'C' performed exceptionally well during tensile testing. All specimens except one (C2) had a bar fracture failure. The failure of the bar was away from the splice region as can be observed in Figure 80 (a & b). Specimen C2 which was a #5 TiABs had a thread strip failure as shown in Figure 80 (c) which indicates that the test pushed the coupler material very close to its limits. Yet, the other two #5(0.625 in. diameter) spliced specimens had bar break. Since the thread strip failure occurred in only one specimen, and the larger bar (e.g., #6) did not have this type of failure can be argued that the failure could have been associated with sample preparation or any existing deficiency in the coupler threads.

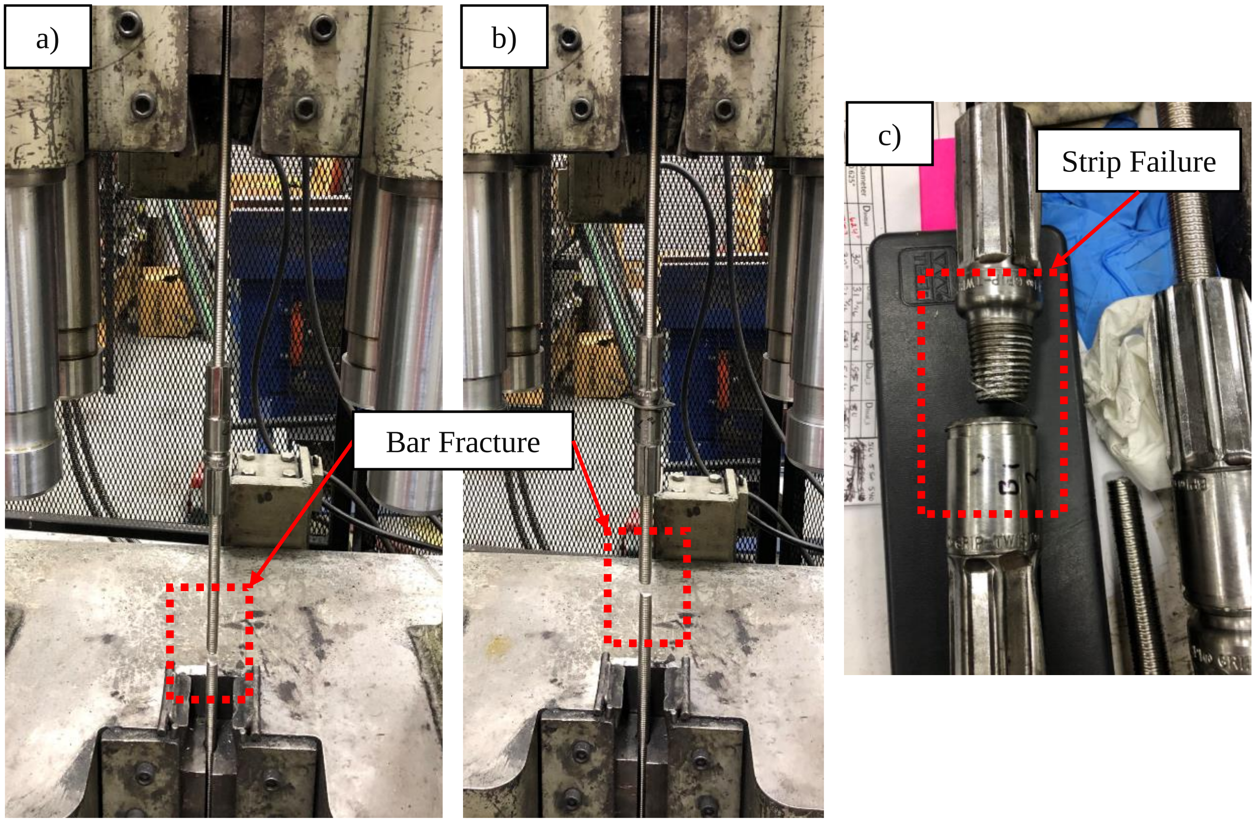

Figure 80. Failure Mode of TiABs with Coupler 'C': a) #5 TiABs (Ø 0.625"), b) #6 TiABs (Ø 0.75"), c) #5 TiABs (Ø 0.625") with Strip Failure

Results from testing are presented in Table 25 and Table 26. The change in diameter of the specimen with #5(0.625 in. diameter) TiABs, i.e., C1, C2 and C3 was found to be 8.6%, 1.0% and 8.0%, respectively. Specimen C2 had small change in the diameter because of the thread strip failure. The change in the diameter of the specimen with #6(0.75 in. diameter) TiABs, i.e., C4, C5 and C6 was found to be 8.7%, 8.8% and 9.5%, respectively.

The change in length of the specimen with #5(0.625 in. diameter) TiABs, i.e., C1, C2 and C3 was found to be 3.3%, 1.2% and 2.7%, respectively. Similarly, the change in length of the specimen with #6(0.75 in. diameter) TiABs, i.e., C4, C5 and C6 was found to be 3.2%, 3.0% and 3.0%, respectively.

Table 25. Dimension Measurements: TiABs with Coupler 'C'

Specimen	$D_{Initial}$ (in.)	$L_{Initial}$ (in.)	L_{Final} (in.)	D_{final} (in.)			
				D_{final_1}	D_{final_2}	D_{final_3}	$D_{final\_average}$
C1	0.627	52.813	54.563	0.570	0.572	0.578	0.573
C2	0.627	52.875	53.500	0.620	0.621	0.621	0.621
C3	0.627	52.875	54.313	0.570	0.572	0.588	0.577
C4	0.750	53.000	54.688	0.676	0.681	0.698	0.685
C5	0.750	52.875	54.438	0.676	0.685	0.692	0.684
C6	0.750	53.000	54.375	0.672	0.681	0.683	0.679

Table 26. Tensile Test Results: TiABs with Coupler 'C'

Specimen	Diameter (in.)	Max Load (lbf)	Stress Value (psi)	Failure Mode
C1	0.625	48,680	157,035	Bar Break
C2	0.625	49,260	158,917	Thread Strip
C3	0.625	49,270	158,950	Bar Break
C4	0.750	67,840	154,187	Bar Break
C5	0.750	67,660	153,776	Bar Break
C6	0.750	67,490	153,393	Bar Break

Figure 81 through Figure 88 present testing results for the samples with Coupler 'C'.

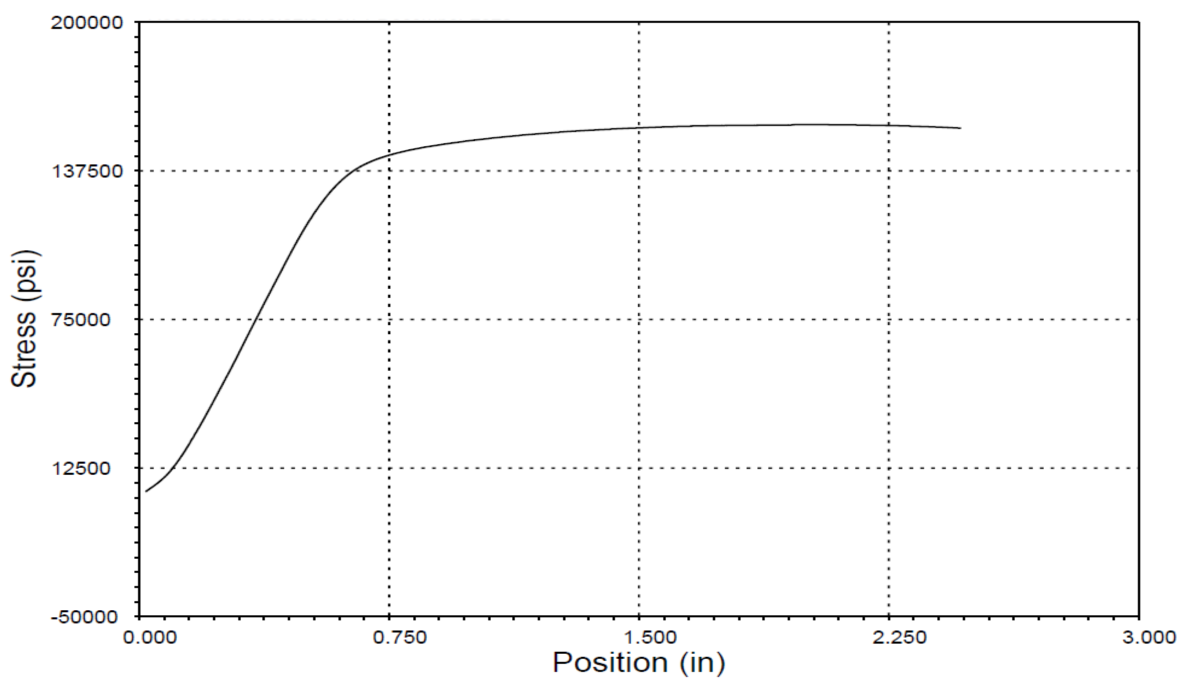

Figure 81. Stress-Displacement Plot for C1

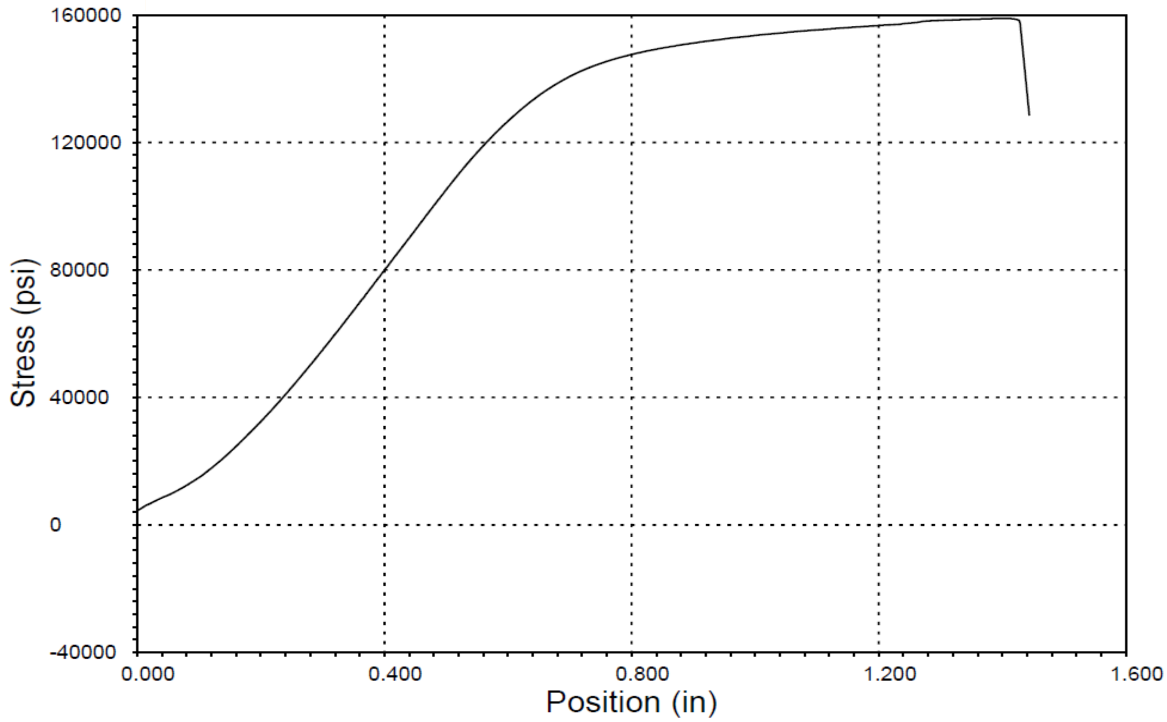

Figure 82. Stress-Displacement Plot for C2

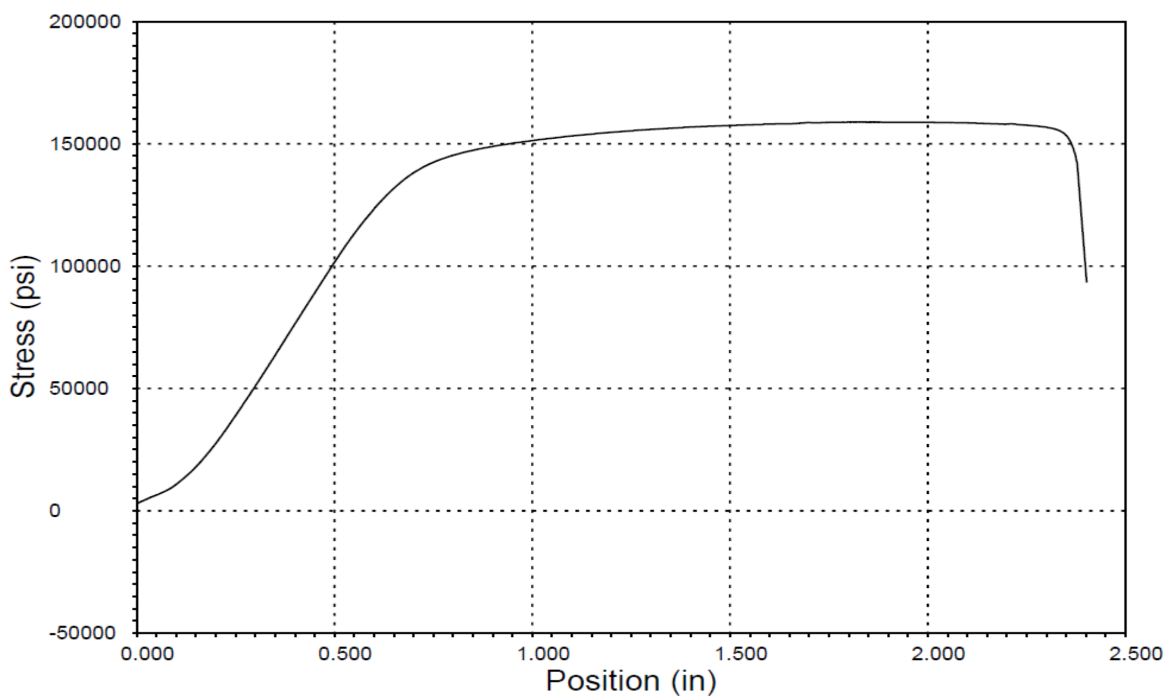

Figure 83. Stress-Displacement Plot for C3

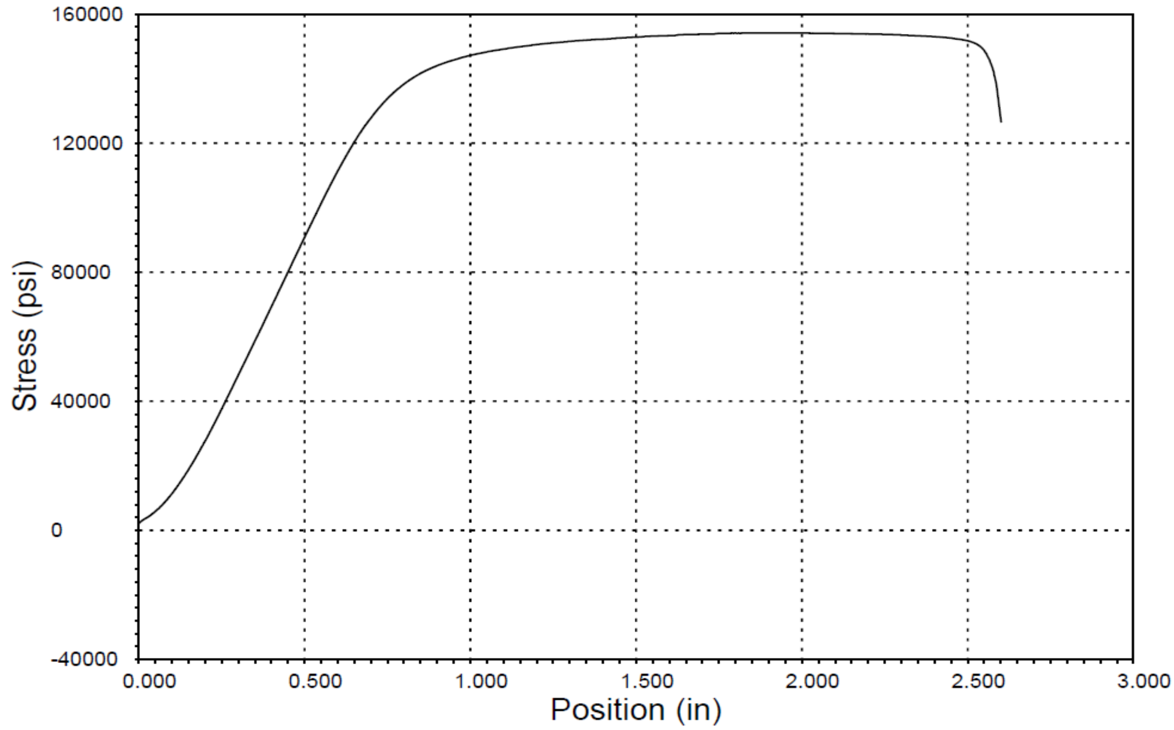

Figure 84. Stress-Displacement Plot for C4

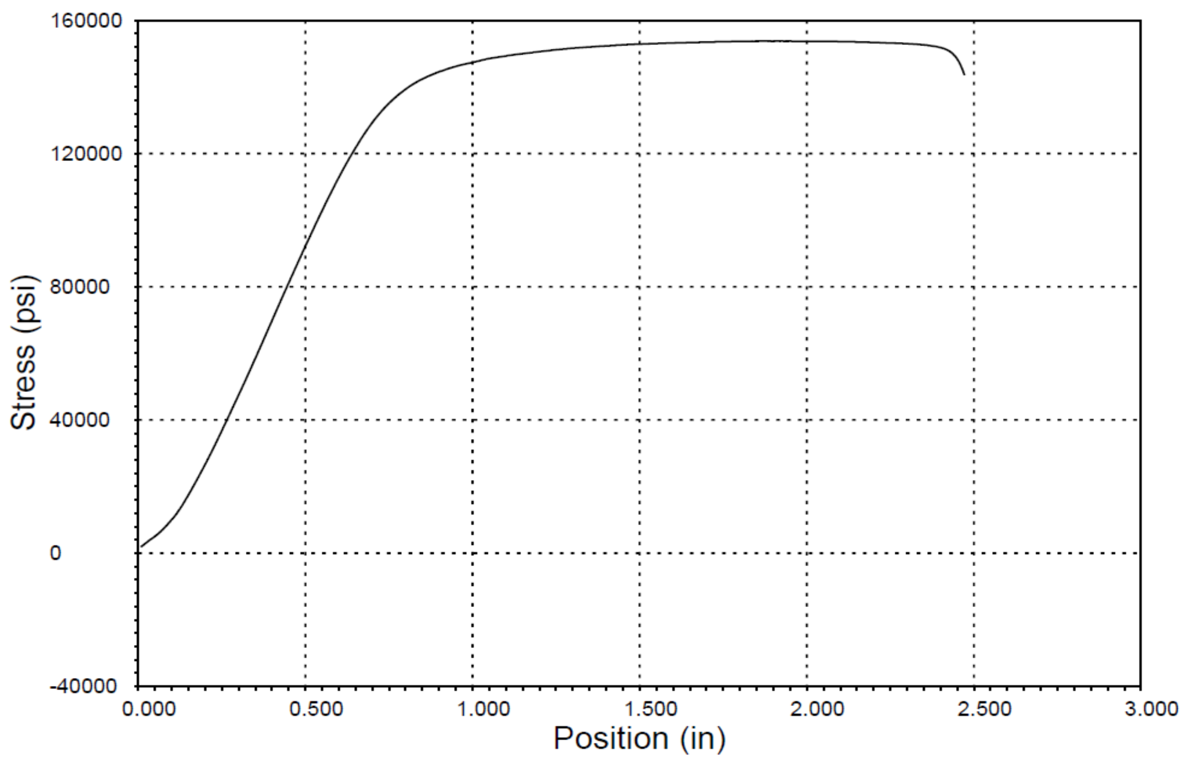

Figure 85. Stress-Displacement Plot for C5

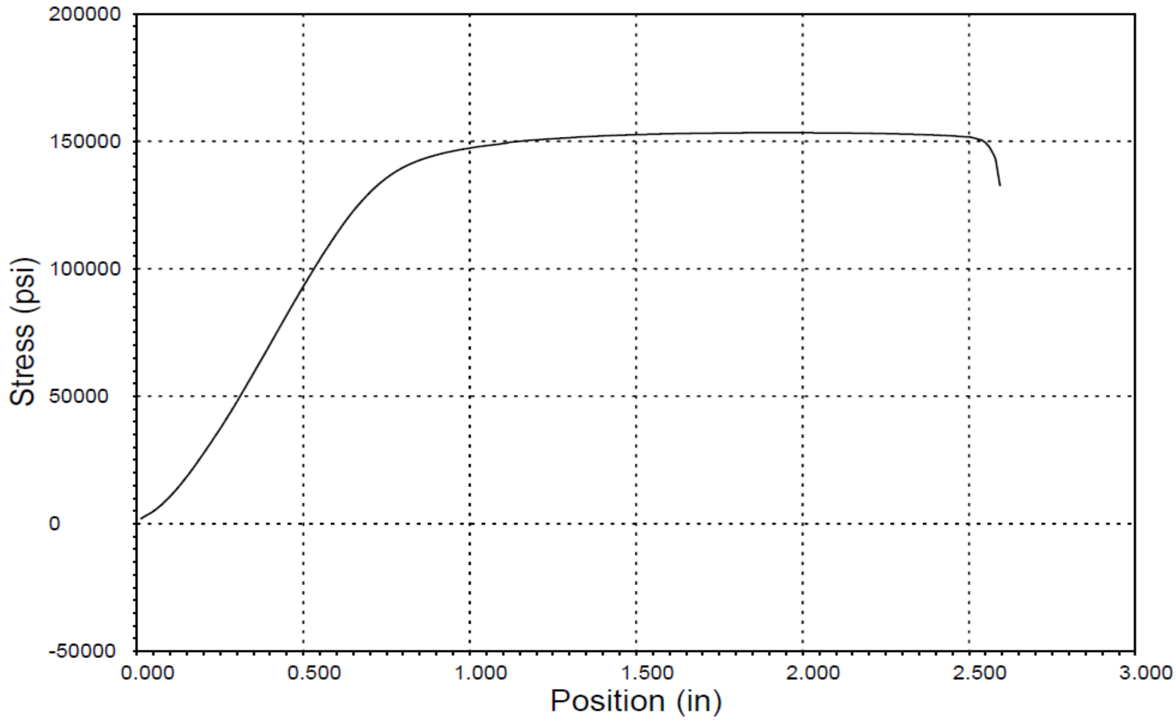

Figure 86. Stress-Displacement Plot for C6

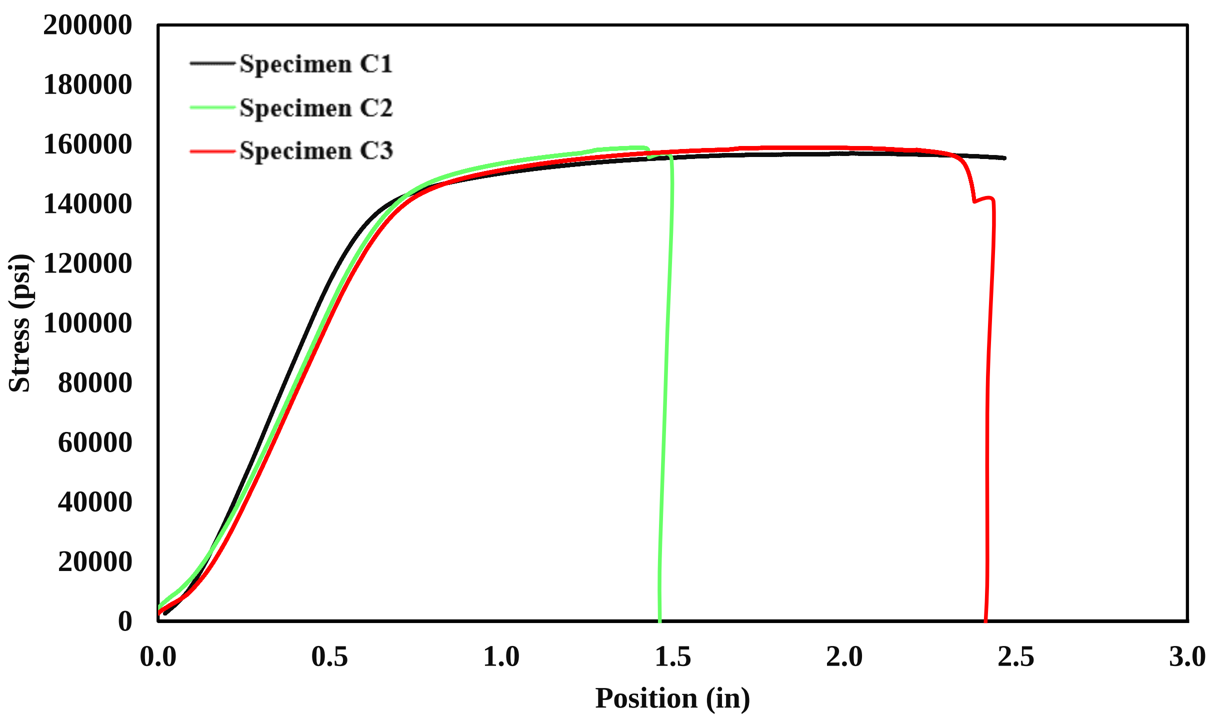

Figure 87. Comparison of Stress-Displacement Plot for #5 TiABs (Ø 0.625 in.) with Coupler 'C'

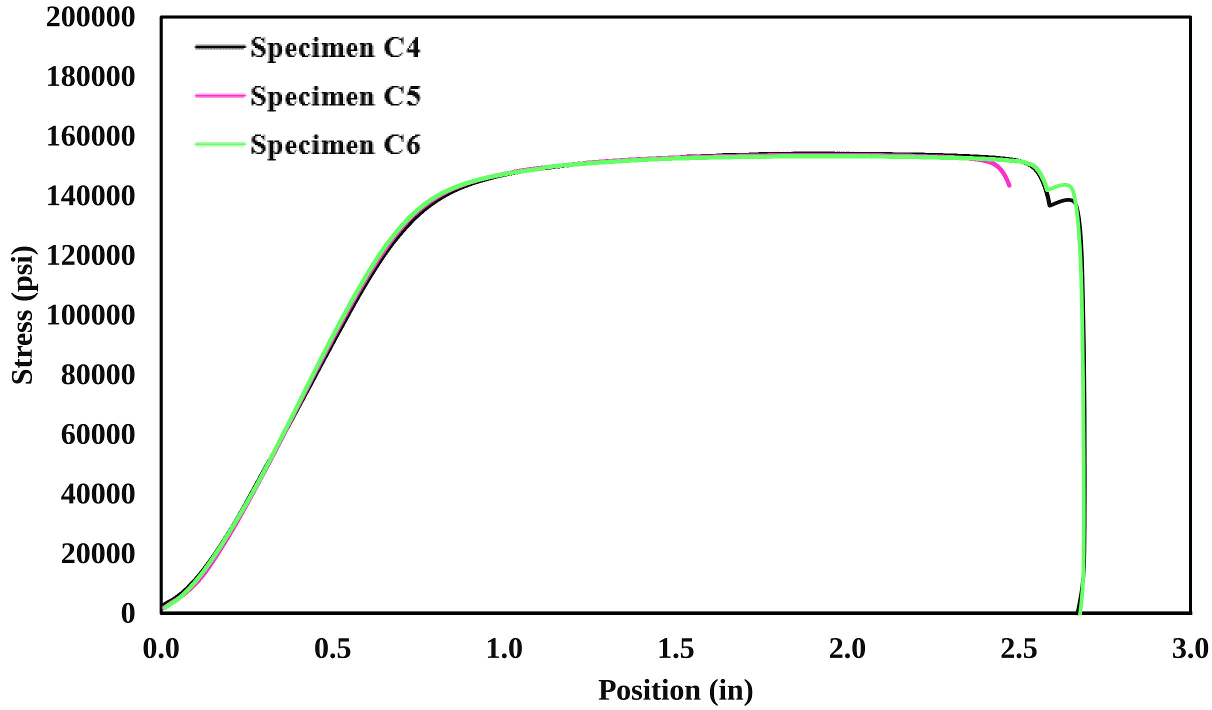

Figure 88. Comparison of Stress-Displacement Plot for #6 TiABs (Ø 0.75 in.) with Coupler 'C'

Coupler 'C' was successful in pushing the failure away from the mechanical coupler to the bar. Since Coupler 'C' proved to be an appropriate mechanical coupler for splicing pseudo-threaded TiABs, it was also investigated for the AASHTO LRFD requirements [25]. According to AASHTO LRFD, when tested to failure, spliced specimens should achieve more than 125% of the yield strength of the bar (125% f_y) or 125% of 140,000 psi. Experimentally, tensile strength of splice system was about 112% on average of the specified yield strength of the bar. And this can be acceptable because, normal steel, which is used to make coupler, goes to strain hardening. However, as far as TiABs are concerned, they do not carry a large overstrength (strain hardening) factor compared to normal or high strength rebars. TiABs have an elastic-perfectly plastic type of behavior under tensile loads. Their overstrength factor is generally about 1.1 compared to 1.5 or similar for normal rebars. Therefore, the research concludes that Coupler 'C' would be one of the choices for mechanical splicing of TiABs.

6.5 Summary

- Mechanical splices are preferred over the lap splices for TiABs. This would result in savings in materials costs.
- Tensile testing of TiABs using three mechanical splice system produced by Producer 'X' in the United States were carried out in accordance with relevant ASTM and AASHTO LRFD requirements. The coupler systems were named 'A', 'B', 'C'.
- Mainly #5 and # 6 TiABs with pseudo threads were investigated.
- Coupler's 'A' and 'B' were not effective in splicing of TiABs. Coupler 'A' had pullout failures while Coupler 'B' failed in tension.
- Coupler 'C' was effective in splicing of #5 and #6 TiABs. All samples developed their capacity and failed outside the coupling region, except one sample that was #5 and had a strip thread failure in the coupler region.
- Coupler 'C' proved to be an appropriate mechanical coupler for splicing of pseudo-threaded TiABs. The coupler was successful in pushing the failure away from the mechanical coupler region and in to the TiABs.
- Tensile strength of splice system with Coupler 'C' was in close compliance with AASHTO LRFD Requirement for spliced specimens to achieve more than 125% of the yield strength of the bar (125% f_y). Given the lower strain hardening of TiABs, Coupler 'C' can be used to splice TiABs in tension zones.

CHAPTER 7. CONCLUSIONS AND RECOMMENDATIONS

Recently, TiABs have emerged as a new advanced material in the civil engineering industry. TiABs have been used in retrofitting of concrete bridges in the United States. Due to lower maintenance cost, TiABs have proved to be less expensive than other materials in terms of life-cycle costs over a span of 50 years or more when it comes to retrofitting of existing bridges. Great corrosion resistance, high strength to weight ratio, flexibility, ductility, and composite compatibility features of TiABs make them a potential material for construction of new structures in seismic and corrosive environments. In this research, a new bridge pier system was introduced that incorporated both seismic resiliency and durability in a single package. The research introduced TiABs for flexural and transverse reinforcing in bridge piers and focused on its application on construction of structures located in seismic and corrosive environment.

A large-scale cantilever bridge pier reinforced with TiABs rebars and spirals was tested under quasi-static cyclic loading protocol to demonstrate seismic resiliency of TiABs, and results were compared against a benchmark specimen reinforced with normal rebars and spirals. The design of the cast-in-place cantilever pier followed the AASHTO LRFD Design Specifications to the extent possible. Both piers were tested up to failure points. The hysteresis plots showed that steel reinforced pier had fatter loop and more area of loop compared to the TiABs reinforced pier which had pinched hysteresis. TiABs have a lower overstrength factor compared to normal rebars which reduces construction and materials cost for the capacity protected elements (e.g., footing, cap beam etc.). The pier reinforced with TiABs outperformed the pier reinforced with normal steel rebars in terms of ultimate ductility. The yield displacement for TiABs reinforced pier was 71.6% higher compared to the pier reinforced with normal rebars (benchmark). However, the base shear for the pier reinforced with TiABs at yield was 58% lower compared to the benchmark. The ultimate displacement for TiABs reinforced pier was 66% higher compared to benchmark pier, however, the ultimate base shear was 76% lower compared to the benchmark pier. The pier with TiABs had lower overstrength factor (1.32) compared to the benchmark (1.48). The displacement ductility at the ultimate base shear and failure points, were 4.56 and 8.82 for the pier with TiABs, and 5.52 and 7.40 for the benchmark pier, respectively.

The total energy dissipated for the pier reinforced with TiABs and pier reinforced with steel rebar were 210.29 kJ and 455.7 kJ, respectively. The total dissipated energy for steel reinforced pier was 54% higher than TiABs reinforced pier, but the pier with TiABs achieved larger number of inelastic cycles. For both piers, more energy was dissipated with increasing drift ratios; however, first loop of cycle dissipated more energy than second loop of cycle which indicated the strength degradation of the pier. The plastic hinge length obtained to be 23.57 in. (1.3 times the diameter) for the pier reinforced with TiABs and 13.67 in. (0.76 times the diameter) for the benchmark specimen. The distribution of curvature along the height for both piers showed that yielding occurred in plastic hinge region of the pier, and the height above the plastic hinge zones remained essentially elastic

Observations from testing showed that the cracks, spalling of the concrete and non-linear deformation occurred mostly at the plastic hinge region for both piers. The pier with TiABs had a gap opening at the base of the pier with considerable bond-slip in the smooth TiABs. The benchmark specimen had more distributed cracks in the plastic hinge zone and performed similar to what can be expected from a well seismically detailed pier. Testing results showed lesser residual drifts of the pier with TiABs. At large drifts, TiABs reinforced pier had almost half of the residual drift of that with steel reinforced pier.

TiABs have less modulus of elasticity compared to normal rebars. The lower modulus of elasticity means that during smaller earthquakes, TiABs would not yield, and would have fewer flexural cracks in the plastic hinge region. Presence of flexural cracks should not be a durability issue for TiABs as they offer excellent corrosion resistance.

In the second part of the research, in order to keep the quantity of TiABs limited (due to their higher cost), tensile testing of spliced TiABs were performed to identify and explore suitability of some available splicing systems for TiABs. Three different coupler systems from Producer ‘X’ in the United States were investigated. One of these systems, Coupler ‘C’, proved to be an appropriate mechanical coupler for splicing of #5 and #6 TiABs with pseudo threads. The coupler was successful in pushing the failure away from the mechanical coupler to the bar. The coupler was close to satisfy the current requirements from AASHTO (e.g., 125% of yield strength)

Based on the results of the testing, TiABs have good potential for applications in civil infrastructure. However, further investigation into the use and performance of TiABs in concrete structures is needed. Some of the recommended research topics for future studies are:

1) Analytical and finite element modeling of the pier reinforced with TiABs.
2) Repeating the testing in this research with pseudo-threaded TiABs instead smooth bars. This can improve energy dissipation and seismic performance (e.g., less bond-slip and rocking).
3) Establishing strain limits for damage control and serviceability of the bridge piers reinforced with TiABs.
4) Performance-based seismic design of bridges reinforced with TiABs.
5) Shake table testing to study the dynamic behavior of piers reinforced with TiABs.
6) Splicing of TiABs with other couplers and under tension/compression cyclic loads.
7) Galvanic corrosion of TiABs when in contact with high strength steel alloys (e.g., mechanical couplers)

8) Identifying appropriate retrofitting solutions for structures reinforced with TiABs in seismic regions.
9) Behavior of TiABs and the effect of rebar size on ductility and bond-slip.
10) Loss assessment and life cycle cost for bridges reinforced with TiABs.
11) Bond properties and behavior of TiABs with concrete under cyclic loading.
12) Development of guidelines and analytical models for structures incorporating TiABs.

REFERENCES

[1] Tazarv M, Saiidi MS. Reinforcing NiTi Superelastic SMA for Concrete Structures. *Journal of Structural Engineering* 2014; 141 (8): 10 pp.

[2] M. Mashal, "*Post-Tensioned Earthquake Damage Resistant Technologies for Accelerated Bridge Construction*," PhD. Dissertation, Civil Engineering, University of Canterbury, Christchurch, New Zealand, 2015.

[3] Tazarv M, Alam MS. Shape Memory Alloy for Bridge Columns. *Proceedings of the 11th National Conference in Earthquake Engineering*, Earthquake Engineering Research Institute, Los Angeles, CA. 2018.

[4] R. DesRoches, J. McCormick, M. Delemont. *Cyclic properties of superelastic shape memory alloy wires and bars,* J. Struct. Eng., 130 (2004), pp. 38-46.

[5] NCHRP Project 12-101 Appendix A

[6] Li, V.C. (2008). "Engineered Cementitious Composites (ECC): Material, Structural, and Durability Performance," in Concrete Construction Engineering Handbook, Chapter 24, Ed. E. Nawy: published by CRC Press.

[7] ACI 440.1R-06. (2006). "Guide for the Design and Construction of Structural Concrete Reinforced with FRP Bars," Reported by American Concrete Institute Committee 440, Farmington Hills, MI.

[8] R. Khadka. "*Mechanical and Bond Testing of Titanium Alloy Bars: Comparison with Steel*," M.S. Thesis, Department of Civil and Environmental Engineering, Idaho State University, USA, 2019.

[9] Adkins, J., and George, W. (2017). "Titanium Finds a Home in Civil Engineering." Concrete International, 39(12), 51–55.

[10] TxDOT Volume 44, Issue 3, May/June 2020, pg 16-17

[11] M. Lostra, "Seismic Performance of Square Reinforced Concrete Columns Retrofitted with Titanium Alloy Bars," M.S. Thesis, School of Civil and Construction Engineering, Oregon State University, USA, 2016.

[12] C. Higgins, D. Amneus, L. Barker, "Methods for Strengthening Reinforced Concrete Bridge Girders Containing Poorly Detailed Flexural Steel Using Near-Surface Mounted Metallics," Final Report to Oregon Dept. of Transportation, Report No. FHWA-OR-RD-16-02, 2015.

[13] C. Higgins, J. Knudtsen, D. Amneus, L. Barker, "Shear and Flexural Strengthening of Reinforced Concrete Beams with Titanium Alloy Bars". *Proceedings of the 2nd World Congress on Civil, Structural, and Environmental Engineering*, Barcelona, Spain, April 2-4, 2017.

[14] ASCE Infrastructure Report Card. 2017. Available at: *https://www.infrastructurereportcard.org/*

[15] Pampanin, S., Marriot, D., and Palermo, A. (2010). *PRESSS Design Handbook*. New Zealand Concrete Society (NZCS) Incorportaion.

[16] ACI 374.2R-13. (2013). "Guide for Testing Reinforced Concrete Structural Elements under Slowly Applied Simulated Seismic Loads," Reported by American Concrete Institute Committee 374, Farmington Hills, MI.

[17] M. Corey. "*A Precast Pier System for Accelerated Bridge Construction in Seismic Zones*," M.S. Thesis, Department of Civil and Environmental Engineering, Idaho State University, USA, 2020.

[18] ASTM. (2007). "*Standard Practice for Making and Curing Concrete Test Specimens in the Laboratory*." ASTM C192/C192M-07, West Conshohocken, PA.

[19] ASTM. (2019). "*Standard Test Method for Compressive Strength of Cylindrical Concrete Specimens*." ASTM C39/C39M-20, West Conshohocken, PA.

[20] ASTM. (2017). "*Standard Test Method for Splitting Tensile Strength of Cylindrical Concrete Specimens.*" ASTM C496/C496M-17, West Conshohocken, PA.

[21] FEMA. (2009). "*Quantification of Building Seismic Performance Factors: Component Equivalency Methodology*." FEMA P-795, Prepared By: Applied Technology Council, Redwood City, CA.

[22] Caltrans. (2013). "*Seismic Design Criteria-Version 1.7. Caltrans*." California Department of Transportation, Sacramento, CA.

[23] Priestley, M. J. N., Calvi, G. M., and Kowalsky, M. J. (2007). "*Displacement-Based Seismic Design of Structures*." Earthquake Spectra, IUSS Press.

[24] ASTM. (2005). "*Standard Test Methods for Testing Mechanical Splices for Steel Reinforcing Bars*." ASTM A 1034/A 1034M-05, West Conshohocken, PA.

[25] AASHTO LRFD. (2017). "*American Association of State Highways and Transportation Officials LRFD Bridge Design Specifications, 8th Edition*." AASHTO LRFD, Washington, DC.

[26] ASTM. (2020). "*Standard Test Methods and Definitions for Mechanical Testing of Steel Products*." ASTM A 370-20, West Conshohocken, PA.

[27] ASTM. (2016). "*Standard Test Methods for Tension Testing of Metallic Materials*." ASTM E8/E8M-16ae1, West Conshohocken, PA.

[28] Saiidi, M.S., O'Brien, M., and Mahmoud, S. (2009). "*Cyclic Response of Concrete Bridge Columns using Superelastic Nitinol and Bendable Concrete.*" ACI Structural Journal, 106 (1): 69-77.

[29] Wang, H., Saiidi, M.S. (2005). "*A Study of RC Columns with Shape Memory Alloy and Engineered Cementitious Composites.*" ScholarWorks, University of Nevada, Reno, Report No. CCEER-05-1.

[30] Ruchin, K., Mustafa, M., Jared, C., (2020). "*Experimental Investigation on Mechanical Properties of Titanium Alloy Bars: Comparison with High-Strength Steel*." ACI Materials Journal, 341: 160-187.

[31] S. Shrestha, "*Seismic Retrofit of Square Reinforced Concrete Bridge Columns using Titanium Alloy Bars*," PhD. Dissertation, Civil Engineering, Oregon State University, United States, 2019.

[32] ASCE Infrastructure Report Card. 2021. Available at: *https://www.infrastructurereportcard.org/*

APPENDIX A: Moment Capacity of Pier Reinforced with Steel Rebar

Column steel						
Diameter of column =	18	in				
Cover =	1.5	in				
Dia of Stirrups (#3) =	0.375	in				
Dia of Longitudional Bars (#6) =	0.75	in				
Ds =	13.5	in				
Ag =	254.4690049	in2				
fy =	60	ksi				
f'c =	4	ksi				
Es =	29000	ksi				
b = Ag/0.80h =	17.67145868	in				
0.80h =	14.4	in				
2/3 Ds =	9	in				
Cover for rectangular =	2.7	in				

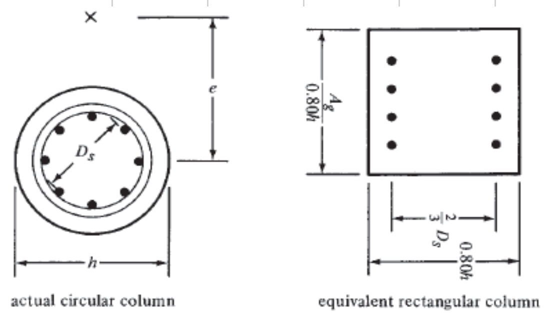

FIGURE 10.9 Replacing a circular column with an equivalent rectangular one.

Strain in left end:	0.002					
Strain in right end:	-0.003					
c =	8.64	in				
ε's =	0.0020625	>	fy/E =	0.002069		
				So, Yields		
εs =	0.00140209					
		So, Does not yield				
	So,	Φ =	0.65	(Tied columns)		
A's (6#6 on top and 6#6 on bottom) =	2.650718801	in2				
a = 0.85c =	7.344	in				
Cc =0.85ab f'c =	-441.249255	k	@	8.028	in	from Ts
C's =f'sA's - 0.85A's f'c =	-150.030684	k	@	9	in	from Ts
Ts = εs Es As =	107.7798388	k				

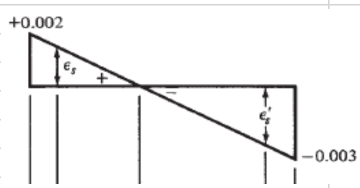

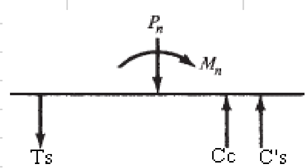

By Statics,						
Pn =	483.5000999	k	@	4.5	in	from Ts
Mn =	2716.874723	k-in				
	226.4062269	k-ft				
ΦMn =	147.1640475	k-ft				

APPENDIX B: Moment Capacity of Pier Reinforced with TiABs

Column Titanium							
Diameter of column =	18	in					
Cover =	1.5	in					
Dia of Stirrups (#3) =	0.375	in					
Dia of Longitudinal Bars (#6) =	0.75	in					
Ds =	13.5	in					
Ag =	254.4690049	in2					
fy =	140	ksi					
f'c =	4	ksi					
Es =	15500	ksi					
b = Ag/0.80h =	17.67145868	in					
0.80h =	14.4	in					
2/3 Ds =	9	in					
Cover for rectangular =	2.7	in					
Strain in left end:	0.002						
Strain in right end:	-0.003						

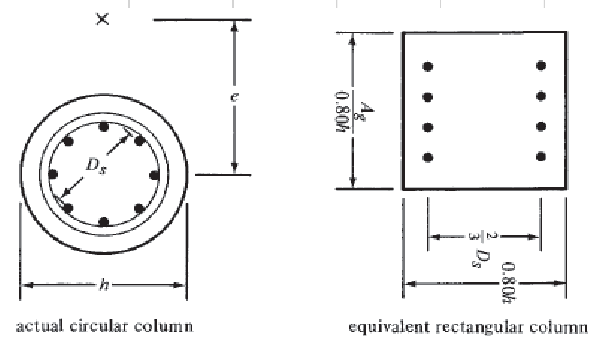

FIGURE 10.9 Replacing a circular column with an equivalent rectangular one.

c =	8.64	in					
ε's =	0.0020625	>	fy/E =	0.009032			
				So, Yields			
εs =	0.00140209						
		So, Does not yield					
	So,	Φ =	0.65	(Tied columns)			
A's (3.5#6 on top and 3.5#6 on bottom) =	1.546252634	in2					
a = 0.85c =	7.344	in					
Cc =0.85ab f'c =	-441.249255	k	@	8.028	in	from Ts	
C's =f'sA's - 0.85A's f'c =	-211.21811	k	@	9	in	from Ts	
Ts = εs Es As =	33.60377158	k					

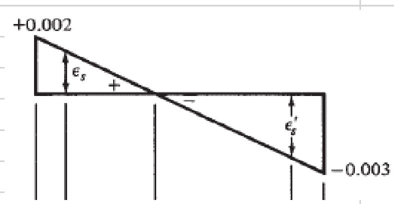

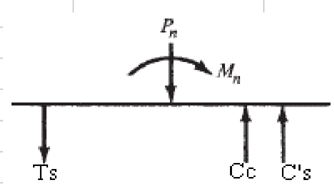

By Statics,							
Pn =	618.8635928	k	@	4.5	in	from Ts	
Mn =	2658.425836	k-in					
	221.5354864	k-ft					
ΦMn =	143.9980661	k-ft					
So, USE 7 #6 Titanium Bars							

APPENDIX C: Experimental Results for Compressive and Tensile Strength: Footing

28-Days cylinder test:

	Diameter/ in			Average Dia/in.	Area/ in2	Force/ lbs	Compressive Strength/ psi	
A	3.991	3.980	3.986	3.985	12.473	69790	5595.13	
B	3.981	3.999	3.980	3.986	12.481	69380	5559.01	
C	3.971	4.004	3.980	3.985	12.470	70920	5687.15	
				Average Compressive Strength:			**5613.76**	**psi**
				Compressive Strength = P/A				

28-Days Split Cylinder:

	Diameter/ in			Average Dia/in.	Length/in	Force/ lbs	Tensile Strength/ psi	
A	5.944	5.970	5.954	5.956	12.000	32510	289.58	
				Average Split Tensile Strength:			**289.58**	**psi**
				Tensile Strength = 2P/pi*DL				

Test Day cylinder test:

	Diameter/ in			Average Dia/in.	Area/ in2	Force/ lbs	Compressive Strength/ psi	
A	3.991	4.022	3.973	3.995	12.534	80380	6412.99	
B	3.948	3.999	3.980	3.975	12.411	89860	7240.45	
C	3.952	3.964	3.991	3.969	12.370	86900	7024.91	
				Average Compressive Strength:			**6892.79**	**psi**
				Compressive Strength = P/A				

Test Day Split Cylinder:

	Diameter/ in			Average Dia/in.	Length/in	Force/ lbs	Tensile Strength/ psi	
A	5.940	6.055	5.989	5.995	12.100	48480	425.49	
				Average Split Tensile Strength:			**425.49**	**psi**
				Tensile Strength = 2P/pi*DL				

APPENDIX D: Experimental Results for Compressive and Tensile Strength: Column

28-Days cylinder test:

	Diameter/ in			Average Dia/in.	Area/ in2	Force/ lbs	Compressive Strength/ psi	
A	3.992	3.980	4.040	4.004	12.592	59840	4752.41	
B	3.980	3.999	3.975	3.985	12.470	63960	5129.02	
C	3.971	4.004	3.980	3.985	12.470	61140	4902.88	
				Average Compressive Strength:			**4928.10**	**psi**
				Compressive Strength = P/A				

28-Days Split Cylinder:

	Diameter/ in			Average Dia/in.	Length/in	Force/ lbs	Tensile Strength/ psi	
A	5.995	5.990	5.989	5.991	12.000	33211	294.07	
				Average Split Tensile Strength:			**294.07**	**psi**
				Tensile Strength = 2P/pi*DL				

Test Day cylinder test:

	Diameter/ in			Average Dia/in.	Area/ in2	Force/ lbs	Compressive Strength/ psi	
A	4.038	3.980	3.972	3.996	12.543	72170	5753.65	
B	4.021	4.028	3.975	4.008	12.616	73310	5811.04	
C	3.971	3.984	3.972	3.975	12.412	76090	6130.43	
				Average Compressive Strength:			**5898.37**	**psi**
				Compressive Strength = P/A				

Test Day Split Cylinder:

	Diameter/ in			Average Dia/in.	Length/in	Force/ lbs	Tensile Strength/ psi	
A	5.975	5.989	6.054	6.006	12.013	37540	331.25	
				Average Split Tensile Strength:			**331.25**	**psi**
				Tensile Strength = 2P/pi*DL				

APPENDIX E: Plastic Hinge Calculation

	(Plastic Hinge Calculation, Priestley et. Al. (2007))			
A) For TiABs				
	H =	78	inch	(Height of the pier)
	fy =	140	ksi	(Longitudinal bar yield strength)
	Fye =	154	ksi	(Fye = 1.1*longitudinal bar yield strength)
	d bl =	0.75	inch	(Diameter of longitudinal bar)
	So,			
	l sp =	17.33		$l_{sp} = 0.15 F_{ye} d_{bl}$
	Now,			
	Lp =	23.57	inch	(Plastic Hinge, $L_p = 0.08H + l_{sp}$
B) For 60 ksi steel rebar				
	H =	78	inch	(Height of the pier)
	fy =	60	ksi	(Longitudinal bar yield strength)
	Fye =	66	ksi	(Fye = 1.1*longitudinal bar yield strength)
	d bl =	0.75	inch	(Diameter of longitudinal bar)
	So,			
	l sp =	7.43		$l_{sp} = 0.15 F_{ye} d_{bl}$
	Now,			
	Lp =	13.67	inch	(Plastic Hinge, $L_p = 0.08H + l_{sp}$

APPENDIX F: Product Data Sheet: Coupler 'A'

BarSplice PRODUCTS INC.
A SUBSIDIARY OF FC INDUSTRIES INC.

DIMENSIONS AND DATA SHEET
INCH-POUND UNITS

Zap Screwlok®

ZAP SCREWLOK® TYPE 2 SERIES
UNCOATED & EPOXY

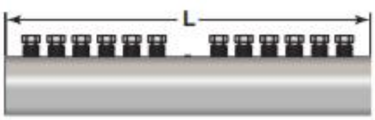

REBAR SIZE US [Metric]	ZAP TYPE 2* PRODUCT CODE BLACK	EPOXY	COUPLER WEIGHT (lb)	DIMENSIONS (in) LENGTH 'L'	'A'	'B'	'C'	'X'	NUMBER SCREWS PER BAR	AVERAGE SCREW TORQUE (ft-lbs)	MIN. IMPACT WRENCH RATING (ft-lbs)
#3 [10]	03ZBA	03ZEA	1.57	5	13/16	5/8	7/16	1 1/8	2	60	250
#4 [13]	04ZBA	04ZEA	2.19	7	1 1/16	11/16	1/2	1 3/8	3		
#5 [16]	05ZBA	05ZEA	3.38	9	1 1/8	3/4	5/8	1 5/8	4		
#6 [19]	06ZBA	06ZEA	4.68	11	1 3/16	15/16	11/16	1 3/4	5		
#7 [22]	07ZBA	07ZEA	7.64	13	1 1/4	1 1/16	13/16	2 1/16	5	105	500
#8 [25]	08ZBA	08ZEA	11.0	15 1/4	1 5/16	1 1/16	7/8	2 1/4	6		
#9 [29]	09ZBA	09ZEA	17.6	16 3/4	1 5/8	1 1/4	1 1/16	2 5/8	6	215	750
#10 [32]	10ZBA	10ZEA	21.5	19 1/8	1 11/16	1 7/16	1 1/8	2 3/4	7		
#11 [36]	11ZBA	11ZEA	25.5	21 1/2	1 13/16	1 1/2	1 1/4	2 15/16	8		
#14 [43]	14ZBA2	14ZEA2	37	18	2 5/16	1 3/4	1 1/2	3 3/4	10	350	1000
#18 [57]	18ZBA	18ZEA	79	29 1/2	2 1/2	2 3/8	1 7/8	4 1/2	21		

* GALVANIZED COUPLER ALSO AVAILABLE - SUBSTITUTE 'ZGA' FOR 'ZBA' IN PART CODE. ALL DIMENSIONS ARE APPROXIMATE

ZAP SCREWLOK® SL SERIES
UNCOATED & EPOXY

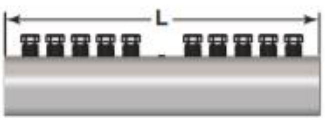

REBAR SIZE US [Metric]	ZAP SL* PRODUCT CODE BLACK	EPOXY	COUPLER WEIGHT (lb)	DIMENSIONS (in) LENGTH 'L'	'A'	'B'	'C'	'X'	NUMBER SCREWS PER BAR	AVERAGE SCREW TORQUE (ft-lbs)	MIN. IMPACT WRENCH RATING (ft-lbs)
#4 [13]	04SZBA	04SZEA	1.53	5	1 1/16	11/16	1/2	1 3/8	2	60	250
#5 [16]	05SZBA	05SZEA	2.59	7	1 1/8	3/4	5/8	1 5/8	3		
#6 [19]	06SZBA	06SZEA	3.78	9	1 3/16	15/16	11/16	1 3/4	4		
#7 [22]	07SZBA	07SZEA	6.27	10 3/4	1 1/4	1 1/16	13/16	2 1/16	4	105	500
#8 [25]	08SZBA	08SZEA	9.24	13	1 5/16	1 1/16	7/8	2 1/4	5		
#9 [29]	09SZBA	09SZEA	14.3	13 7/8	1 5/8	1 1/4	1 1/16	2 5/8	4	215	750
#10 [32]	10SZBA	10SZEA	18.3	16 1/2	1 11/16	1 7/16	1 1/8	2 3/4	5		
#11 [36]	11SZBA	11SZEA	22.4	19 1/8	1 13/16	1 1/2	1 1/4	2 15/16	6		
#14 [43]	14SZBA1	14SZEA1	33	15 3/8	2 5/16	1 3/4	1 1/2	3 3/4	8	350	1000
#18 [57]	18SZBA	18SZEA	63	23 1/2	2 1/2	2 3/8	1 7/8	4 1/2	16		

* GALVANIZED COUPLER ALSO AVAILABLE - SUBSTITUTE 'SZGA' FOR 'SZBA' IN PART CODE. ALL DIMENSIONS ARE APPROXIMATE

ZAP SCREWLOK® TRANSITIONS

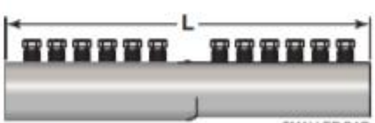

REBAR SIZE (US/US)	ZAP PRODUCT CODE TRANSITION*	COUPLER WEIGHT (lb)	DIMENSIONS (in) LENGTH 'L'	'A'	'B'	'C'	'X'	NUMBER SCREWS PER BAR	AVERAGE SCREW TORQUE (ft-lbs)	MIN. IMPACT WRENCH RATING (ft-lbs)
5/4	05/04ZBA	2.59	7	1 1/8	3/4	5/8	1 5/8	3	60	250
6/4 6/5	06/04ZBA 06/05ZBA	3.78	9	1 3/16	15/16	11/16	1 3/4	4		
7/5 7/6	07/05ZBA 07/06ZBA	6.27	10 3/4	1 1/4	1 1/16	13/16	2 1/16	4	105	500
8/5 8/6 8/7	08/05ZBA 08/06ZBA 08/07ZBA	9.24	13	1 5/16	1 1/16	7/8	2 1/4	5		
9/6 9/7 9/8	09/06ZBA 09/07ZBA 09/08ZBA	14.3	13 7/8	1 5/8	1 1/4	1 1/16	2 5/8	4	215	750
10/7 10/8 10/9	10/07ZBA 10/08ZBA 10/09ZBA	18.3	16 1/2	1 11/16	1 7/16	1 3/16	2 3/4	5		
11/7 11/8 11/9	11/07ZBA 11/08ZBA 11/09ZBA	18.3	16 1/2	1 13/16	1 1/2	1 1/4	2 3/4	5		
11/10	11/10ZBA	22.4	19 1/8	1 13/16	1 1/2	1 1/4	2 15/16	6		
14/9 14/10 14/11	14/09ZBA 14/10ZBA 14/11ZBA	33	15 3/8	2 5/16	1 3/4	1 1/2	3 3/4	8	350	1000
18/11 18/14	18/11ZBA 18/14ZBA	56	18 9/16	2 1/2	2 1/4	1 13/16	4 3/8	12		

* EPOXY & GALVANIZED TRANS. ALSO AVAILABLE - SUBSTITUTE 'ZEA' OR 'ZGA' FOR 'ZBA' IN PART CODE. ALL DIMENSIONS ARE APPROXIMATE

SINGLE ROW ZAP SCREWLOK® (SIZES #4 – #11) BEFORE AND AFTER ASSEMBLY

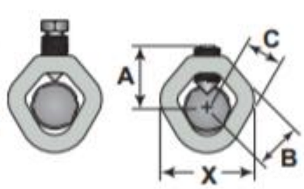

DOUBLE ROW ZAP SCREWLOK® (SIZES #14 – #18) BEFORE AND AFTER ASSEMBLY

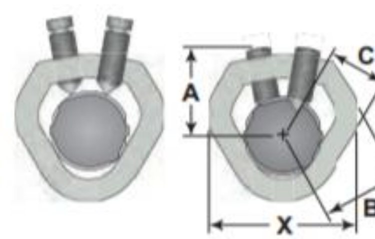

BarSplice PRODUCTS INC. A SUBSIDIARY OF FC INDUSTRIES INC.

DIMENSIONS AND DATA SHEET
INCH-POUND UNITS

Zap Screwlok®

ZAP STRUCTURAL CONNECTOR

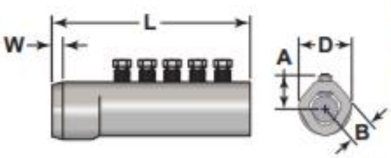

REBAR SIZE US [Metric]	ZAP PRODUCT CODE STR. CONNECTOR	COUPLER WEIGHT (lb)	DIMENSIONS (in) LENGTH 'L'	'A'	'B'	DIA. 'D'	'W'	NUMBER SCREWS PER BAR	AVERAGE SCREW TORQUE (ft-lbs)	MIN. IMPACT WRENCH RATING (ft-lbs)
#4 [13]	04SZSC	0.95	3 1/8	1 1/16	11/16	1 7/16	3/16	2	60	250
#5 [16]	05SZSC	1.53	4 1/8	1 1/8	3/4	1 5/8	1/4	3	60	250
#6 [19]	06SZSC	2.26	5 3/8	1 3/16	15/16	1 13/16	1/4	4	60	250
#7 [22]	07SZSC	3.66	6 3/8	1 1/4	1 1/16	2 1/16	3/8	4	105	500
#8 [25]	08SZSC	5.53	7 7/8	1 5/16	1 1/16	2 5/16	3/8	5	105	500
#9 [29]	09SZSC	8.19	8	1 5/8	1 1/4	2 5/8	7/16	4	215	750
#10 [32]	10SZSC	10.4	9 1/2	1 11/16	1 7/16	2 13/16	1/2	5	215	750
#11 [36]	11SZSC	12.9	11 1/8	1 13/16	1 1/2	2 15/16	9/16	6	215	750
#14 [43]	14SZSC	19.8	9 3/4	2 5/16	1 3/4	3 3/4	11/16	8	350	1000
#18 [57]	18SZSC	40	15 3/8	2 1/2	2 1/4	4 1/2	7/8	16	350	1000

ALL DIMENSIONS ARE APPROXIMATE

DOUBLE BARREL ZAP SCREWLOK®
UNCOATED & EPOXY

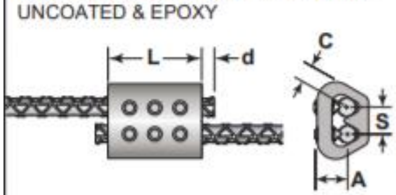

REBAR SIZE US [Metric]	DOUBLE BARREL PRODUCT CODE* BLACK	EPOXY	COUPLER WEIGHT (lb)	DIMENSIONS (in) LENGTH 'L'	'A'	'C'	'S'	'd'	NUMBER SCREWS PER BAR	AVERAGE SCREW TORQUE (ft-lbs)	MIN. IMPACT WRENCH RATING (ft-lbs)
#3 [10]	03DBZA	03DBZEA	1.41	2 1/8	1 1/8	3/8	15/16	3/8	2	60	250
#4 [13]	04DBZA	04DBZEA	1.38	2 1/8	1 1/16	1/2	15/16	1/2	2	60	250
#5 [16]	05DBZA	05DBZEA	2.17	3	1 1/8	5/8	15/16	5/8	3	60	250
#6 [19]	06DBZA	06DBZEA	3.07	3 7/8	1 3/16	3/4	15/16	3/4	4	60	250
#7 [22]	07DBZA	07DBZEA	6.76	5 3/8	1 5/16	7/8	1 3/8	7/8	4	105	500
#8 [25]	08DBZA	08DBZEA	10.2	6 1/2	1 3/4	1	1 3/16	1	5	105	500

* GALVANIZED COUPLER ALSO AVAILABLE - SUBSTITUTE 'DBZGA' FOR 'DBZBA' IN PART CODE. ALL DIMENSIONS ARE APPROXIMATE

DOUBLE BARREL ZAP TRANSITIONS
UNCOATED & EPOXY

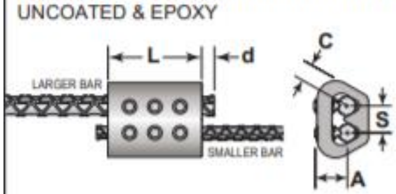

REBAR SIZE (US/US)	DOUBLE BARREL PRODUCT CODE* TRANSITION	COUPLER WEIGHT (lb)	DIMENSIONS (in) LENGTH 'L'	'A'	'C'	'S'	'd'	NUMBER SCREWS PER BAR	AVERAGE SCREW TORQUE (ft-lbs)	MIN. IMPACT WRENCH RATING (ft-lbs)
4/3	04/03DBZA	1.40	2 1/8	1 1/16	1/2	15/16	1/2	2	60	250
5/4	05/04DBZA	2.20	3	1 1/8	5/8	15/16	5/8	3	60	250
6/4	06/04DBZA	3.11	3 7/8	1 3/16	3/4	15/16	3/4	4	60	250
6/5	06/05DBZA	3.11	3 7/8	1 3/16	3/4	15/16	3/4	4	60	250
7/5	07/05DBZA	6.86	5 3/8	1 5/16	7/8	1 3/8	7/8	4	105	500
7/6	07/06DBZA	6.86	5 3/8	1 5/16	7/8	1 3/8	7/8	4	105	500
8/7	08/07DBZA	10.3	6 1/2	1 3/4	1	1 3/16	1	5	105	500

* EPOXY & GALVANIZED TRANS. ALSO AVAILABLE - SUBSTITUTE 'DBZEA' OR 'DBZGA' FOR 'DBZA' IN PART CODE. ALL DIMENSIONS ARE APPROXIMATE

ZAP SCREWLOK® MECHANICAL SPLICES AND CONNECTORS FOR REINFORCING BARS

ZAP SCREWLOK® mechanical splices and connectors are compatible with reinforcing bars that comply with ASTM A615, ASTM A706, ASTM A996, or equal, and consist of smooth, shaped, steel sleeves with converging sides. A series of cone-pointed hex-head screws are arranged along the longitudinal axis in one or two rows. In the case of butt splices, reinforcing bars are inserted from each end to a center stop. No special bar-end preparation is required, so ends can be sheared, sawed, or flame-cut. When a splice is required between fixed points, the center pin can be knocked out completely allowing the coupler sleeve to be slipped entirely onto one bar and subsequently repositioned over both bar ends being spliced.

During mechanical splice assembly, the specially designed screws are tightened until they embed into the rebar surface whereupon the heads twist off at a prescribed tightening torque. Forces from the screws cause rebar deformations to interlock within the coupler wedge. The DUAL mechanical action results in a full positive connection for transferring tension or compression forces from bar-to-bar. Screws can be tightened using suitable impact wrenches. Linear alignment is preserved across the splice by using reinforcing bars with straight ends and securing the continuation bar in the desired position at the time of assembly.

Mechanical butt splices and connectors are available for reinforcing bar sizes #3 through #18 (Ø10 – 57 mm), and **mechanical lap splices** are available for bar sizes #3 through #8 (Ø10 – 25 mm), per the above ***Dimensions and Data*** charts. Transition splices are used to connect reinforcement bars of different sizes or different types, such as square bar or threaded rod.

Epoxy-coated reinforcing bars that comply with ASTM A775 can be spliced by means of epoxy coated Zap Screwlok® couplers without shielding or removing the epoxy coating from the bar. Zinc-coated (galvanized) bars per ASTM A767 or A1094 can be mechanically spliced by means of galvanized Zap Screwlok® couplers.

ZAP SCREWLOK® is an engineered mechanical splice system whose strength is independent of the concrete which surrounds it, thereby providing true structural continuity. Applications include new construction, field repairs, splicing of column steel, beam reinforcement, concrete piles and deck steel, and splicing of older types of reinforcing bars. The Zap Screwlok® system is commonly used for rehab / retrofit projects, strengthening and upgrading concrete elements, extending deck steel to widen bridges, highway patch and repair projects, and splicing bars across closure pours. Zap Screwlok® Type 2 splices can be used for mechanically splicing reinforcement in members resisting earthquake induced forces. Benefits include a field installed splice with easy visual inspection, no specialized equipment, minimal clearance requirements, a positive rebar center-stop and no rebar end preparation.

Field splicing of reinforcing bars by the Zap Screwlok® method is most popular because of the systems simplicity, cost effectiveness and adaptability. Instructions provided with Zap Screwlok® splices and connectors, or available at www.barsplice.com, explain step-by-step installation and safety information.

Barsplice Products, Inc., 4900 Webster Street, Dayton OH 45414, USA
Tel: (937) 275-8700 • Fax: (937) 275-9566 • E-mail: bar@barsplice.com

aci MEMBER | CRSI MEMBER

REV.P 07/15/2020

BarSplice PRODUCTS INC.
A SUBSIDIARY OF FC INDUSTRIES INC.

DIMENSIONS AND DATA SHEET
INCH-POUND UNITS

BarGrip® XL

BarGrip® XL COUPLER

REBAR SIZE US [metric]	BarGrip XL PRODUCT CODE	BarGrip XL COLOR CODE*	COUPLER WEIGHT (lb)	COUPLER DIMENSIONS (in) LENGTH 'L'	OUTSIDE DIA. 'D'	INSIDE DIA. 'd'	BAR INSERTION 'i'	FIELD INSTALLATION DIMENSIONS (in) (SEE BELOW) PRESS MODEL	'H'	'S'	'T'	'X'	'U'
#3 [10]	03XL	ORANGE	0.24	3 1/4	3/4	1/2	1 5/8	BG 250	3 1/4	1 5/8	2	4 5/8	2 1/4
#4 [13]	04XL	PINK	0.40	4	15/16	5/8	2		3 3/4	1 3/4	2 1/8	5	2 3/8
#5 [16]	05XL	RED	0.69	4 3/4	1 1/8	3/4	2 3/8		4 1/4	1 7/8	2 1/4	6 3/4	2 1/2
#6 [19]	06XL	YELLOW	1.25	5 1/2	1 3/8	15/16	2 3/4	BG 400	5 5/8	3	4 1/4	7 5/8	5 1/4
#7 [22]	07XL	BLUE	1.76	6 1/4	1 9/16	1 1/16	3 1/8		6 1/4	3	4 1/2	8 3/4	5 1/2
#8 [25]	08XL	BLACK	2.57	7	1 3/4	1 3/16	3 1/2		6 3/4	3 1/4	4 1/2	9 1/2	5 1/2
#9 [29]	09XL	RED	3.30	7 1/2	1 15/16	1 3/8	3 3/4	BG 750	7 1/2	3 1/4	5 1/4	11 1/2	6 1/4
#10 [32]	10XL	YELLOW	4.52	8 1/4	2 3/16	1 1/2	4 1/8		8	3 1/2	5 1/2	12 1/2	6 1/2
#11 [36]	11XL	BLUE	5.73	9	2 3/8	1 11/16	4 1/2		8 5/8	3 1/2	5 3/4	13 1/8	6 1/2
#14 [43]	14XL	PINK	11.9	11	2 15/16	1 15/16	5 1/2	BG 1140	10 3/8	4 3/4	7	15 1/8	9
#18 [57]	18XL	RED	24.1	14	3 13/16	2 5/8	7		13	5 1/4	8	20 3/4	9 1/2

ALL DIMENSIONS ARE APPROXIMATE

BarGrip® XL TRANSITION SERIES

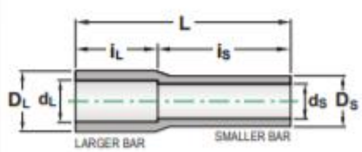

REBAR SIZE	TRANSITION PRODUCT CODE	COLOR CODE* LG	SM	COUPLER WEIGHT (lb)	COUPLER DIMENSIONS (in) LENGTH 'L'	OUTSIDE DIA. LARGE 'D_L'	OUTSIDE DIA. SMALL 'D_S'	INSIDE DIA. LARGE 'd_L'	INSIDE DIA. SMALL 'd_S'	BAR INSERTION LARGE 'i_L'	BAR INSERTION SMALL 'i_S'	FIELD PRESS MODEL
5/4	05/04XL	RED	PINK	0.38	3 7/16	1 1/16	7/8	3/4	5/8	1 3/8	2 1/16	BG 250
6/4	06/04XL	YEL.	PINK	0.60	4 1/16	1 3/8	7/8	15/16	5/8	1 5/16	2 3/4	BG 400
6/5	06/05XL		RED	0.72	4 1/16	1 3/8	1 1/16	15/16	3/4	1 9/16	2 1/2	
7/5	07/05XL	BLUE	RED	1.00	4 3/4	1 9/16	1 1/16	1 1/16	3/4	1 11/16	3 1/16	
7/6	07/06XL		YEL.	1.20	4 3/4	1 9/16	1 3/8	1 1/16	15/16	2 1/16	2 11/16	
8/6	08/06XL	BLK	YEL.	1.72	5 3/8	1 3/4	1 3/8	1 3/16	15/16	2 1/2	2 7/8	
8/7	08/07XL		BLUE	1.75	5 3/8	1 3/4	1 9/16	1 3/16	1 1/16	2 1/2	2 7/8	
9/7	09/07XL	RED	BLUE	1.90	6 1/8	1 15/16	1 9/16	1 5/16	1 1/16	2 7/8	3 1/4	BG 750
9/8	09/08XL		BLK	2.50	6 1/8	1 15/16	1 3/4	1 5/16	1 3/16	2 7/8	3 1/4	
10/8	10/08XL	YEL.	BLK	3.50	6 7/8	2 3/16	1 3/4	1 1/2	1 3/16	2 15/16	3 15/16	
10/9	10/09XL		RED	3.52	6 7/8	2 3/16	1 15/16	1 1/2	1 5/16	3 1/16	3 13/16	
11/8	11/08XL	BLUE	BLK	3.79	7 1/4	2 3/8	1 3/4	1 5/8	1 3/16	2 5/8	4 5/8	
11/9	11/09XL		RED	3.95	7 1/4	2 3/8	1 15/16	1 5/8	1 5/16	3 1/8	4 1/8	
11/10	11/10XL		YEL.	4.38	7 1/4	2 3/8	2 3/16	1 5/8	1 1/2	3 1/4	4	
14/10	14/10XL	PINK	YEL.	6.90	8 7/8	2 7/8	2 3/16	1 15/16	1 1/2	3 5/8	5 1/4	BG 1140
14/11	14/11XL		BLUE	7.05	8 7/8	2 7/8	2 3/8	1 15/16	1 5/8	3 5/8	5 1/4	
18/11	18/11XL	RED	BLUE	14.6	11 9/16	3 13/16	2 3/8	2 5/8	1 5/8	4 1/8	7 7/16	
18/14	18/14XL		PINK	16.7	11 9/16	3 13/16	2 7/8	2 5/8	1 15/16	4 1/8	7 3/16	

ALL DIMENSIONS ARE APPROXIMATE

BarGrip® STRUCTURAL CONNECTOR

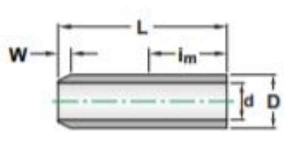

REBAR SIZE US [metric]	BarGrip XL PRODUCT CODE	BarGrip XL COLOR CODE*	COUPLER WEIGHT (lb)	DIMENSIONS (in) LENGTH 'L'	OUTSIDE DIA. 'D'	INSIDE DIA. 'd'	MINIMUM INSERTION 'i_m'**	WELDING BEVEL 'W'
#3 [10]	03LB	ORANGE	0.24	3 1/4	3/4	1/2	1	3/16
#4 [13]	04LB	PINK	0.39	4	15/16	5/8	1 1/4	3/16
#5 [16]	05LB	RED	0.67	4 3/4	1 1/8	3/4	1 5/8	1/4
#6 [19]	06LB	YELLOW	1.22	5 1/2	1 3/8	15/16	1 7/8	1/4
#7 [22]	07LB	BLUE	1.72	7 1/4	1 9/16	1 1/16	2 1/4	5/16
#8 [25]	08LB	BLACK	2.50	7	1 3/4	1 3/16	2 1/2	3/8
#9 [29]	09LB	RED	3.20	6 1/2	1 15/16	1 3/8	2 3/4	7/16
#10 [32]	10LB	YELLOW	4.40	8 1/4	2 3/16	1 1/2	3 1/8	1/2
#11 [36]	11LB	BLUE	5.55	9	2 3/8	1 11/16	3 1/2	9/16
#14 [43]	14LB	PINK	11.6	11	2 15/16	1 15/16	4 1/2	11/16
#18 [57]	18LB	RED	23.5	14	3 13/16	2 5/8	6 1/8	7/8

** Minimum insertion equals the swage length. Maximum Rebar Insertion can be up to the full coupler length.

ALL DIMENSIONS ARE APPROXIMATE

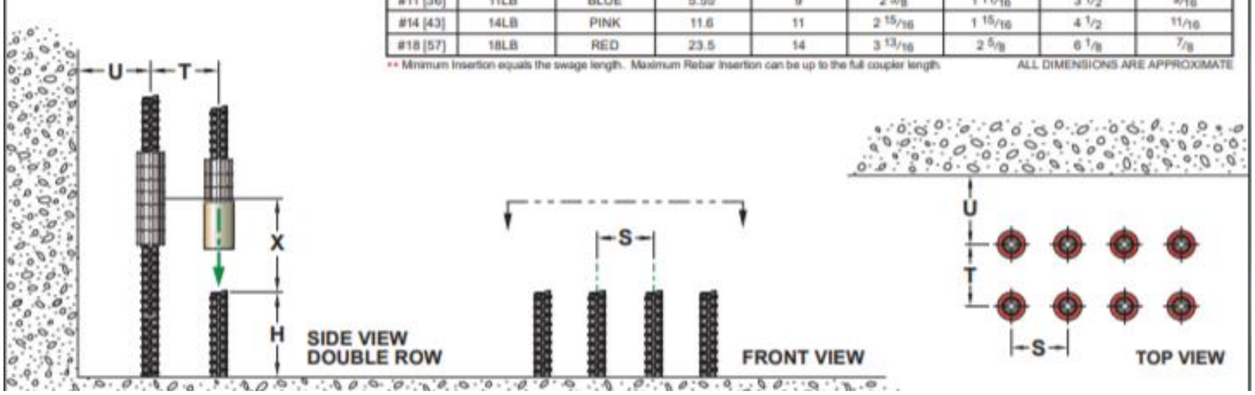

BPI BarGrip® SWAGING EQUIPMENT

[See BarGrip Splicing Manual (SM02) for more details]

BPI® Equipment is available for lease or purchase.

Equipment must be used in accordance with manuals, lease agreements, manufacturers' directions and all safety instructions.

BG750M

MIDSIZE FIELD PRESS
weighs 90 lbs [41 kg]
(mostly used on #8, #9, #10 & #11 bar)

#5 #6 #7 #8 #9 #10 #11

BG1140M

HEAVY-DUTY FIELD PRESS
weighs 200 lbs [91 kg]
(mostly used on #10, #11, #14 & #18 bar)

#7 #8 #9 #10 #11 #14 #18

BG400

COMPACT FIELD PRESS
weighs 60 lbs [28 kg]
(mostly used on #6, #7 & #8 bar)

#3 #4 #5 #6 #7 #8

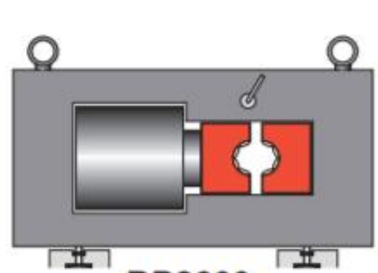

BP2600

BENCH PRESS for swaging all sizes up to No. 18 [Ø 57mm]
weighs 1,600 lbs [725 kg]

Double acting cylinder produces 300 tons of force connected to 10 or 15 hp pump for high fabrication shop productivity.

Press includes foot control, lifting eyes and leveling feet.

#3 #4 #5 #6 #7 #8 #9 #10 #11 #14 #18

BG250

MINI FIELD PRESS
weighs 20 lbs [9 kg]
(mostly used on #4 & #5 bar)

#3 #4 #5

BPI® swaging equipment for the installation of **BarGrip®** cold swaged coupling sleeves and structural connectors consists of a hydraulic **PRESS**, **PUMP** and **HOSE** with suitable swaging **DIES**.

Press models for field swaging range in size from the BG 250 for splicing #3 – 5 reinforcement bars (Ø10 – 16 mm), to the BG 1140M for splicing bars up to #18 (Ø57 mm). Each press is provided with a lifting handle and/or lifting eye for support. With a simple change of the die set, each press is capable of swaging multiple sizes of coupling sleeve inclusive of BarGrip XL, XL Transitions and Structural Connectors. For ease of use, dies and coupling sleeves are stamped and color-coded to match.

A hydraulic pump (electrically-driven or gasoline-driven) connects to the press by means of a hose with quick-disconnect ends. The equipment operator depresses a foot control to actuate the system. As the ram of the press extends and pushes the dies towards each other, a portion of the coupling sleeve is forced to deform around the rebar and interlock with the bar profile. When each swaging bite has been completed, a pressure switch, built into the pump, automatically stops the process to allow the ram of the press to retract for the next bite. After a coupling sleeve has been fully swaged, the operator simply removes the outer die pin and slides the outer die out of the press for convenient removal of the press from around the spliced rebar.

Pump Model	PE 55	PE 400	PG 400
Driver	1 ¼ HP Electric Motor	10 HP Electric Motor	18 HP Gasoline Engine
Power Supply	115V 1-phase	230V or 460V 3-phase	Battery Start
Weight with fluid	147 lbs (66 kg)	605 lbs (274 kg)	545 lbs (247 kg)
Most common use	Rebar #3 - #11 [Ø10-36mm]	Rebar #9 - #18 [Ø28-57mm]	Rebar #9 - #18 [Ø28-57mm]
Attributes	Compact / Maneuverable	Fast / High volume jobs	No power supply required

* COLOR CODE OF COUPLER MUST MATCH COLOR OF DIE SET

A BP 2600 Bench Press can be utilized by the rebar fabricator to efficiently half-swage coupling sleeves to reinforcement bar ahead of shipping, thereby saving time and labor on the jobsite.

NOTE: In lieu of shop half-swaging with a Bench Press, it may sometimes be appropriate to use a field press such as a BG 750M or BG 1140M – Contact BPI for assistance with your specific application.

aci MEMBER

Barsplice Products, Inc., 4900 Webster Street, Dayton OH 45414, USA
Tel: (937) 275-8700 • Fax: (937) 275-9566 • E-mail: bar@barsplice.com

CRSI MEMBER

REV.N 11/13/2019

APPENDIX H: Product Data Sheet: Coupler 'C'

BarSplice PRODUCTS INC. A SUBSIDIARY OF FC INDUSTRIES INC.

DIMENSIONS AND DATA SHEET
INCH-POUND UNITS

Grip-Twist®

GRIP–TWIST® XT MECHANICAL SPLICES

COLD–SWAGED STEEL COUPLER WITH TAPER THREADED ENDS & OPTIONAL FLANGE

- ***FOR HIGH STRENGTH, LOW CARBON, CHROMIUM STEEL BARS, ASTM A1035***
- ***FAST, EFFICIENT INSTALLATION***
- ***ELIMINATES LONG LAP LENGTHS, REDUCES CONGESTION***
- ***DEVELOPED STRENGTH –*** 1.25 x specified yield strength (*fy*) ASTM A1035 Grades 100 & 120.
- ***ULTIMATE CAPACITY –*** ASTM A1035 Grades 100 & 120, equal to 150 ksi.
- ***FULL MECHANICAL SPLICE –*** ACI 318–19 Chapter 18 - Exceeds specified tensile strength (f_u) ASTM A615 Grade 100, equal to 115 ksi.

TAPER THREADED GRIP–TWIST® XT

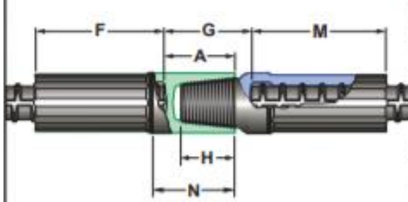

REBAR SIZE US [Metric]	TAPER THREADED GRIP–TWIST XT COLOR CODE*	COUPLER WEIGHT (lb) FEMALE	COUPLER WEIGHT (lb) MALE	BAR INSERTION (AFTER SWAGING) F	BAR INSERTION (AFTER SWAGING) M	REBAR GAP G	MALE INSERTION H	END ALLOWANCE A	NON-SWAGED LENGTH N
				DIMENSIONS (in)					
#4 [13]	RED	0.62	0.61	2 1/4	2 1/4	1 7/8	15/16	1 5/16	1 1/2
#5 [16]	YELLOW	1.18	1.07	2 11/16	2 11/16	2	1 1/8	1 9/16	1 13/16
#6 [19]	BLUE	1.64	1.57	3 1/16	3 1/16	2 7/16	1 5/16	1 7/8	2 1/8
#7 [22]	RED	3.34	3.33	3 15/16	3 15/16	3 1/8	1 3/4	2 7/16	2 3/4
#8 [25]	YELLOW	4.74	4.71	4 7/16	4 7/16	3 1/2	2	2 3/4	3 1/8
#9 [29]	BLUE	5.8	6.0	4 13/16	4 13/16	3 1/2	2 1/8	2 3/4	3 1/8
#10 [32]	BLACK	9.3	9.1	5 3/8	5 3/8	4 1/8	2 3/8	3 1/4	3 5/8
#11 [36]	PINK	10.6	10.7	5 5/8	5 5/8	4 5/8	2 11/16	3 5/8	4 1/16
#14 [43]	RED	26	26	6 7/8	6 7/8	7 1/8	3 1/4	5 3/16	5 11/16
#18 [57]	YELLOW	43	41	8 1/2	8 1/2	7 1/4	4 3/8	5 13/16	6 13/16

ALL DIMENSIONS ARE APPROXIMATE

GRIP–TWIST® XT TRANSITION SERIES

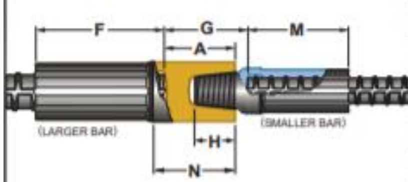

REBAR SIZE	XT COLOR CODE* TRANS. FEMALE	XT COLOR CODE* TAPER MALE	COUPLER WEIGHT (lb) FEMALE	COUPLER WEIGHT (lb) MALE	BAR INSERTION (AFTER SWAGING) F	BAR INSERTION (AFTER SWAGING) M	REBAR GAP G	MALE INSERTION H	END ALLOWANCE A	NON-SWAGED LENGTH N
					DIMENSIONS (in)					
5/4	YELLOW	RED	1.28	0.61	2 11/16	2 1/4	1 15/16	15/16	1 9/16	1 13/16
6/5	BLUE	YELLOW	1.80	1.07	3 1/16	2 11/16	2 5/16	1 1/8	1 7/8	2 1/8
7/6	RED	BLUE	3.83	1.57	3 15/16	3 1/16	3	1 5/16	2 7/16	2 3/4
8/7	YELLOW	RED	5.23	3.33	4 7/16	3 15/16	3 7/16	1 3/4	2 3/4	3 1/8
9/8	BLUE	YELLOW	6.27	4.71	4 13/16	4 7/16	3 1/2	2	2 3/4	3 1/8
10/9	BLACK	BLUE	9.9	6.0	5 3/8	4 13/16	4	2 1/8	3 1/4	3 5/8
11/10	PINK	BLACK	10.9	9.1	5 5/8	5 3/8	4 1/2	2 3/8	3 5/8	4 1/16
14/11	RED	PINK	30	10.7	6 7/8	5 5/8	6 1/8	2 11/16	5 3/16	5 11/16

ALL DIMENSIONS ARE APPROXIMATE – OTHER TRANSITION SIZES AVAILABLE UPON REQUEST

GRIP–TWIST® XT POSITION SERIES

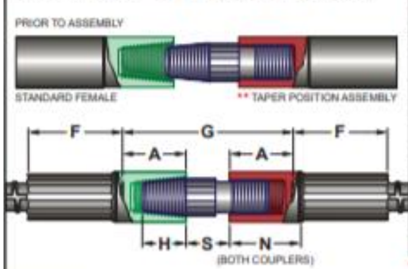

REBAR SIZE US [Metric]	GRIP–TWIST XT POSITION COLOR CODE*	COUPLER WEIGHT (lb) FEMALE	COUPLER WEIGHT (lb) POSITION w/ STUD	BAR INSERTION (AFTER SWAGE) F	SPACE (AFTER ASSY) S	REBAR GAP G	MALE INSERTION H	END ALLOWANCE A	NON-SWAGED LENGTH N
					DIMENSIONS (in)				
#4 [13]	RED	0.62	0.98	2 1/4	1 1/8	3 3/4	15/16	1 5/16	1 1/2
#5 [16]	YELLOW	1.18	1.75	2 11/16	1 1/4	4 3/8	1 1/8	1 9/16	1 13/16
#6 [19]	BLUE	1.64	2.66	3 1/16	1 5/8	5 3/8	1 5/16	1 7/8	2 1/8
#7 [22]	RED	3.34	5.29	3 15/16	1 1/2	6 3/8	1 3/4	2 7/16	2 3/4
#8 [25]	YELLOW	4.74	7.65	4 7/16	1 5/8	7 1/8	2	2 3/4	3 1/8
#9 [29]	BLUE	5.8	9.8	4 13/16	1 7/8	7 3/8	2 1/8	2 3/4	3 1/8
#10 [32]	BLACK	9.3	14.4	5 3/8	1 3/4	8 1/4	2 3/8	3 1/4	3 5/8
#11 [36]	PINK	10.6	16.6	5 5/8	2 1/8	9 3/8	2 11/16	3 5/8	4 1/16
#14 [43]	RED	26	40	6 7/8	2 1/8	12 1/2	3 1/4	5 3/16	5 11/16
#18 [57]	YELLOW	43	67	8 1/2	2 3/4	14 3/8	4 3/8	5 13/16	6 13/16

** EACH TAPER POSITION ASSEMBLY (XTMTPA) CONSISTS OF (1) POSITION COUPLER (XTMPF) AND (1) PRE-INSTALLED STUD (TTMRP) EACH MARKED WITH SEPARATE CODE FOR TRACEABILITY

GRIP–TWIST® XT FLANGED SERIES

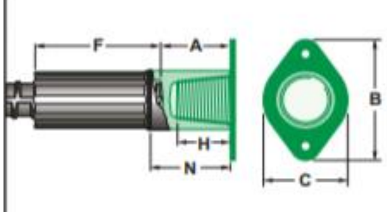

REBAR SIZE US [Metric]	GRIP–TWIST XT w/ METAL FLANGE COLOR CODE*	FEMALE COUPLER w/ FLANGE WEIGHT (lb)	BAR INSERTION (AFTER SWAGE) F	FLANGE HEIGHT B	FLANGE WIDTH C	MALE INSERTION H	END ALLOWANCE A	NON-SWAGED LENGTH N
				DIMENSIONS (in)				
#4 [13]	RED	0.67	2 1/4	2 7/16	1 5/8	15/16	1 5/16	1 1/2
#5 [16]	YELLOW	1.26	2 11/16	2 15/16	2	1 1/8	1 9/16	1 13/16
#6 [19]	BLUE	1.72	3 1/16	2 15/16	2	1 5/16	1 7/8	2 1/8
#7 [22]	RED	3.44	3 15/16	3 3/8	2 3/8	1 3/4	2 7/16	2 3/4
#8 [25]	YELLOW	4.87	4 7/16	3 11/16	2 5/8	2	2 3/4	3 1/8
#9 [29]	BLUE	5.9	4 13/16	3 3/4	2 3/4	2 1/8	2 3/4	3 1/8
#10 [32]	BLACK	9.5	5 3/8	4 1/8	3 1/8	2 3/8	3 1/4	3 5/8
#11 [36]	PINK	10.8	5 5/8	4 1/4	3 1/4	2 11/16	3 5/8	4 1/16
#14 [43]	RED	27	6 7/8	5 3/4	3 13/16	3 1/4	5 3/16	5 11/16

ALL DIMENSIONS ARE APPROXIMATE – PLASTIC FLANGE ALSO AVAILABLE FOR SIZES #4 AND #5 – ASK FOR DETAILS

BarSplice PRODUCTS INC.

A SUBSIDIARY OF FC INDUSTRIES INC.

DIMENSIONS AND DATA SHEET
INCH-POUND UNITS

Grip-Twist®

GRIP–TWIST® XT DoughNUT™

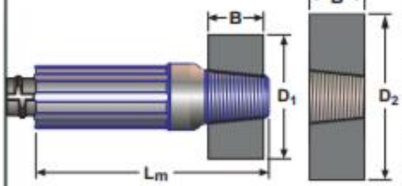

REBAR SIZE US [Metric]	COMPLETE XT MALE SWAGED LENGTH Lm (in)	THICKNESS (in) B	HEAD DIAMETER AND WEIGHT TDS SERIES [5Ab] D1 (in)	TDS SERIES [5Ab] Wt (lb)	TDX SERIES [10Ab] D2 (in)	TDX SERIES [10Ab] Wt (lb)
#4 [13]	3 5/8	7/8	1 5/8	0.38	2 3/16	0.85
#5 [16]	4 5/16	15/16	1 7/8	0.57	2 1/2	1.15
#6 [19]	5	1 1/4	2 3/16	1.02	2 7/8	1.98
#7 [22]	6 1/2	1 1/2	2 3/4	1.86	3 7/8	4.32
#8 [25]	7 1/4	1 5/8	3	2.34	4 1/4	5.59
#9 [29]	7 5/8	1 7/8	3 3/8	3.54	4 5/8	7.74
#10 [32]	8 9/16	2	3 7/8	4.97	5 1/4	10.5
#11 [36]	9 3/8	2 1/8	4	5.5	5 1/2	12.3
#14 [43]	12 3/16	2 3/4	5 1/2	13.5	7 1/2	29
#18 [57]	14 5/16	3 5/8	6 1/8	23	8 3/8	48

ALL DIMENSIONS ARE APPROXIMATE

TTGT XT STRUCTURAL CONNECTOR

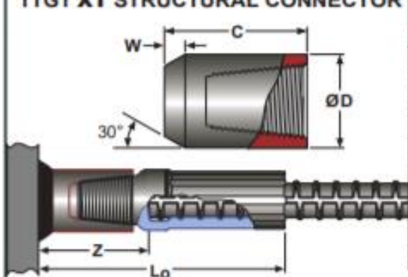

REBAR SIZE US [Metric]	TAPER THREADED GRIP-TWIST XT MALE COLOR CODE *	STRUCTURAL CONNECTOR WEIGHT (lb)	DIMENSIONS (in) XT STR CONN. OUTSIDE DIA D	XT STR CONN. LENGTH C	WELD BEVEL LENGTH W	REBAR GAP Z	OVERALL LENGTH Lo
#4 [13]	RED	0.32	1 1/8	1 11/16	1/4	2 1/8	4 5/16
#5 [16]	YELLOW	0.58	1 3/8	2	1/4	2 1/2	5 1/8
#6 [19]	BLUE	0.83	1 9/16	2 5/16	5/16	2 15/16	6
#7 [22]	RED	1.58	1 15/16	3	7/16	3 13/16	7 3/4
#8 [25]	YELLOW	2.24	2 3/16	3 3/8	1/2	4 3/16	8 9/16
#9 [29]	BLUE	2.8	2 3/8	3 5/8	9/16	4 1/2	9 3/8
#10 [32]	BLACK	4.5	2 3/4	4 1/8	5/8	5	10 5/16
#11 [36]	PINK	5.1	2 7/8	4 3/8	11/16	5 3/8	11 1/4
#14 [43]	RED	12	3 13/16	5 3/4	7/8	7 1/16	14 11/16
#18 [57]	YELLOW	20	4 9/16	6 5/8	1	3 5/8	16 9/16

ALL DIMENSIONS ARE APPROXIMATE

REBAR SIZE US [Metric]	COUPLER OUTSIDE DIAMETER (in)	TAPER GRIP–TWIST XT PART NUMBERS FEMALE	TAPER GRIP–TWIST XT PART NUMBERS MALE	TTGT XT TRANSITION PART NUMBERS TRANSITION FEMALE	TTGT XT TRANSITION PART NUMBERS MALE	TAPER GRIP–TWIST XT POSITION PART NUMBERS FEMALE	STUD	POSITION COUPLER	TTGT XT FLANGED FEMALE P/N	GRIP-TWIST XT DoughNUT PART NUMBERS ** TDS [5Ab]	TDX [10Ab]	TTGT XT STRUCTURAL CONN. P/N
#4 [13]	1 1/8	XT04F	XT04M			XT04F	XT04RP	XT04PF	XT04FWFL	05TDS	05TDX	XT04SC
#5 [16]	1 3/8	XT05F	XT05M	XT05/04F	XT04M	XT05F	XT05RP	XT05PF	XT05FWFL	06TDS	06TDX	XT05SC
#6 [19]	1 9/16	XT06F	XT06M	XT06/05F	XT05M	XT06F	XT06RP	XT06PF	XT06FWFL	07TDS	07TDX	XT06SC
#7 [22]	1 15/16	XT07F	XT07M	XT07/06F	XT06M	XT07F	XT07RP	XT07PF	XT07FWFL	09TDS	09TDX	XT07SC
#8 [25]	2 3/16	XT08F	XT08M	XT08/07F	XT07M	XT08F	XT08RP	XT08PF	XT08FWFL	10TDS	10TDX	XT08SC
#9 [29]	2 3/8	XT09F	XT09M	XT09/08F	XT08M	XT09F	XT09RP	XT09PF	XT09FWFL	11TDS	11TDX	XT09SC
#10 [32]	2 3/4	XT10F	XT10M	XT10/09F	XT09M	XT10F	XT10RP	XT10PF	XT10FWFL	13TDS	13TDX	XT10SC
#11 [36]	2 7/8	XT11F	XT11M	XT11/10F	XT10M	XT11F	XT11RP	XT11PF	XT11FWFL	14TDS	14TDX	XT11SC
#14 [43]	3 13/16	XT14F	XT14M	XT14/11F	XT11M	XT14F	XT14RP	XT14PF	XT14FWFL	18TDS	18TDX	XT14SC
#18 [57]	4 5/8	XT18F	XT18M	XT18/14F	XT14M	XT18F	XT18RP	XT18PF		20TDS	20TDX	XT18SC

** MATCHING THREAD SIZE COINCIDES WITH LARGER, STANDARD GRIP-TWIST® DoughNUT™

TAPER THREADED GRIP–TWIST® XT – Equipment and Installation

A Bench Press BP2600 fitted with a two-piece die set and powered by an electrically-driven hydraulic pump is used by the rebar fabricator to efficiently swage Grip-Twist® **XT** coupler components. The equipment operator depresses a foot control to actuate the system. As the ram extends and pushes the dies towards each other, the coupler component is forced to deform around the rebar and interlock with the bar profile. When a swaging bite has been completed, a pressure switch automatically stops the process and the operator retracts the ram for the next bite. For ease of use, swaging dies are color coded to indicate the rebar and coupler size. Color codes are shown on Grip-Twist® **XT** Dimensions and Data Charts.

NOTE: Taper Threaded Grip-Twist® **XT** coupler components are dimensionally different from standard Grip-Twist® products. Consequently, the swaging dies that are used to swage the Grip-Twist **XT** components are color coded differently from the swaging dies used to swage standard Grip-Twist products.

*** COLOR CODE OF COUPLER MUST MATCH COLOR OF DIE SET**

BP2600

Bench press for swaging all sizes up to No. 18 [Ø 57mm].

Double acting cylinder produces 300 tons of force connected to 10 or 15 hp pump for high fabrication shop productivity.

Press includes foot control, lifting eyes and leveling feet.

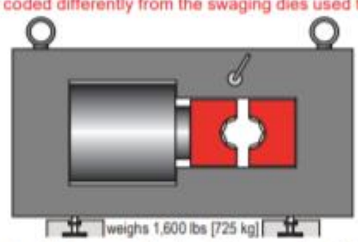

BPI® Equipment is available for lease or purchase.

Equipment must be used in accordance with manuals, lease agreements, manufacturers' directions and all safety instructions.

aci MEMBER

Barsplice Products, Inc., 4900 Webster Street, Dayton OH 45414, USA
Tel: (937) 275-8700 • Fax: (937) 275-9566 • E-mail: bar@barsplice.com

CRSI MEMBER

REV.G 07/13/2020

APPENDIX I: AASHTO LRFD Requirement Check for Coupler 'C'

THEORETICAL								
Grip-Twist XT			fu for coupler =	100000	psi	(A519 Steel)		
			Inside Dia.	Inside Area	Outside Dia.	Out. Area	Area Coupler (Ac)		*Fu/ lb
	#5	05XL	0.63	0.3068	1.375	1.4849	1.1781	in2	117809.72
	#6	06XL	0.75	0.4418	1.5625	1.9175	1.4757	in2	147568.95
			(*Fu = fu × Ac)						
Pure Titanium									
			fy for TiABs =	130000	psi	(TiAB class 130)			
		dia/in	area At /in2	#Fy / lb					
	#5	0.625	0.3068	39883.50					
	#6	0.75	0.4418	57432.24					
		(#Fy = fy × At)							
Tensile strength of splice system shall not be less than 125% of specified minimum yield strength of spliced bar									
			Calculated:				By: Fu Coup / Fy Ti		
A.	For #5	Fu coupler:	117809.72	Should be >	49854.38	OK)	2.954		
B.	For #6	Fu coupler:	147568.95	Should be >	71790.30	OK)	2.569		

EXPERIMENTAL							
fy for TiABs =		130000	psi	(TiAB class 130)			
125% fy =		162500	psi				
	Splice System		Tensile Strenght / psi			which is	
	D1		157,035	<	162500	120.8	% fy
	D2		158,917	<	162500	122.2	% fy
	D3		158,950	<	162500	122.3	% fy
	D4		154,187	<	162500	118.6	% fy
	D5		153,776	<	162500	118.3	% fy
	D6		153,393	<	162500	118.0	% fy
					Average:	120.0	% fy